Climate4you update November 2024
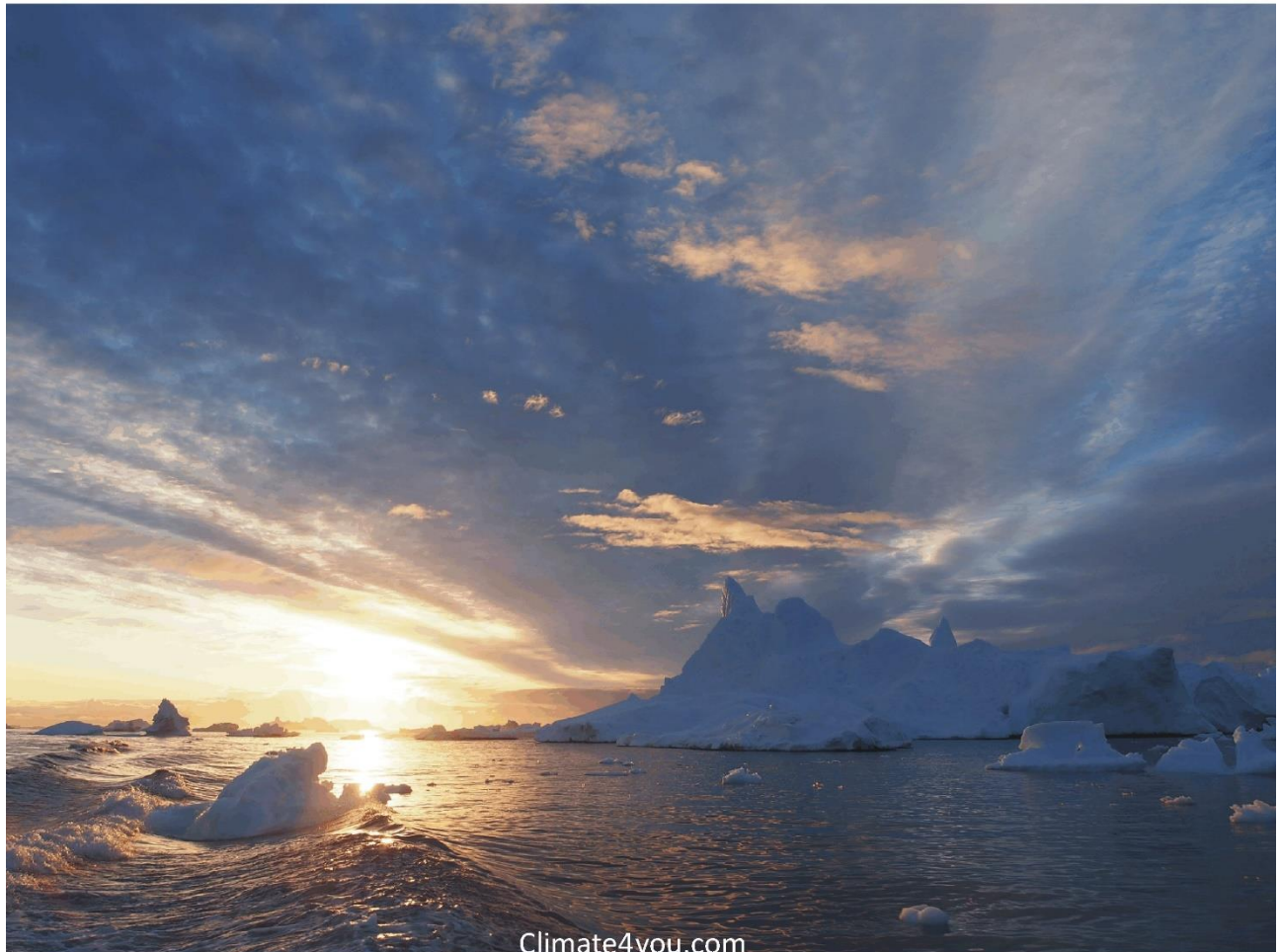

Climate4you.com

Summary of observations until November 2024:

1: Observed average annual global air temperature change since 1979 (46 years) is +0.0152°C (UAH).
If unchanged, additional average global air temperature increase by year 2100 will be about +1.14°C.

2: Tide gauges along coasts indicate a typical global sea level increase of about 1-2 mm/yr.
Coastal sea level change rate last 100 year has essential been stable, but with periodic variations.
If unchanged, global sea level at coasts will typically increase 8-16 cm by year 2100, although many
locations in regions affected by glaciation 20,000 years ago, will experience a relative sea level drop.

3: Since 2004 the global oceans above 1900 m depth on average have warmed about 0.037°C.
The maximum warming (about 0.2°C, 0-100 m depth) mainly affects oceans near Equator,
where the incoming solar radiation is at maximum.

4: Sources and sinks for CO_2 are many. However, changes in atmospheric CO_2 follow changes in global
air temperature, and changes in global air temperature follow changes in ocean surface temperature.

5: There was no perceptible effect on atmospheric CO_2 due to the 2020-21 COVID-related drop in
GHG emissions, underlining the fact that natural sinks and sources for atmospheric CO_2 far outweigh
human contributions. Therefore, any future reductions in the use of fossil fuels are unlikely
to have any significant effect on the amount of atmospheric Co_2.

Contents:

2

November 2024 global surface air temperature overview

General: This newsletter contains graphs and diagrams showing a selection of key meteorological variables, updated to the most recent past month, if possible. All temperatures are given in degrees Celsius.

Traditionally, a 30 -year reference period is often used by various meteorological institutions for comparison purposes and are supposed to be updated through the end of each decade ending in zero (e.g., 1951-1980, 1961-1990, 1971-2000, etc.). The concept of a normal climate goes back to the first part of the 20th century. At that time, lasting to about 1960, it was generally believed that for all practical purpose's climate could be considered constant, no matter how obvious year-to-year fluctuations might have been. On this basis meteorologist decided to operate with an average or normal climate, defined by a 30-year period, called the normal period, assuming that it was of sufficient length to iron out all intervening variations.

In fact, using a 30-yr 'normal' period is rather unfortunate, as observations clearly demonstrate that various global climate parameters (see, e.g., page 20) are influenced by periodic changes of 50-70 years duration. The frequently used 30-yr reference period is roughly half this time interval and is therefore highly unsuited as reference period. In the maps on page 4, showing the geographical pattern of surface air temperature anomalies, the last previous 10 years are therefore used as reference period. This decadal approach corresponds well to the typical memory horizon for many people and is also adopted as reference period by other institutions, e.g., the Danish Meteorological Institute (DMI).

In many diagrams shown in this newsletter the thin line represents the monthly global average value, and the thick line indicate a simple running 37-month average, nearly corresponding to a three-year average. The year 1979 has been chosen as starting point in many diagrams, as this approximately corresponds to both the beginning of satellite observations and the onset of the late 20th century warming period. However, most of the data series have a longer record length, which may be inspected in greater detail on www.climate4you.com.

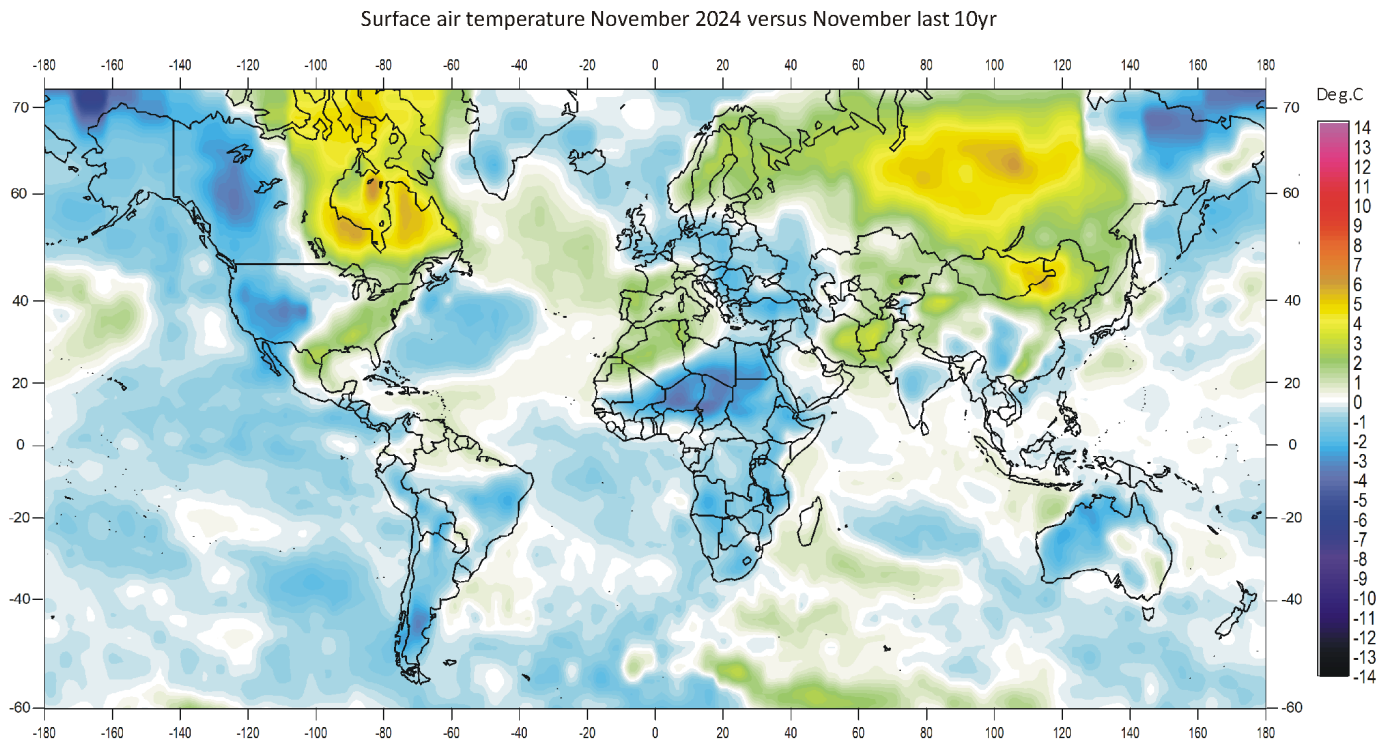**November 2024 surface air temperature**

General: For November 2024, the GISS data portal provided AIRS interpolated surface air data, based on satellite observations (p.4-5). According to the GISS and NCDC records, the November global temperature anomaly was almost unchanged from the October anomaly. The UAH and RSS lower troposphere satellite series show the November temperature anomaly as lower than the October anomaly. The AIRS v6 November global average temperature anomaly compared to the average for the last 10 years also is somewhat lower (p.4). This especially applies when compared to November last year (p.5). The previous months of elevated temperature anomalies are evident from surface up to the Tropopause (p.34).

The Northern Hemisphere surface temperature anomality pattern (p.4) was characterised by strong regional contrasts, mainly controlled by the dominant jet stream position. Especially eastern and northern Canada and central Russia were warm relative to the average for the last 10 years. In contrast, Siberia, Alaska and western Canada was relatively cold. Ocean wise, except a region around 50°N much of the North Atlantic was relatively cold, especially the Greenland and Norwegian Seas. The Pacific Ocean was relatively cold, except for a region centred around 40°N. PDO (p.20) remains negative. Arctic Ocean surface air temperatures were a mixture of above and below the 10-yr average.

Near the Equator temperatures were generally near or below the 10-year average. Evidently, ocean heat released during the previous warm El Niño episode has now dissipated from this important and huge region.

Southern Hemisphere temperatures were near or below the 10-yr average for September. All main land areas were relatively cold. The entire Antarctic had temperatures below the average for the previous 10 years.

November 2024 global surface air temperature overview versus average November last 10 years

Surface air temperature November 2024 versus November last 10yr
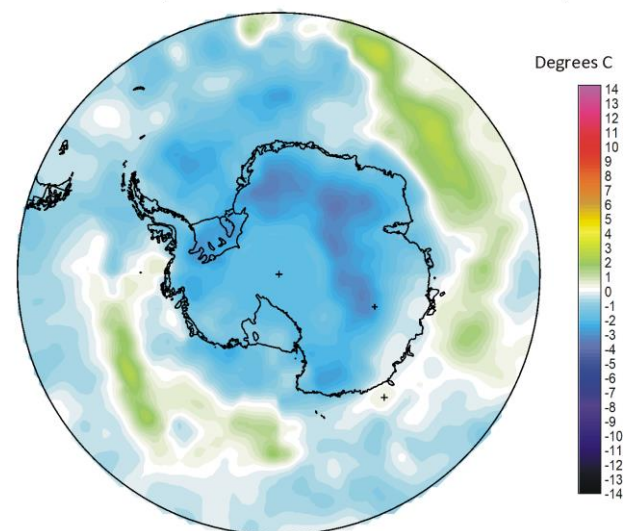
November 2024 surface air temperature compared to the average of November over the last 10 years. Green-yellow-red colours indicate areas with higher temperature than the 10-year average, while blue colours indicate lower than average temperatures. Data source: Remote Sensed Surface Temperature Anomaly, AIRS/Aqua L3 Monthly Standard Physical Retrieval 1-degree x 1-degree V006 (https://airs.jpl.nasa.gov/), obtained from the GISS data portal (https://data.giss.nasa.gov/gistemp/maps/index_v4.html).
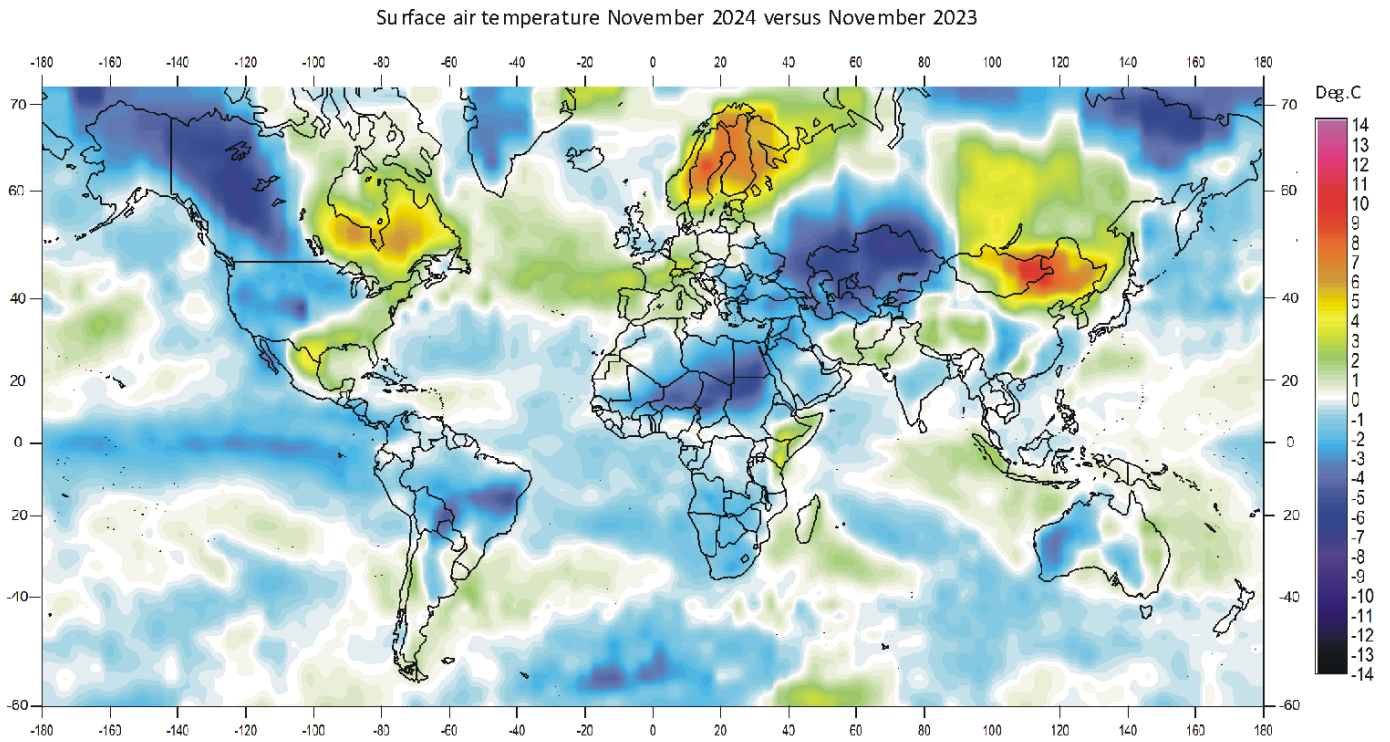
November 2024 global surface air temperature compared to November 2023

Surface air temperature November 2024 versus November 2023
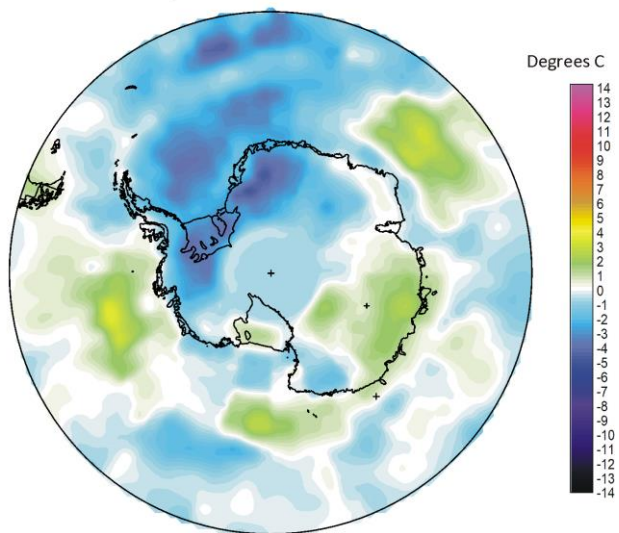
November 2024 surface air temperature compared to November 2023. Green-yellow-red colours indicate regions where the present month was warmer than last year, while blue colours indicate regions where the present month was cooler than last year. Variations in monthly temperature from one year to the next has no tangible climatic importance but may nevertheless be interesting to study. Data source: Remote Sensed Surface Temperature Anomaly, AIRS/Aqua L3 Monthly Standard Physical Retrieval 1-degree x 1-degree V006 (https://airs.jpl.nasa.gov/), obtained from the GISS data portal (https://data.giss.nasa.gov/gistemp/maps/index_v4.html).
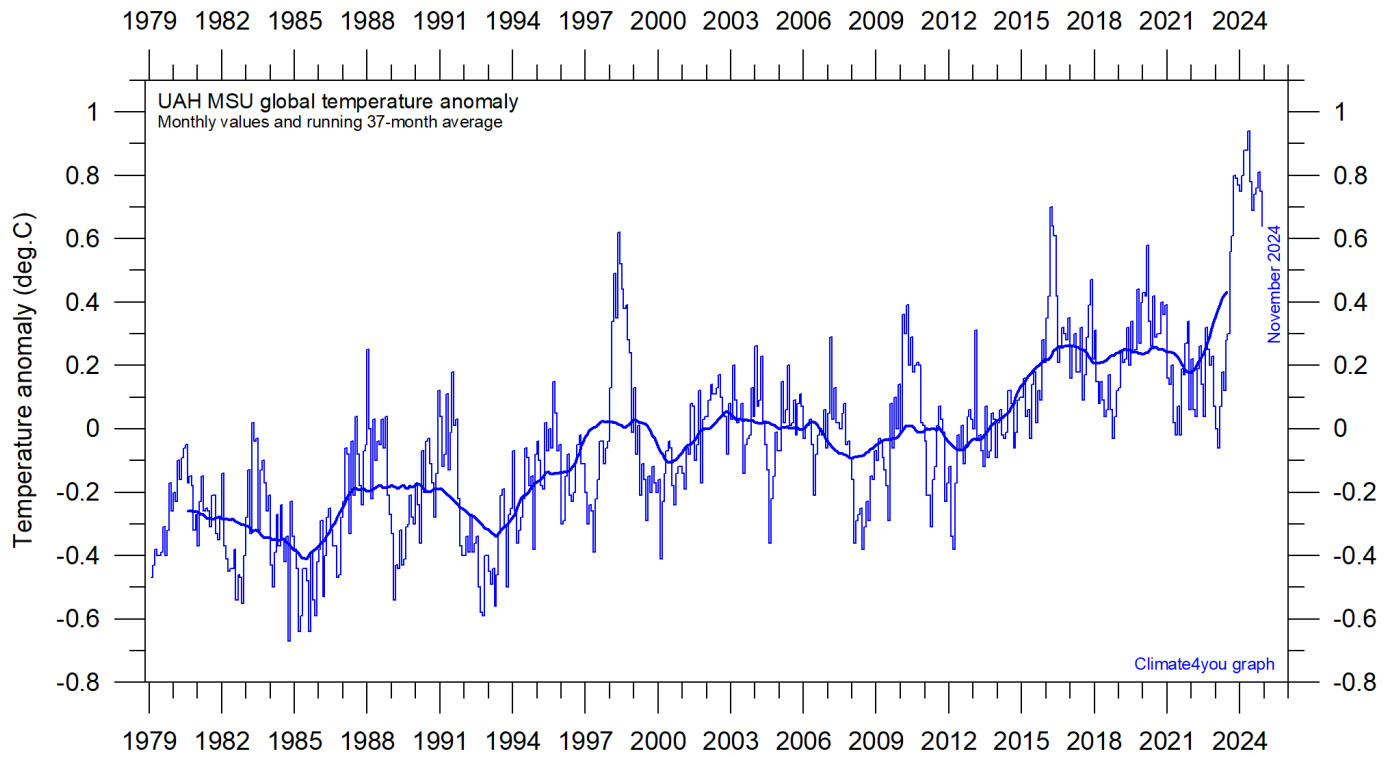
Global monthly average lower troposphere temperature (thin line) since 1979 according to University of Alabama at Huntsville, USA. The thick line is the simple running 37-month average. Reference period 1991-2020.

6

Global monthly average lower troposphere temperature (thin line) since 1979 according to according to Remote Sensing Systems (RSS), USA. The thick line is the simple running 37-month average.

Temperature quality class 2: HadCRUT global surface air temperature, updated to October 2024

HadCRUT5 non-infilled global temperature anomaly
Monthly values and running 37-month average

October 2024

Climate4you graph

Temperature anomaly (deg.C)
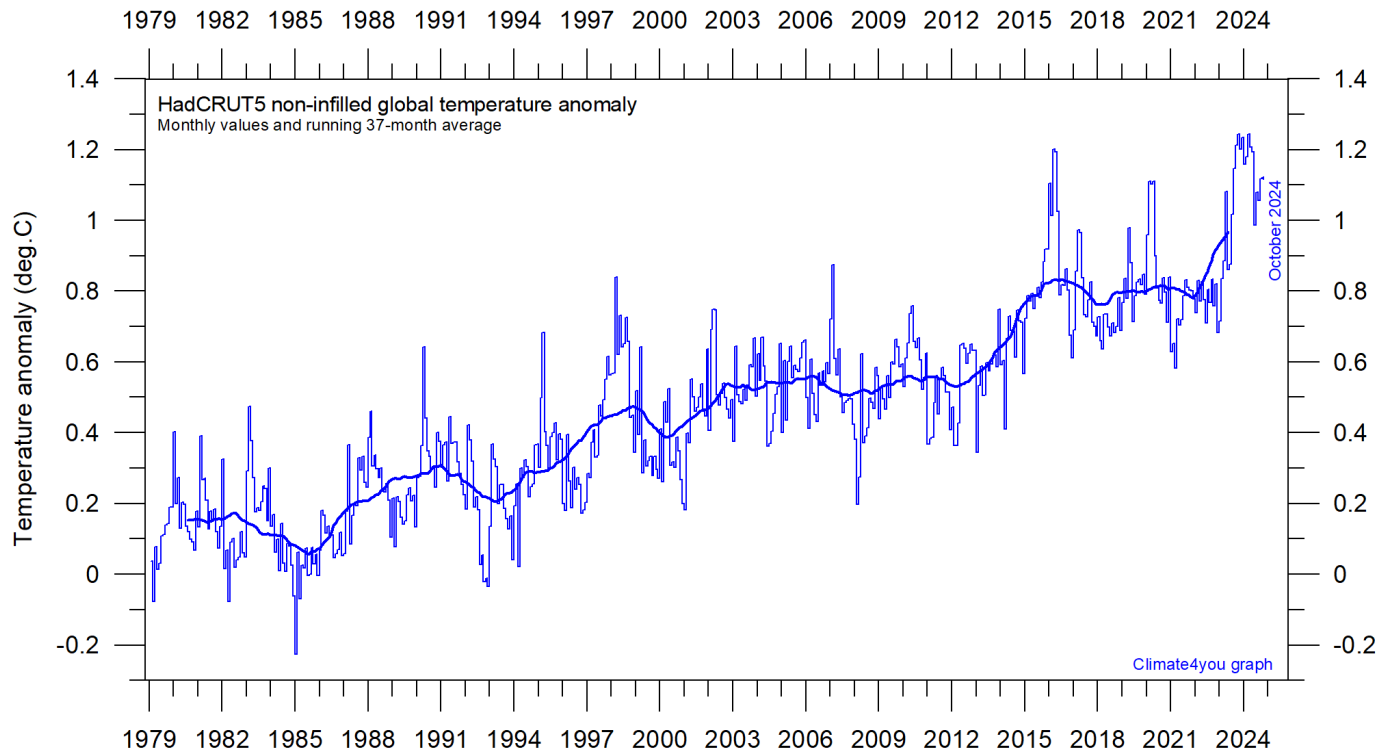
7   *Global monthly average surface air temperature (thin line) since 1979 according to the Hadley Centre for Climate Prediction and Research and the University of East Anglia's Climatic Research Unit (CRU), UK. The thick line is the simple running 37-month average.*

Temperature quality class 3: GISS and NCDC global surface air temperature, updated to November 2024
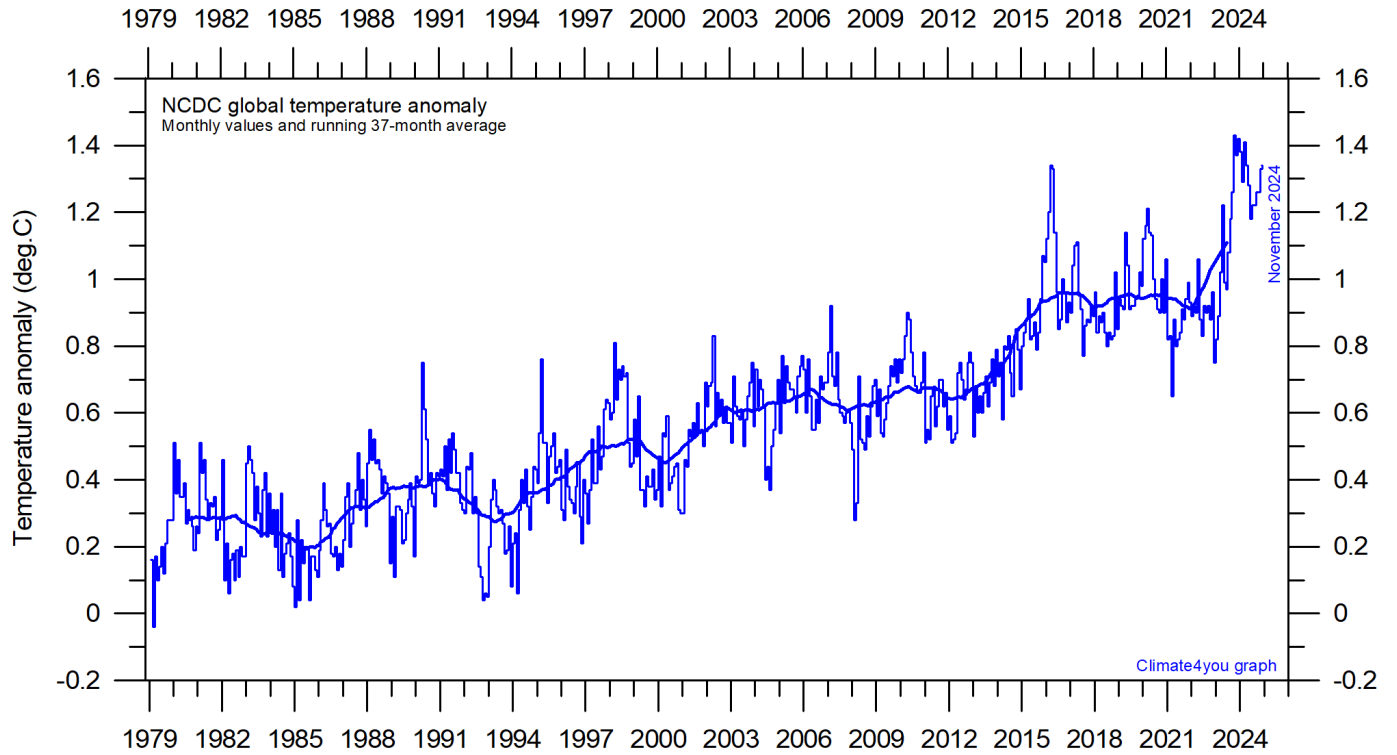
Global monthly average surface air temperature since 1979 according to according to the _National Climatic Data Center_ (NCDC), USA. The thick line is the simple running 37-month average.
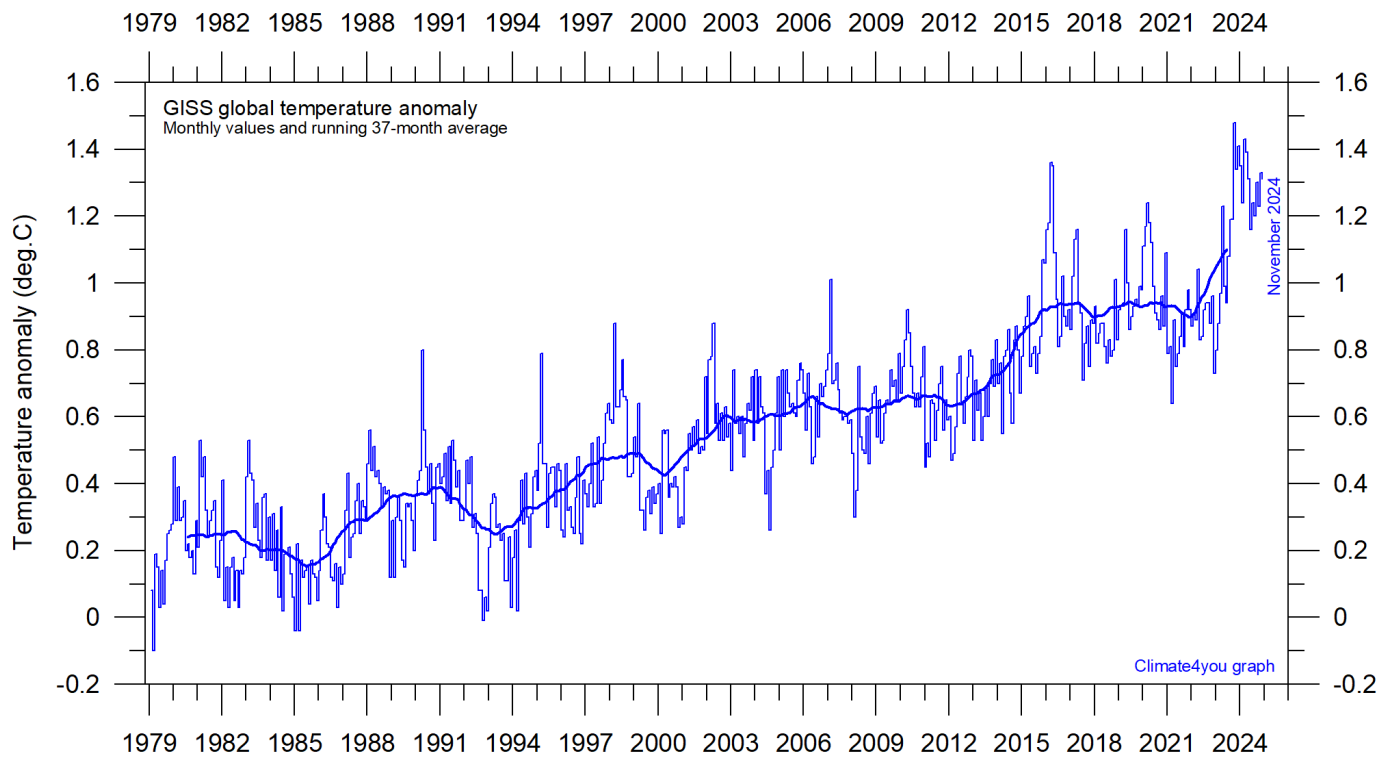
Global monthly average surface air temperature (thin line) since 1979 according to according to the _Goddard Institute for Space Studies_ (GISS), at Columbia University, New York City, USA, using ERSST_v4 ocean surface temperatures. The thick line is the simple running 37-month average.

A note on data record stability and -quality:

The temperature diagrams shown above all have 1979 as starting year. This roughly marks the beginning of the recent episode of global warming, after termination of the previous episode of global cooling from about 1940. In addition, the year 1979 also represents the starting date for the satellite-based global temperature estimates (UAH and RSS). For the three surface air temperature records (HadCRUT, NCDC and GISS), they begin much earlier (in 1850 and 1880, respectively), as can be inspected on www.climate4you.com.

For all three surface air temperature records, but especially NCDC and GISS, administrative changes to anomaly values are quite often introduced, even affecting observations many years back in time. Some changes from the recent past may be due to the delayed addition of new station data or change of station location, while others probably have their origin in changes of the technique implemented to calculate average values from the raw data. It is clearly impossible to evaluate the validity of such administrative changes for the outside user of these records; it is only possible to note that such changes quite often are introduced (se example diagram next page).

In addition, the three surface records represent a blend of sea surface data collected by moving ships or by other means, plus data from land stations of partly unknown quality and unknown degree of representativeness for their region. Many of the land stations also has been moved geographically during their period of operation, instrumentation have been changed, and they are influenced by changes in their near surroundings (vegetation, buildings, etc.). The surface network is inherently heterogeneous (dense over continents but sparse over oceans) and probably contaminated by urbanization surrounding many measurement sites.

The satellite temperature records also have their problems, but these are generally of a more technical nature and probably therefore better correctable. In addition, the temperature sampling by satellites is more regular and complete on a global basis than that represented by the surface records. It is also important that the sensors on satellites measure temperature directly by microwave radiance (thereby unobstructed by clouds), while most modern surface temperature measurements are indirect, using electronic resistance.

Everybody interested in climate science should gratefully acknowledge the big efforts put into maintaining the different temperature databases referred to in the present newsletter. At the same time, however, it is also important to realise that all temperature records cannot be of equal scientific quality. The simple fact that they to some degree differ shows that they cannot all be correct.

On this background, and for practical reasons, Climate4you therefore operates with three quality classes (1-3) for global temperature records, with 1 representing the highest quality level:

Quality class 1: The satellite records (UAH and RSS).
Quality class 2: The HadCRUT surface record.
Quality class 3: The NCDC and GISS surface records.

The main reason for discriminating between the three surface records is the following:

While both NCDC and GISS often experience quite large administrative changes (see example on p.10), and therefore essentially must be considered as unstable records, the changes introduced to HadCRUT are fewer and smaller. For obvious reasons, as the past does not change, any record undergoing continuing changes cannot describe the past correctly all the time. Frequent and large corrections in a database unavoidably signal a fundamental uncertainty about what is likely to represent the correct values.

You can find more on the issue of lack of temporal stability on www.climate4you.com (go to: *Global Temperature*, and then proceed to *Temporal Stability*).
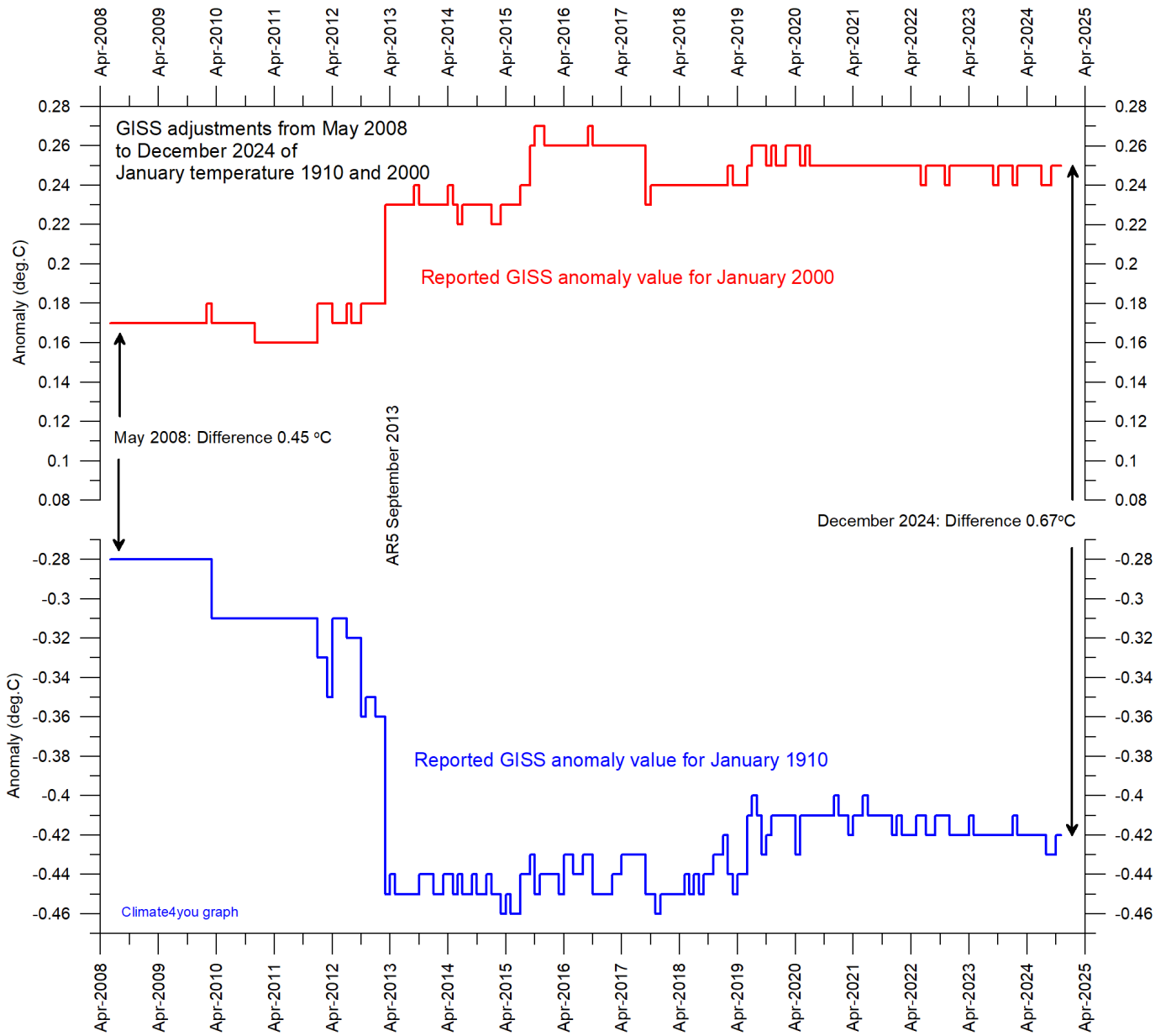
Diagram showing the monthly adjustments made since May 2008 by the Goddard Institute for Space Studies (GISS), USA, as recorded by published anomaly values for the two months January 1910 and January 2000. AR5 indicates timing of publication of IPCC report AR5 Climate Change 2013: The Physical Science Basis.

The administrative upsurge of the temperature increase from January 1915 to January 2000 has grown from 0.45°C (reported May 2008) to 0.67°C (reported December 2024). This represents an about 49% administrative temperature increase over this period, meaning that a substantial part (nearly half) of the apparent global temperature increases from January 1910 to January 2000 (as reported by GISS) is caused by administrative changes of the original data since May 2008.
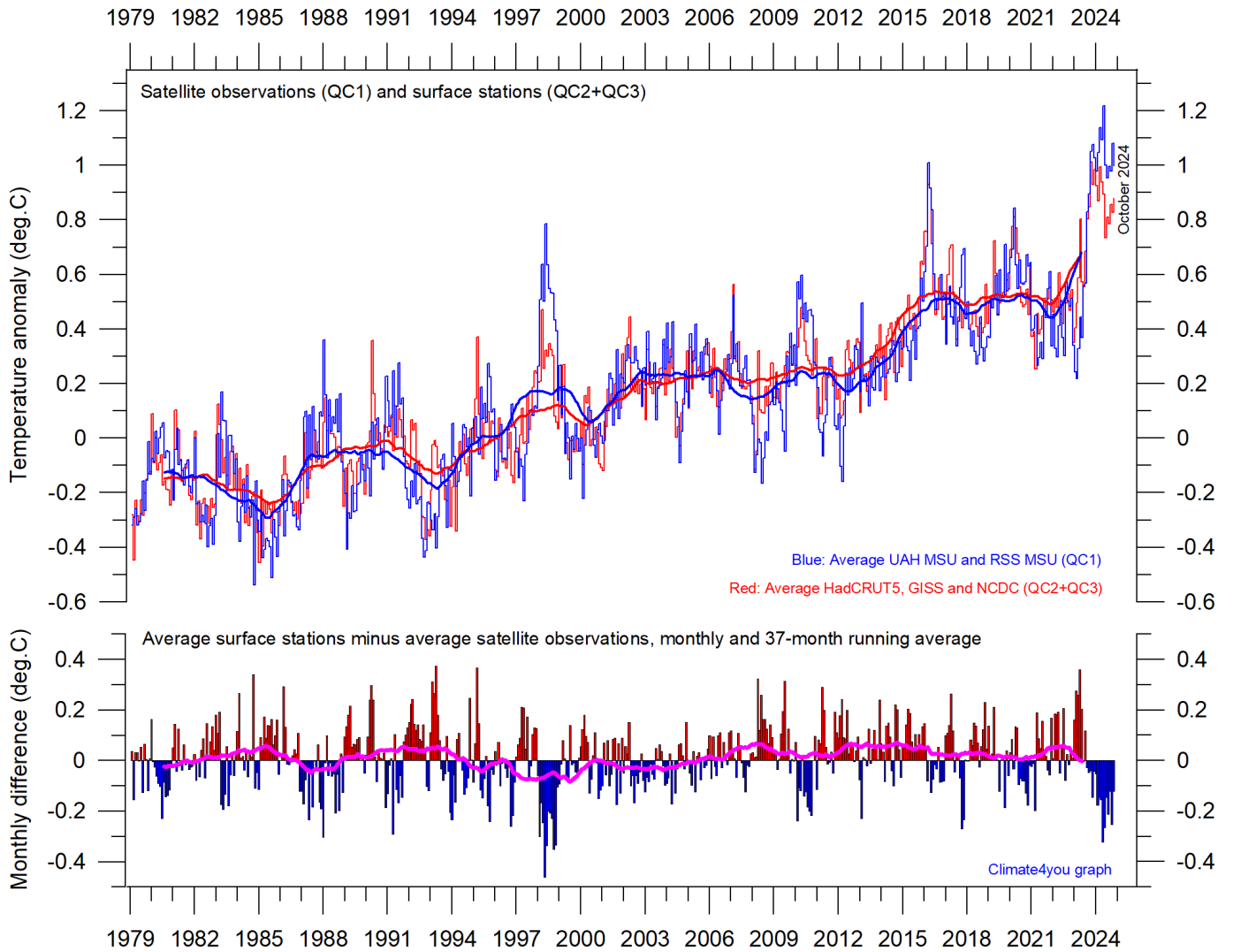
Plot showing the average of monthly global surface air temperature estimates (HadCRUT5, GISS and NCDC) and satellite-based temperature estimates (RSS MSU and UAH MSU). The thin lines indicate the monthly value, while the thick lines represent the simple running 37-month average, nearly corresponding to a running 3-yr average. The lower panel shows the monthly difference between average surface air temperature and satellite temperatures. As the base period differs for the different temperature estimates, they have all been normalised by comparing to the average value of 30 years from January 1979 to December 2008.

Global air temperature linear trends updated to October 2024
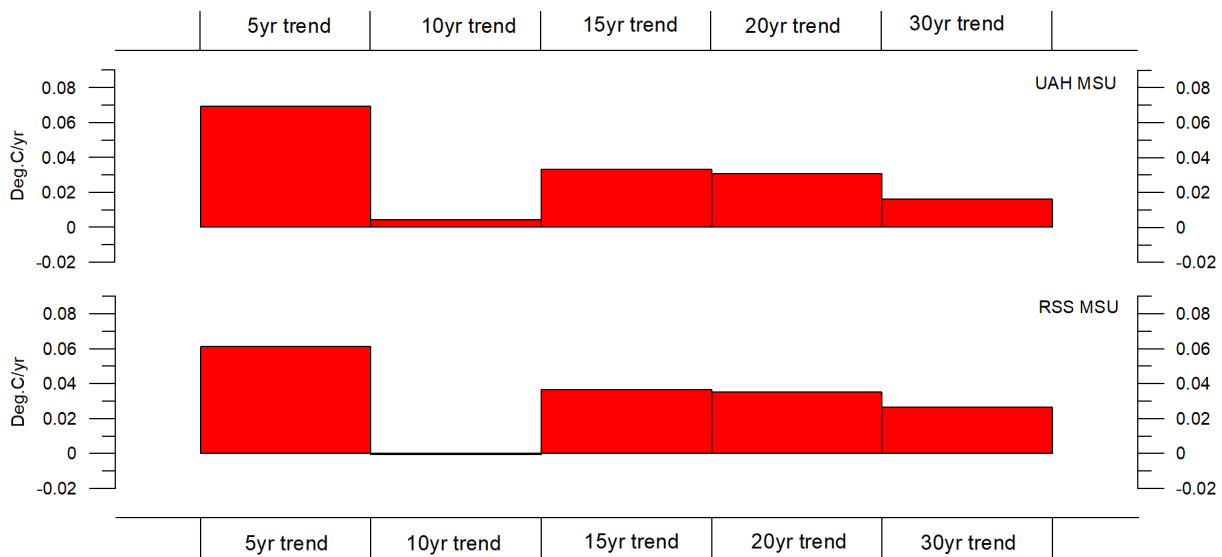
Diagram showing the latest 5, 10, 20 and 30-yr linear annual global temperature trend, calculated as the slope of the linear regression line through the data points, for two satellite-based temperature estimates (UAH MSU and RSS MSU).

Diagram showing the latest 5, 10, 20, 30, 50, 70 and 100-year linear annual global temperature trend, calculated as the slope of the linear regression line through the data points, for three surface-based temperature estimates (GISS, NCDC and HadCRUT5).

All in one, Quality Class 1, 2 and 3; updated to October 2024
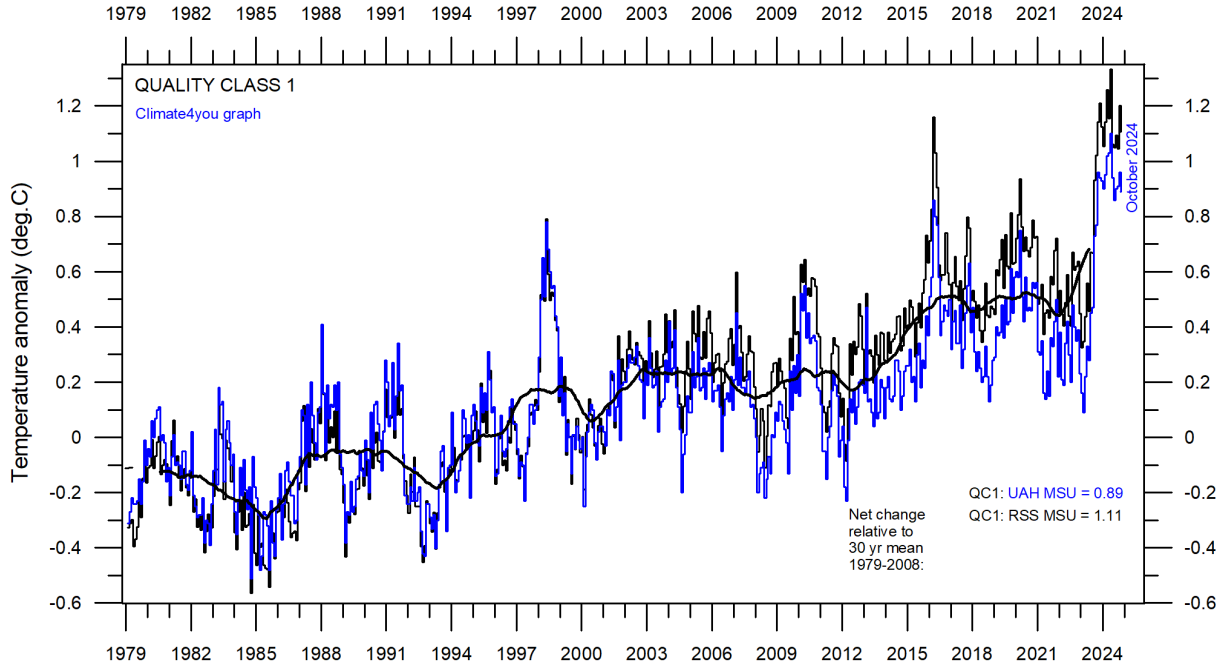
Superimposed plot of Quality Class 1 (UAH and RSS) global monthly temperature estimates. As the base period differs for the individual temperature estimates, they have all been normalised by comparing with the average value of the initial 120 months (30 years) from January 1979 to December 2008. The heavy black line represents the simple running 37 month (c. 3 year) mean of the average of both temperature records. The numbers shown in the lower right corner represent the temperature anomaly relative to the individual 1979-2008 averages.
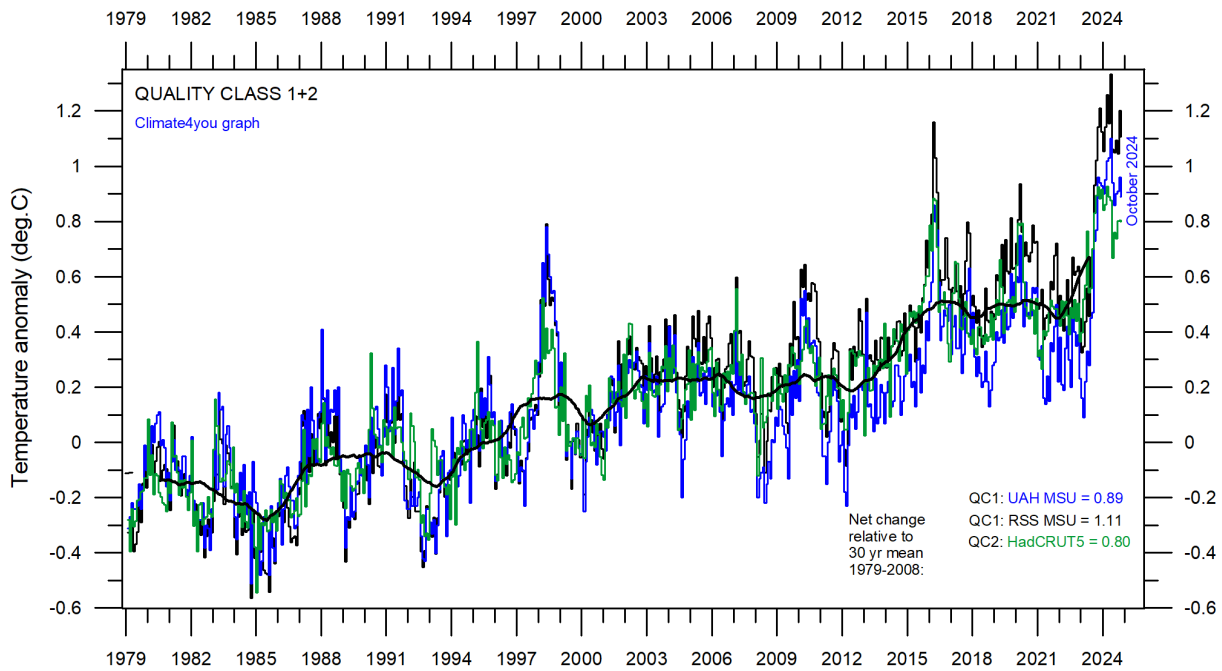
Superimposed plot of Quality Class 1 and 2 (UAH, RSS and HadCRUT) global monthly temperature estimates. As the base period differs for the individual temperature estimates, they have all been normalised by comparing with the average value of the initial 120 months (30 years) from January 1979 to December 2008. The heavy black line represents the simple running 37 month (c. 3 year) mean of the average of all three temperature records. The numbers shown in the lower right corner represent the temperature anomaly relative to the individual 1979-2008 averages.
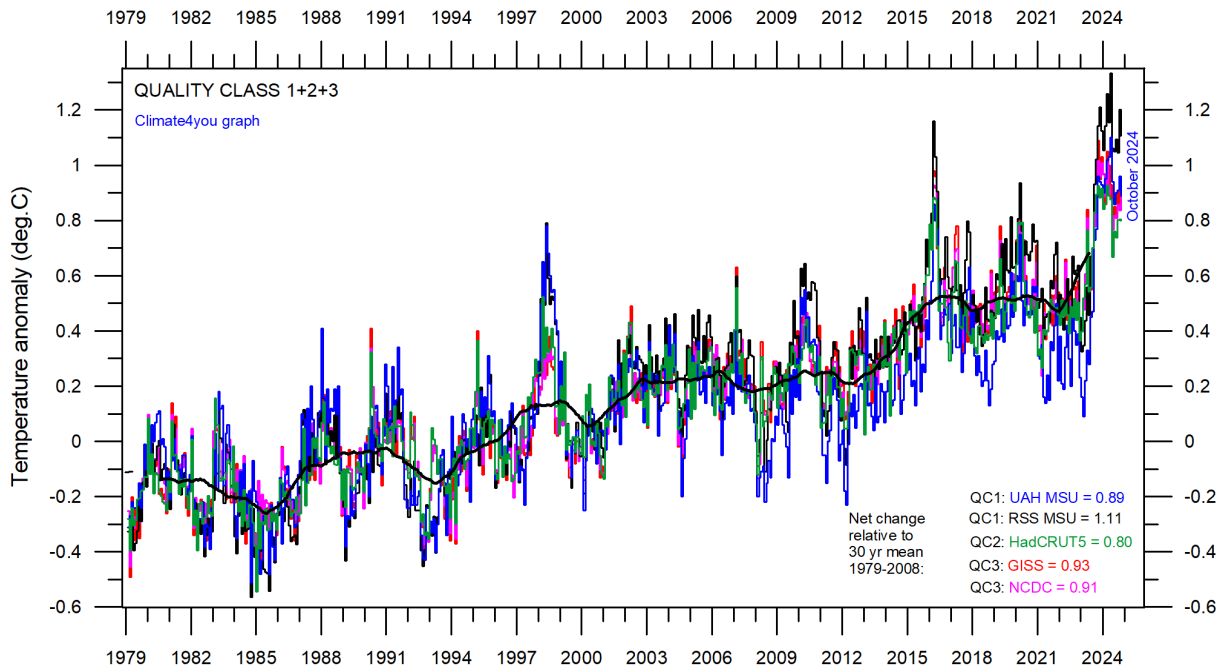
Superimposed plot of Quality Class 1, 2 and 3 global monthly temperature estimates (UAH, RSS, HadCRUT, GISS and NCDC). As the base period differs for the individual temperature estimates, they have all been normalised by comparing with the average value of the initial 120 months (30 years) from January 1979 to December 2008. The heavy black line represents the simple running 37 month (c. 3 year) mean of the average of all five temperature records. The numbers shown in the lower right corner represent the temperature anomaly relative to the individual 1979-2008 averages.

14   *Please see reflections on page 9 relating to the above three quality classes.*

Satellite- and surface-based temperature estimates are derived from different types of measurements and comparing them directly as in the above diagrams therefore may be somewhat ambiguous.

However, as both types of estimates often are discussed together in various news media, the above composite diagrams may nevertheless be of some interest.

In fact, the different types of temperature estimates appear to agree as to the overall temperature variations on a 2-3-year scale, although on a shorter time scale there are often considerable differences between the individual records. However, since about 2003 the surface records used to be drifting towards higher temperatures than the combined satellite record, but this overall tendency was much removed by the major adjustment of the RSS satellite series in 2015 (see lower diagram on page 6).

The combined records (diagram above) suggest a modest global air temperature increase over the last 40 years, about 0.2°C per decade. It should be noted that the apparent temperature increases since about 2003 at least partly is the result of ongoing administrative adjustments (page 9-10). At the same time, none of the temperature records considered here indicates any overall temperature decrease during the last 20 years.

The present temperature development does not exclude the possibility that global temperatures may begin to increase significantly later. On the other hand, it also remains a possibility that Earth just now is passing an overall temperature peak, and that global temperatures may begin to decrease during the coming 5-10 years.

As always, time will show which of these possibilities is correct.

Global sea surface temperature, updated to November 2024
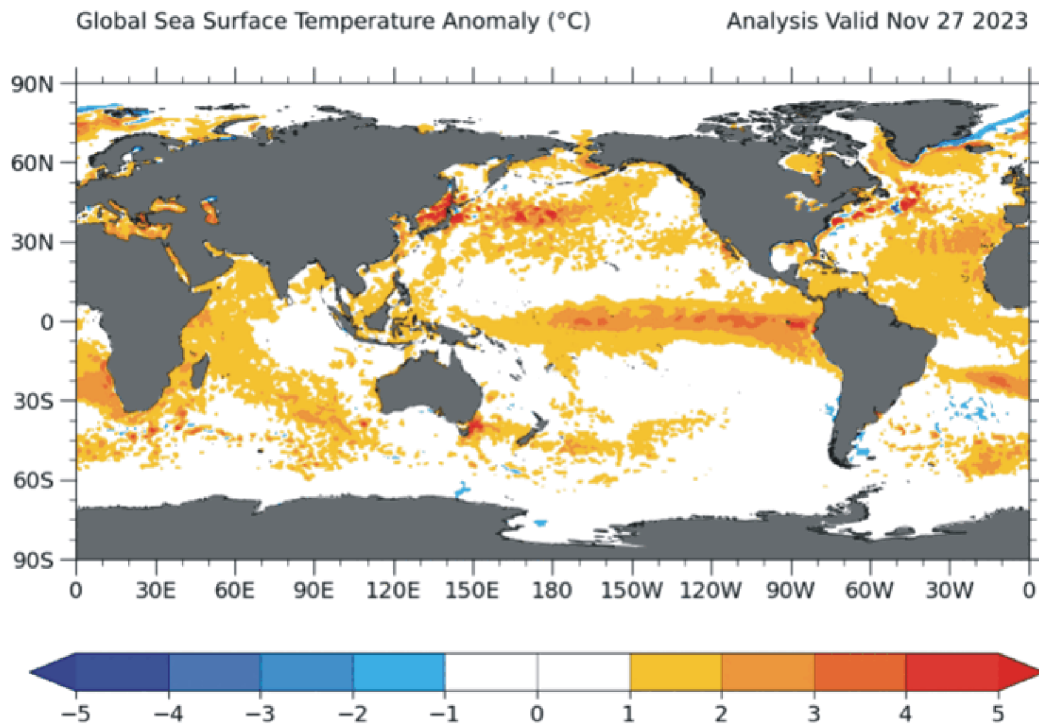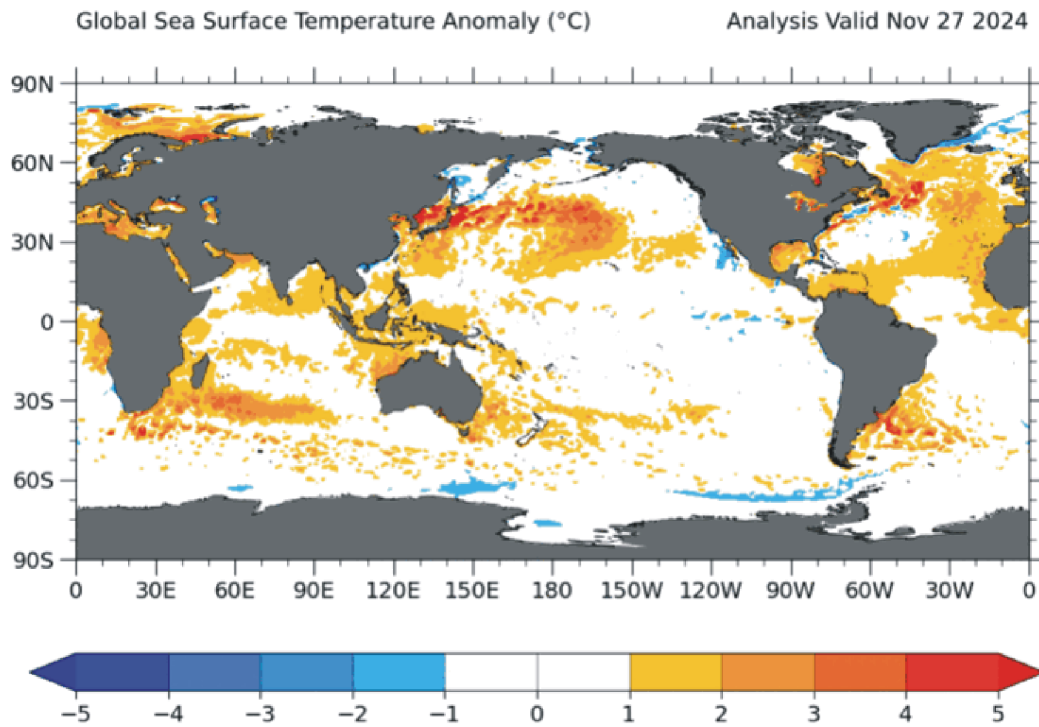
Sea surface temperature anomaly on 27 November 2024 (upper map) and 2023 (lower map). Map source: Plymouth State Weather Center. Reference period: 1977-1991.

Because of the large surface areas near Equator, the temperature of the surface water in these regions is especially important for the global atmospheric temperature (p. 6-8). In fact, 50% of planet Earth's surface area is located within 30ºN and 30ºS.

A mixture of relatively warm and cold water presently dominates much of the global ocean surface, but with notable variations from month to month. All such ocean surface temperature changes will be influencing global air temperatures in the months to come. A cold La Niña episode (Pacific Ocean) has recently ended and was followed by a warm (now also ended) El Niño episode (maps p.15 and diagram p.25).

The significance of short-term cooling or warming reflected in air temperatures should never be overstated. Whenever Earth experiences cold La Niña or warm El Niño episodes major heat exchanges take place between the Pacific Ocean and the atmosphere above, sooner or later showing up in estimates of the global air temperature.

However, this does not necessarily reflect similar changes in the total heat content of the atmosphere-ocean system. In fact, global net changes can be small and such heat exchanges may mainly reflect redistribution of energy between ocean and atmosphere. What matters is the overall temperature development when seen over several years.
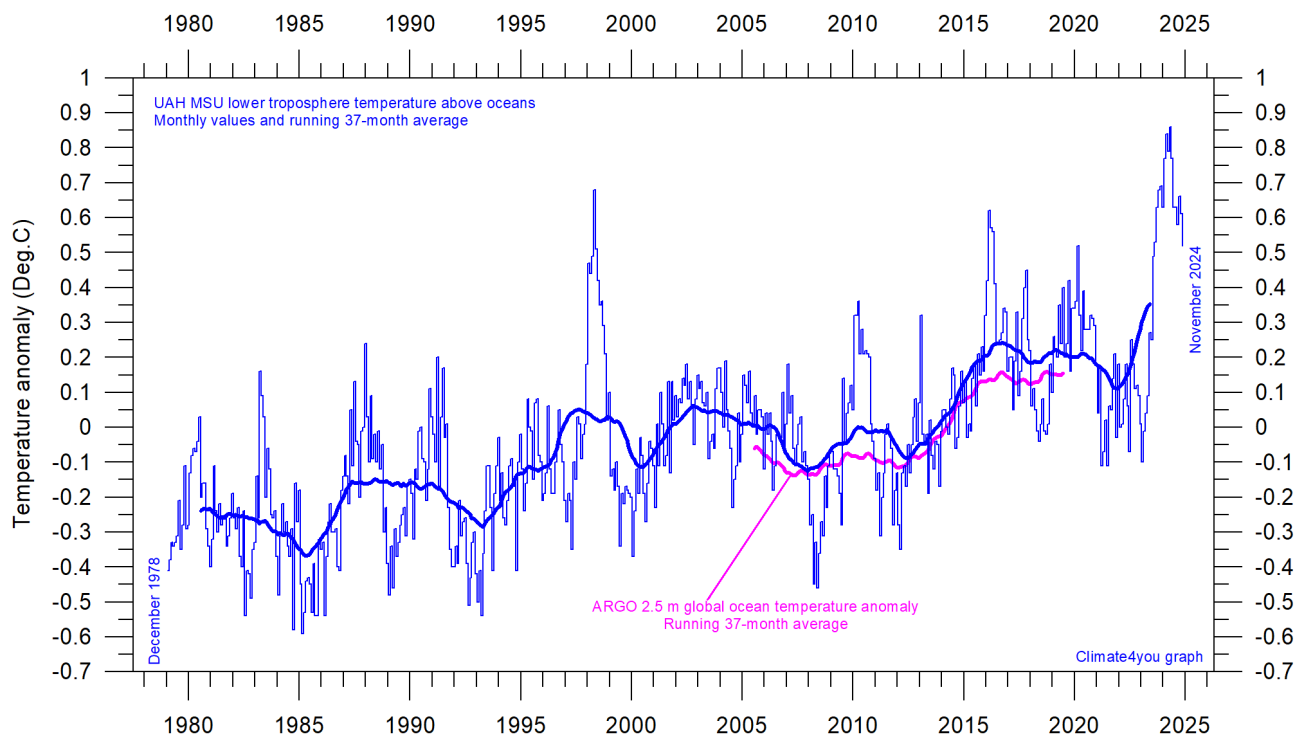
Global monthly average lower troposphere temperature over oceans (thin line) since 1979 according to University of Alabama at Huntsville, USA. The thick line is the simple running 37-month average. Insert: Argo global ocean temperature anomaly from floats, displaced vertically to make visual comparison easier. UAH reference period: 1991-2020.
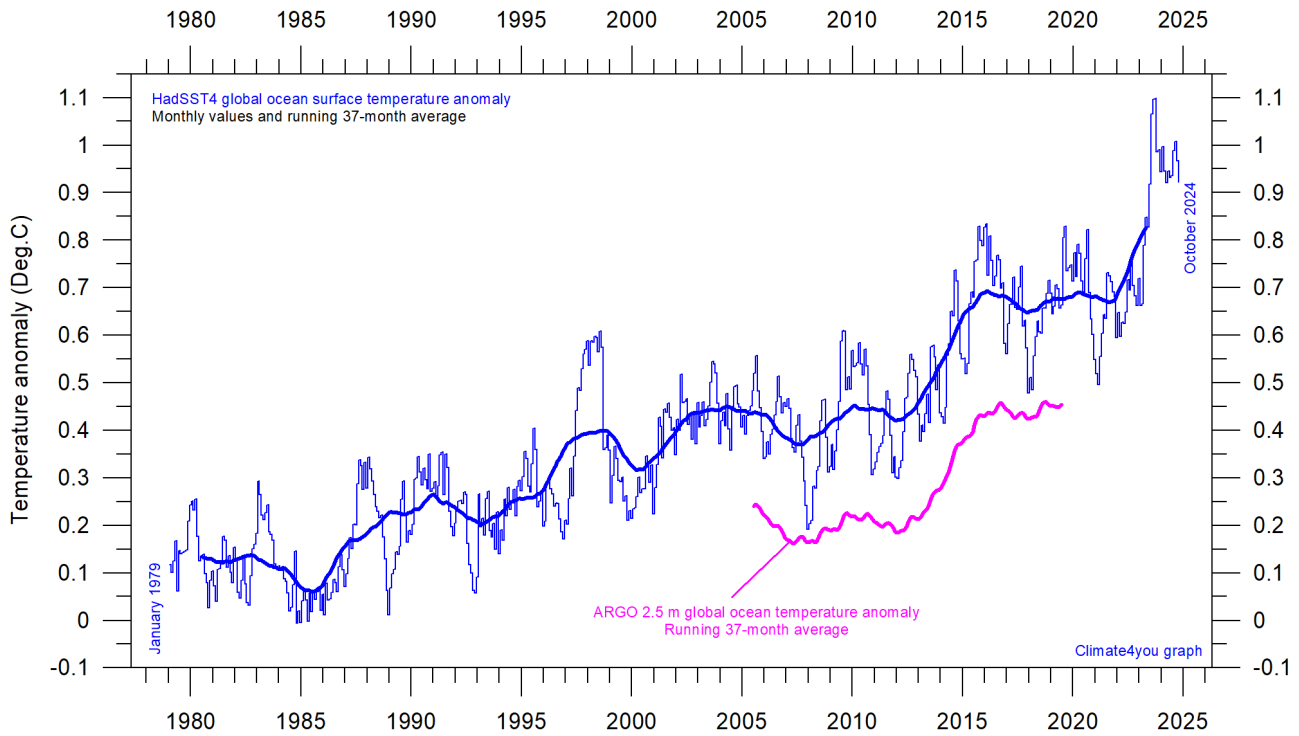
Global monthly average sea surface temperature since 1979 according to University of East Anglia's [Climatic Research Unit](#) ([CRU](#)), UK. Base period: 1961-1990. The thick line is the simple running 37-month average. Insert: Argo global ocean temperature anomaly from floats, displaced vertically to make visual comparison easier.
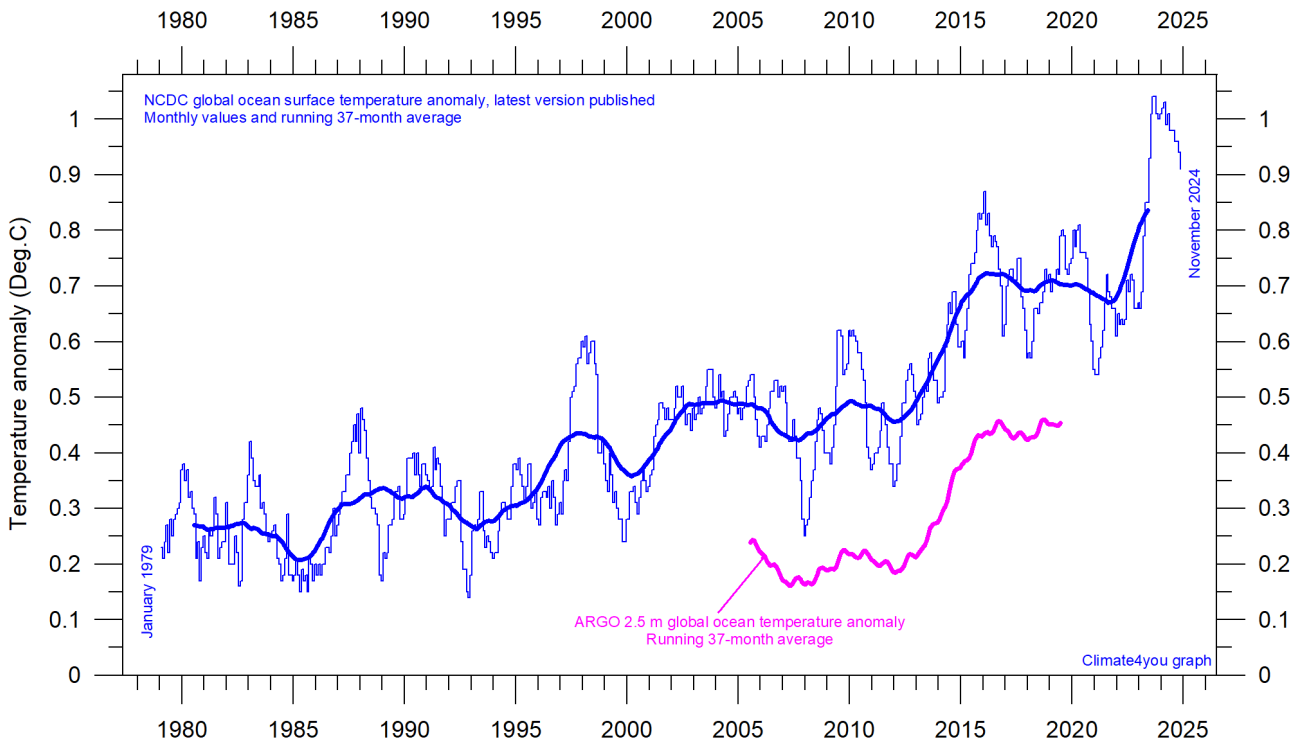
Global monthly average sea surface temperature since 1979 according to the [National Climatic Data Center](#) (NCDC), USA. Base period: 1901-2000. The thick line is the simple running 37-month average. Insert: Argo global ocean temperature anomaly from floats, displaced vertically to make visual comparison easier.

Ocean temperature in uppermost 100 m, updated to June 2024

World Oceans, vertical mean temperature anomaly 0-100 m depth; NODC, NOAA
3-month and running 39-month average, base period 1955-2010

January-March 1955

April-June 2024

Climate4you graph
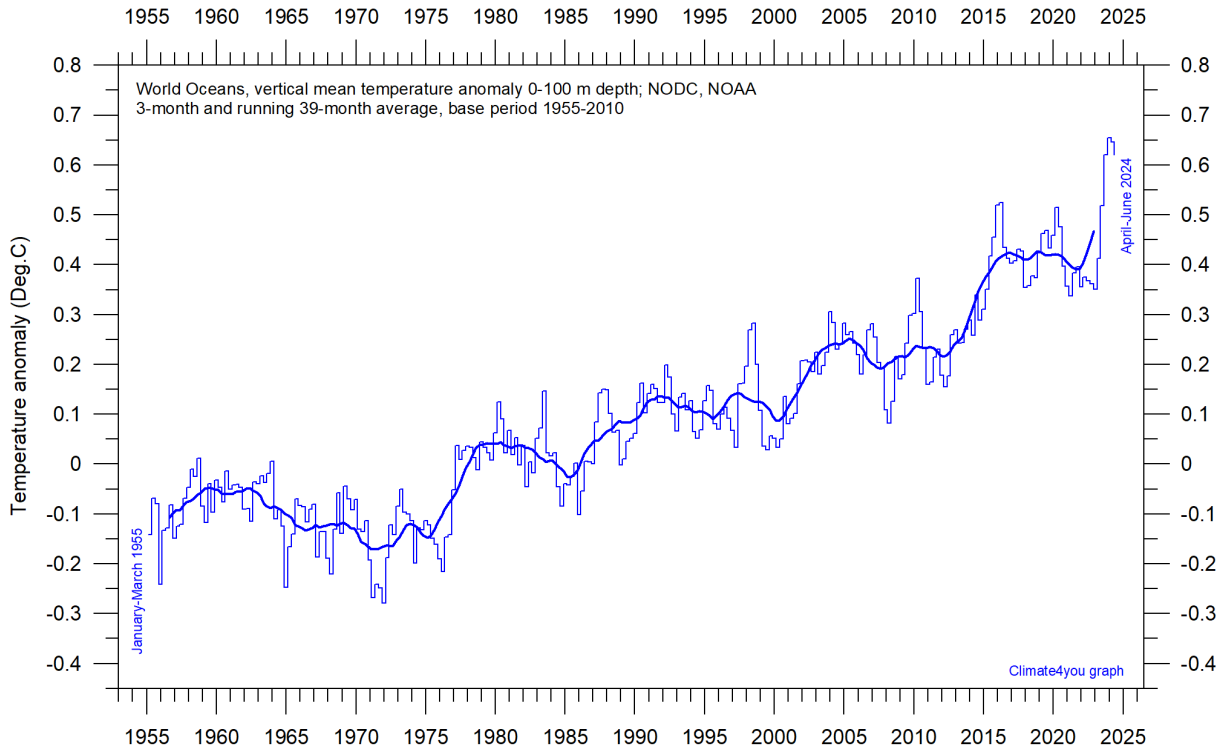
World Oceans vertical average temperature 0-100 m depth since 1955. The thin line indicates 3-month values, and the thick line represents the simple running 39-month (c. 3 year) average. Data source: NOAA National Oceanographic Data Center (NODC). Base period 1955-2010.

18
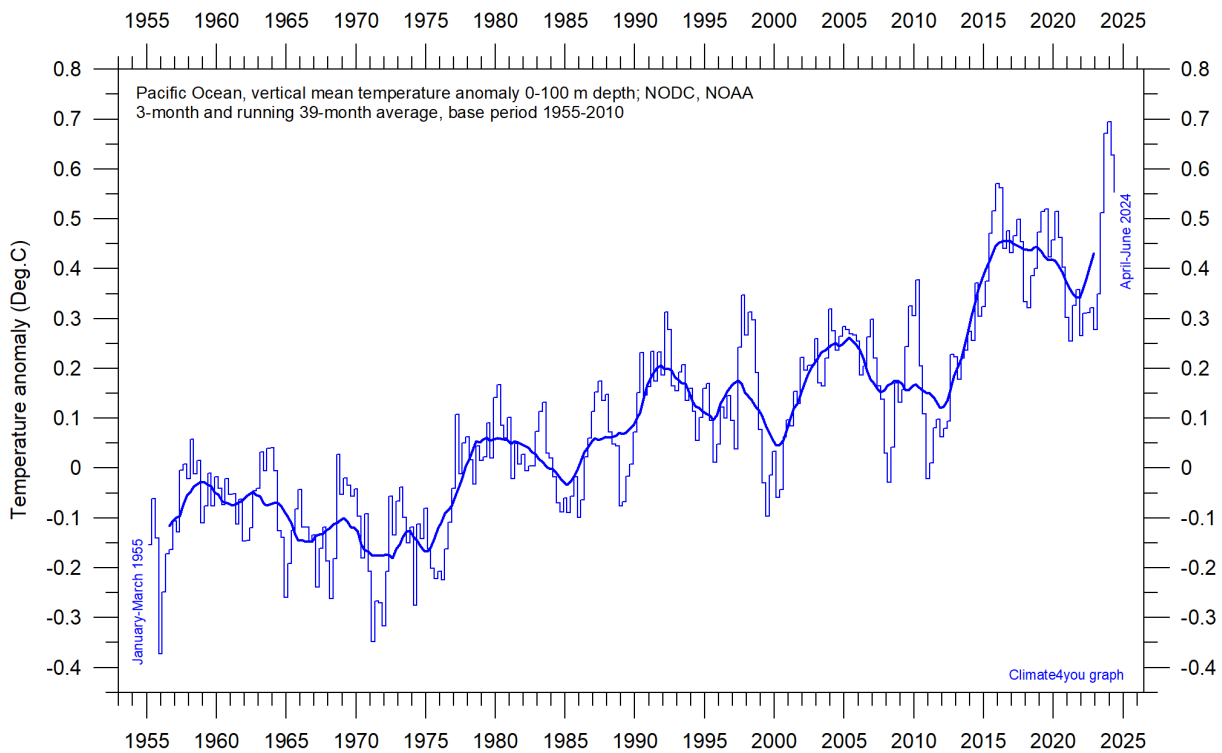
Pacific Ocean, vertical mean temperature anomaly 0-100 m depth; NODC, NOAA
3-month and running 39-month average, base period 1955-2010

January-March 1955

April-June 2024

Climate4you graph

Pacific Ocean vertical average temperature 0-100 m depth since 1955. The thin line indicates 3-month values, and the thick line represents the simple running 39-month (c. 3 year) average. Data source: NOAA National Oceanographic Data Center (NODC). Base period 1955-2010.
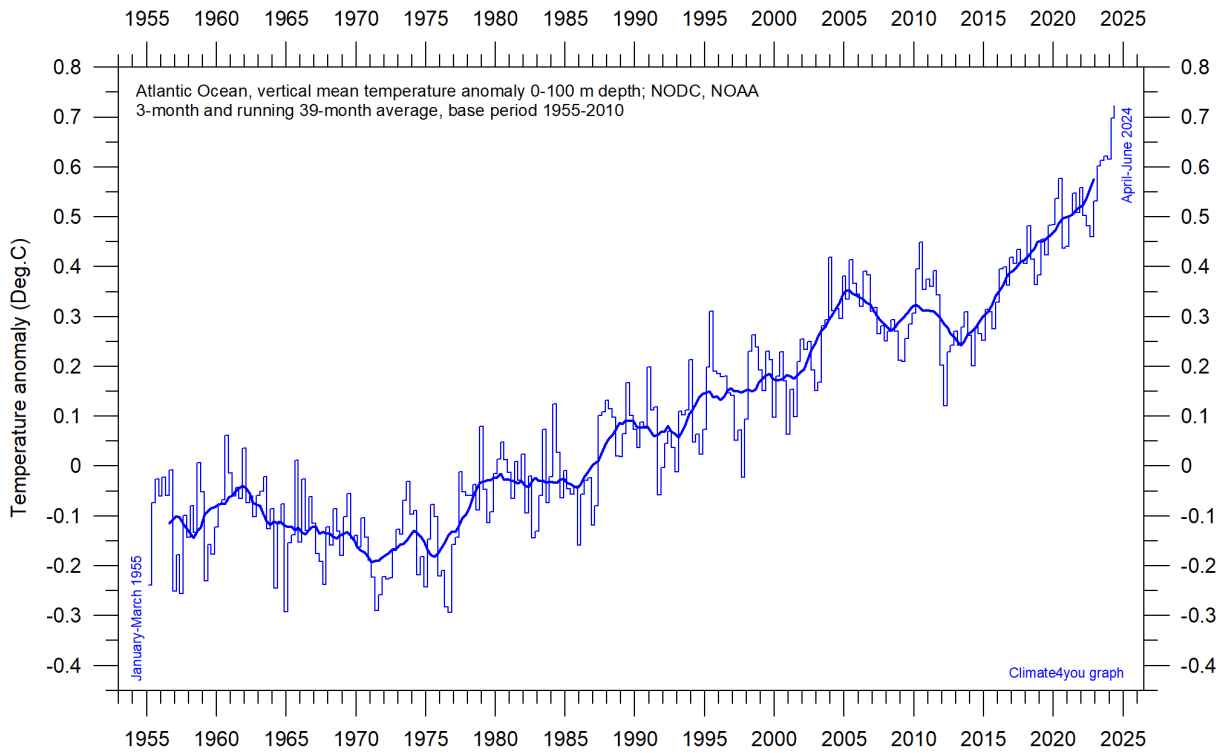
Atlantic Ocean vertical average temperature 0-100 m depth since 1955. The thin line indicates 3-month values, and the thick line represents the simple running 39-month (c. 3 year) average. Data source: NOAA National Oceanographic Data Center (NODC). Base period 1955-2010.

Indian Ocean vertical average temperature 0-100 m depth since 1955. The thin line indicates 3-month values, and the thick line represents the simple running 39-month (c. 3 year) average. Data source: NOAA National Oceanographic Data Center (NODC). Base period 1955-2010.

Pacific Decadal Oscillation (PDO), updated to November 2024

Monthly values of the Pacific Decadal Oscillation (PDO) since January 1979. The PDO is a long-lived El Niño-like pattern of Pacific climate variability, a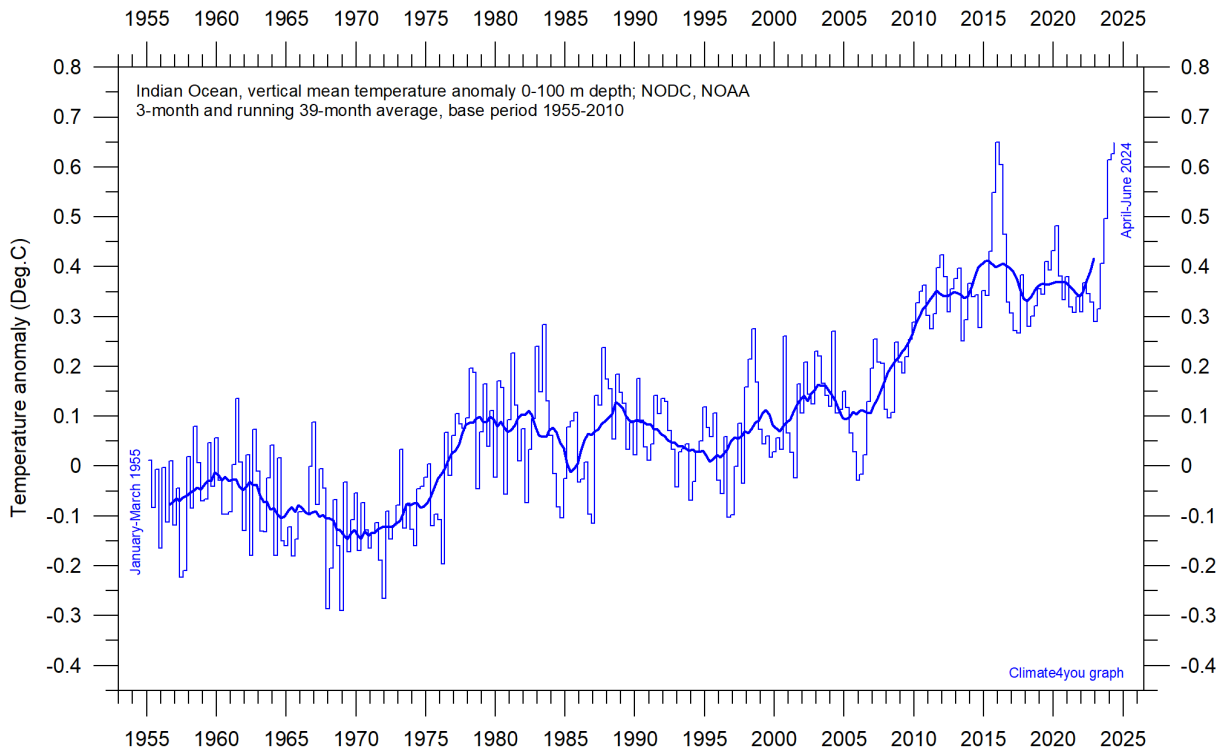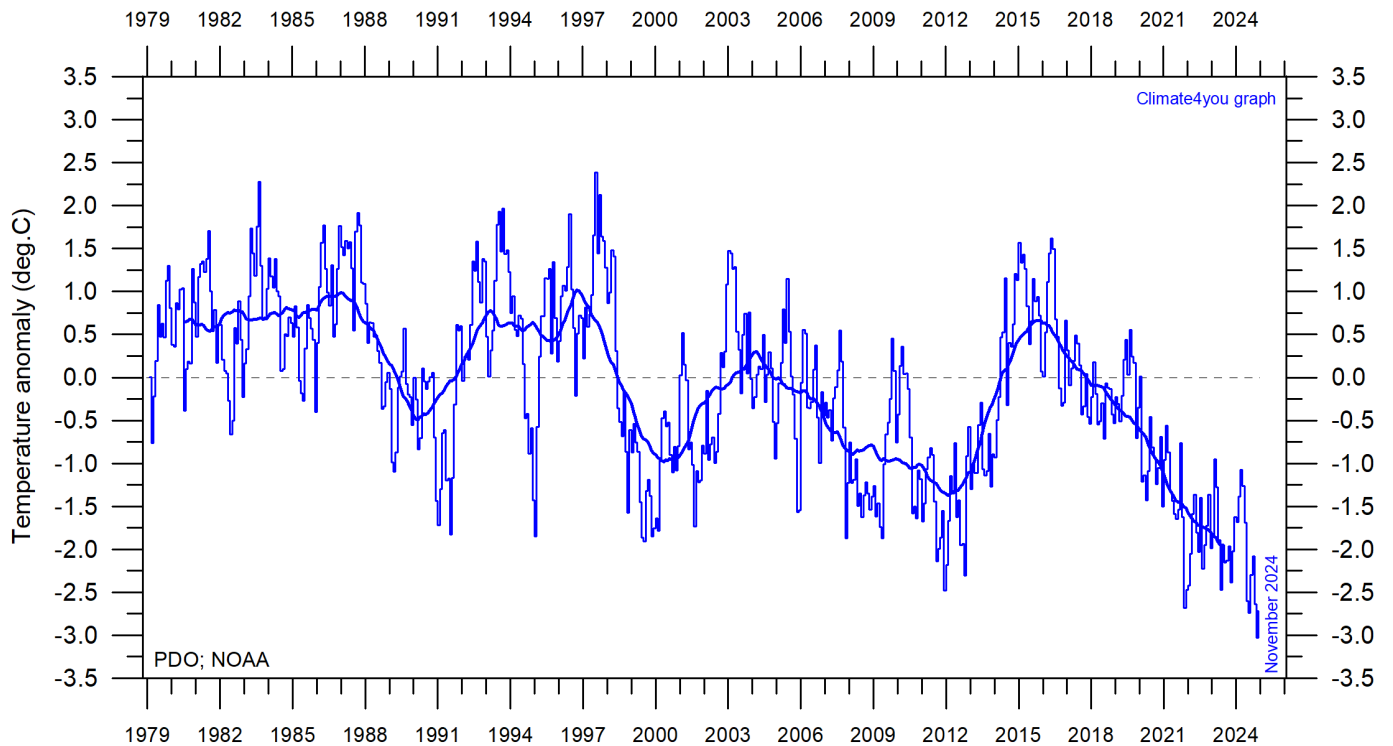nd the data series goes back to January 1854. Base period: 1982-2002. The thin line indicates monthly PDO values, and the thick line is the simple running 37-month average. Data source: NOAA Physical Science Laboratory (version PDO ERSST V5 plotted above).

The PDO is a long-lived El Niño-like pattern of Pacific climate variability, with data extending back to January 1854. Causes for PDO are not currently known, but even in the absence of a theoretical understanding, PDO climate information improves season-to-season and year-to-year climate forecasts for North America because of its strong tendency for multi-season and multi-year persistence. The PDO also appears to be roughly in phase with global temperature changes. Thus, from a societal impact's perspective, recognition of PDO is important because it shows that "normal" climate conditions can vary over time periods comparable to the length of a human's lifetime.

The PDO illustrates how global temperatures are tied to sea surface temperatures in the Pacific Ocean, the largest ocean on Earth. When sea surface temperatures are relatively low (negative phase PDO), as it was from 1945 to 1977, global air temperature often decreases. When Pacific Ocean surface temperatures are high (positive phase PDO), as from 1977 to 1998, global surface air temperature often increases.

A Fourier frequency analysis (not shown here) shows the PDO record to be influenced by a significant 5.6-year cycle, and feasibly also by a longer 18.6-year long period, corresponding to the length of the lunar nodal tide.

North Atlantic heat content uppermost 700 m, updated to June 2021
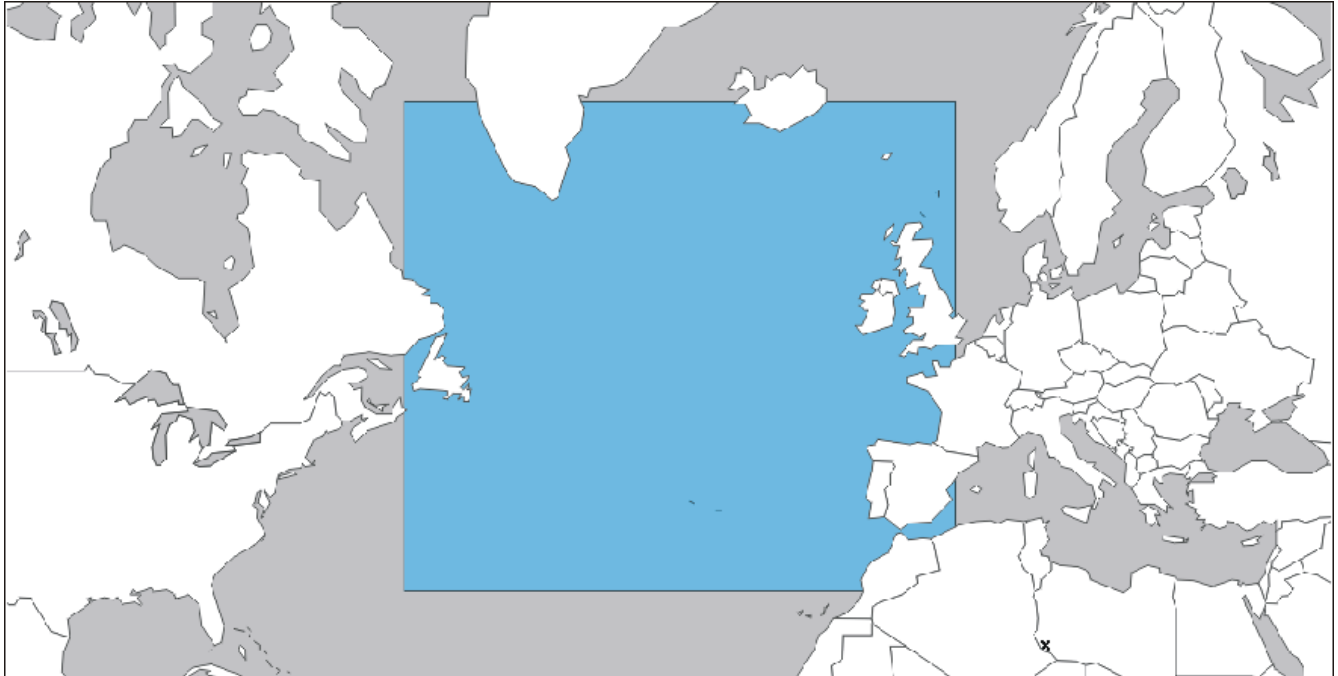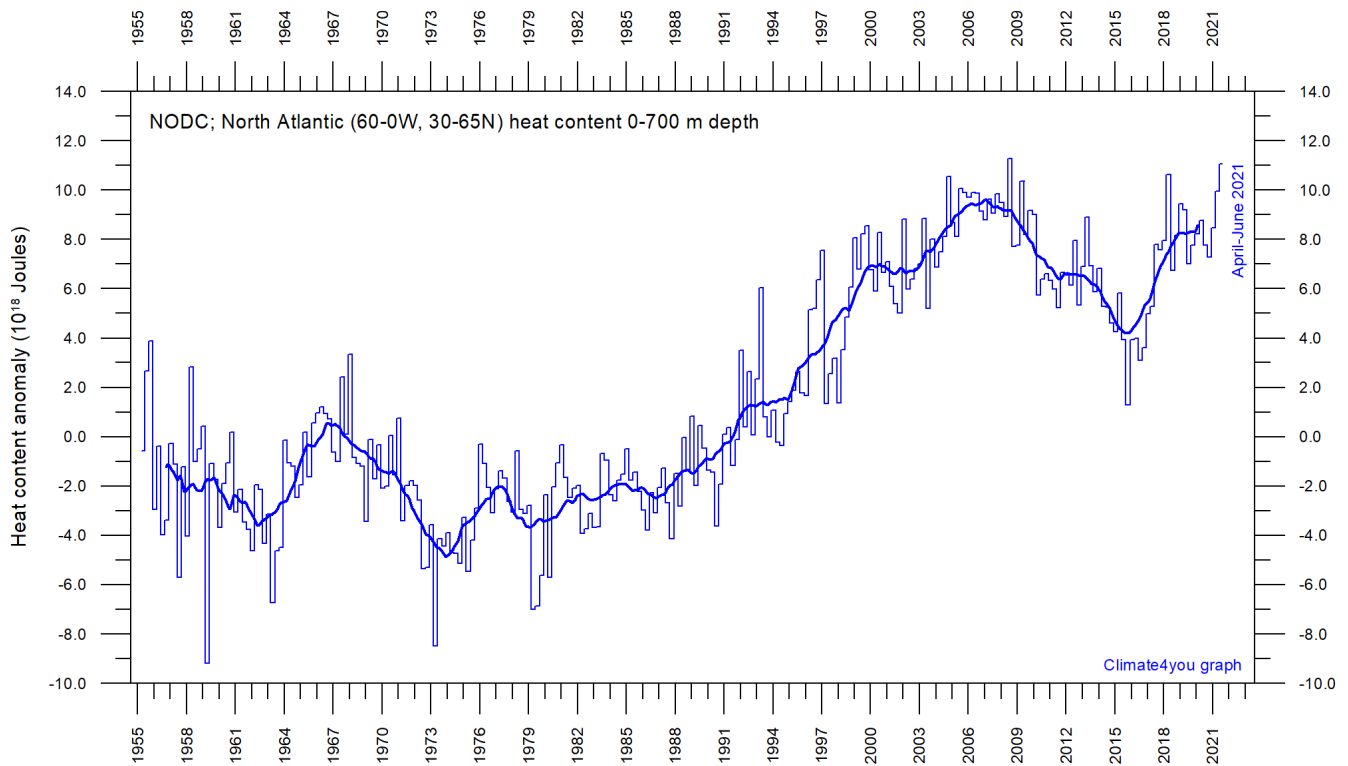
Global monthly heat content anomaly (10^{18} Joules) in the uppermost 700 m of the North Atlantic (60-0W, 30-65N; see map above) *ocean since January 1955. The thin line indicates monthly values, and the thick line represents the simple running 37-month (c. 3 year) average. Data source: National Oceanographic Data Center (NODC).*

North Atlantic temperatures 0-800 m depth along 59⁰N, 30-0W, updated to December 2021
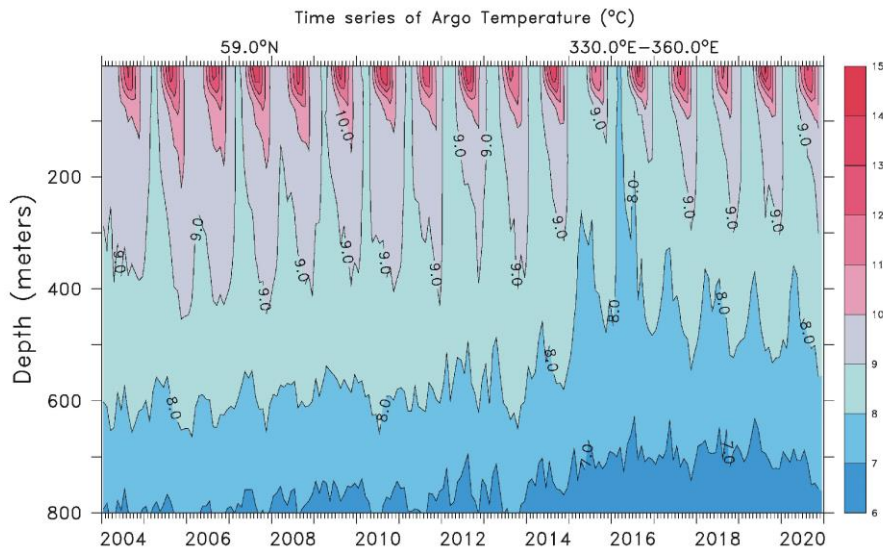
Time series depth-temperature diagram along 59 N across the North Atlantic Current from 30°W to 0°W, from surface to 800 m depth. Source: Global Marine Argo Atlas. See also the diagram below.
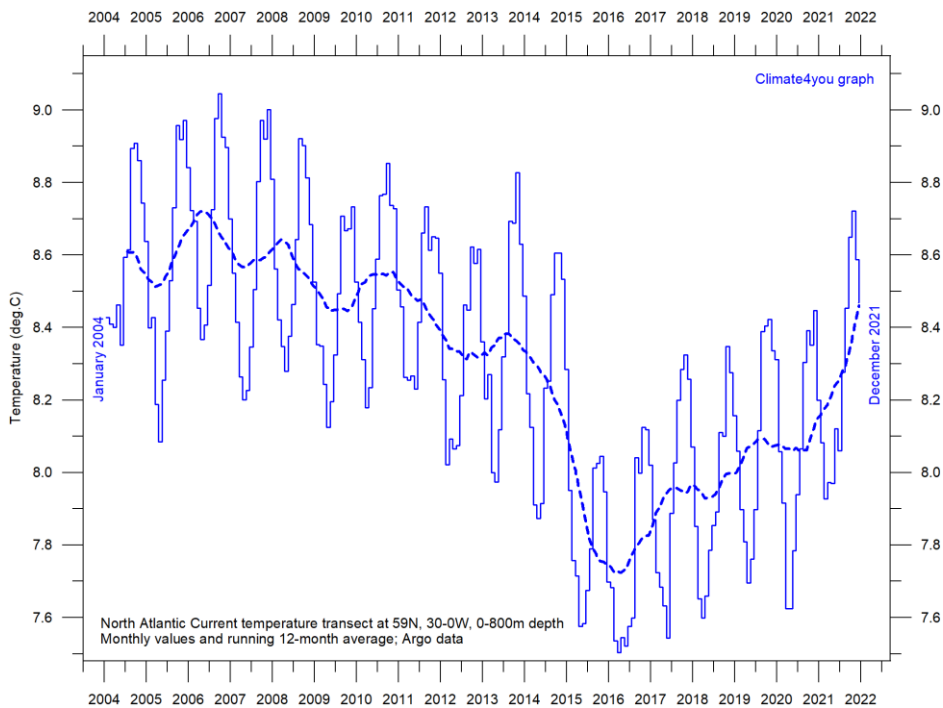
Average temperature along 59 N, 30-0W, 0-800m depth, corresponding to the main part of the North Atlantic Current, using Argo-data. Source: Global Marine Argo Atlas. Additional information can be found in: Roemmich, D. and J. Gilson, 2009. The 2004-2008 mean and annual cycle of temperature, salinity, and steric height in the global ocean from the Argo Program. Progress in Oceanography, 82, 81-100.

Global ocean temperature 0-1900 m depth summary, updated to December 2021
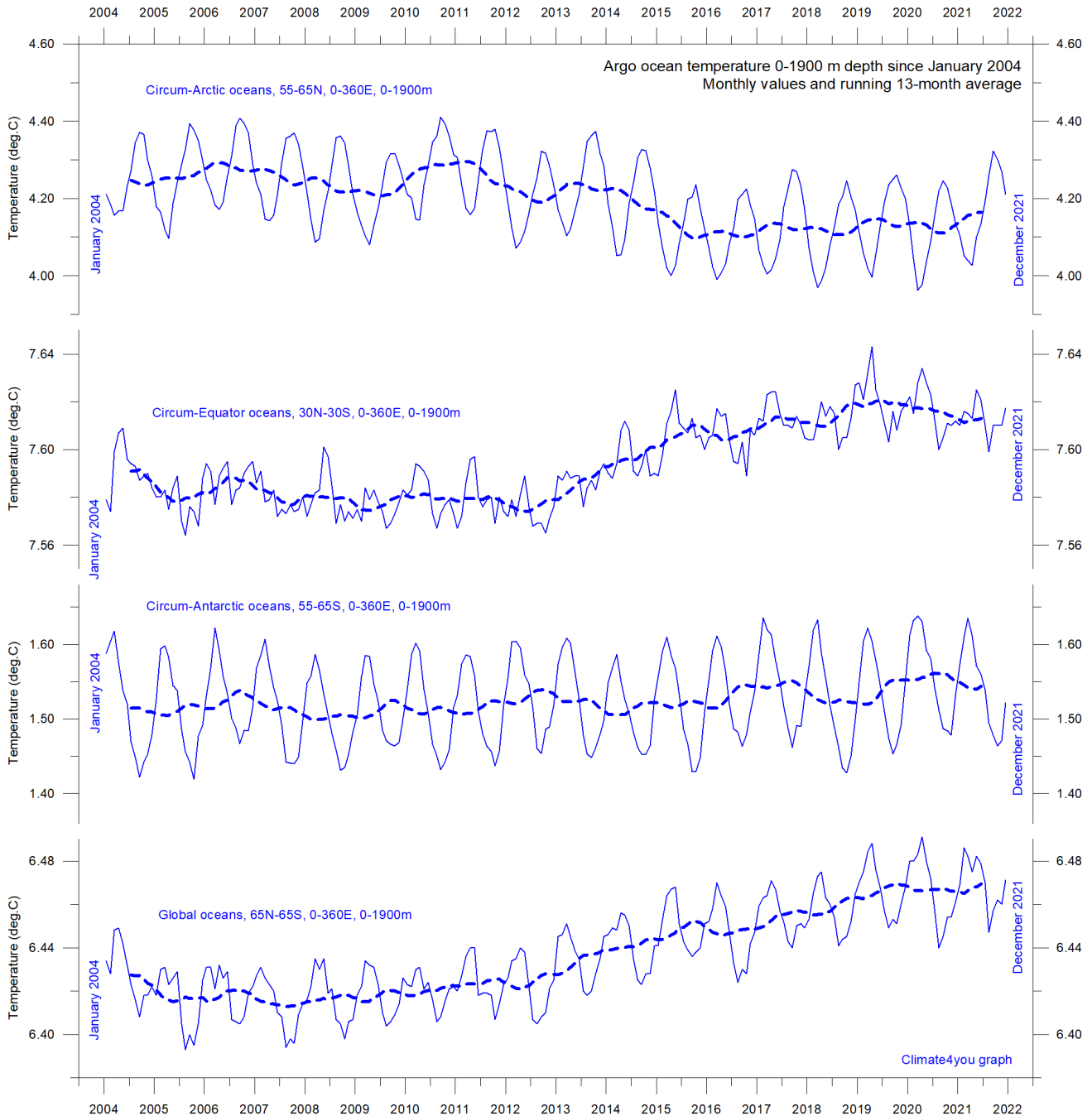
Summary of average temperature in uppermost 1900 m in different parts of the global oceans, using Argo-data. Source: Global Marine Argo Atlas. Additional information can be found in: Roemmich, D. and J. Gilson, 2009. The 2004-2008 mean and annual cycle of temperature, salinity, and steric height in the global ocean from the Argo Program. Progress in Oceanography, 82, 81-100.

The temperature of the global oceans down to 1900 m depth has been increasing since about 2011, but with a possible peak around 2020. The global increase since 2013 is mainly due to changes occurring near the Equator, between 30°N and 30°S. In contrast, for the circum-Arctic oceans north of 55°N, depth-integrated ocean temperatures have been decreasing since 2011, but with a possible low around 2019. Near the Antarctic, south of 55°S, temperatures have essentially been stable. At most latitudes, a clear annual rhythm is evident.

Global ocean net temperature change since 2004 at different depths, updated to December 2020
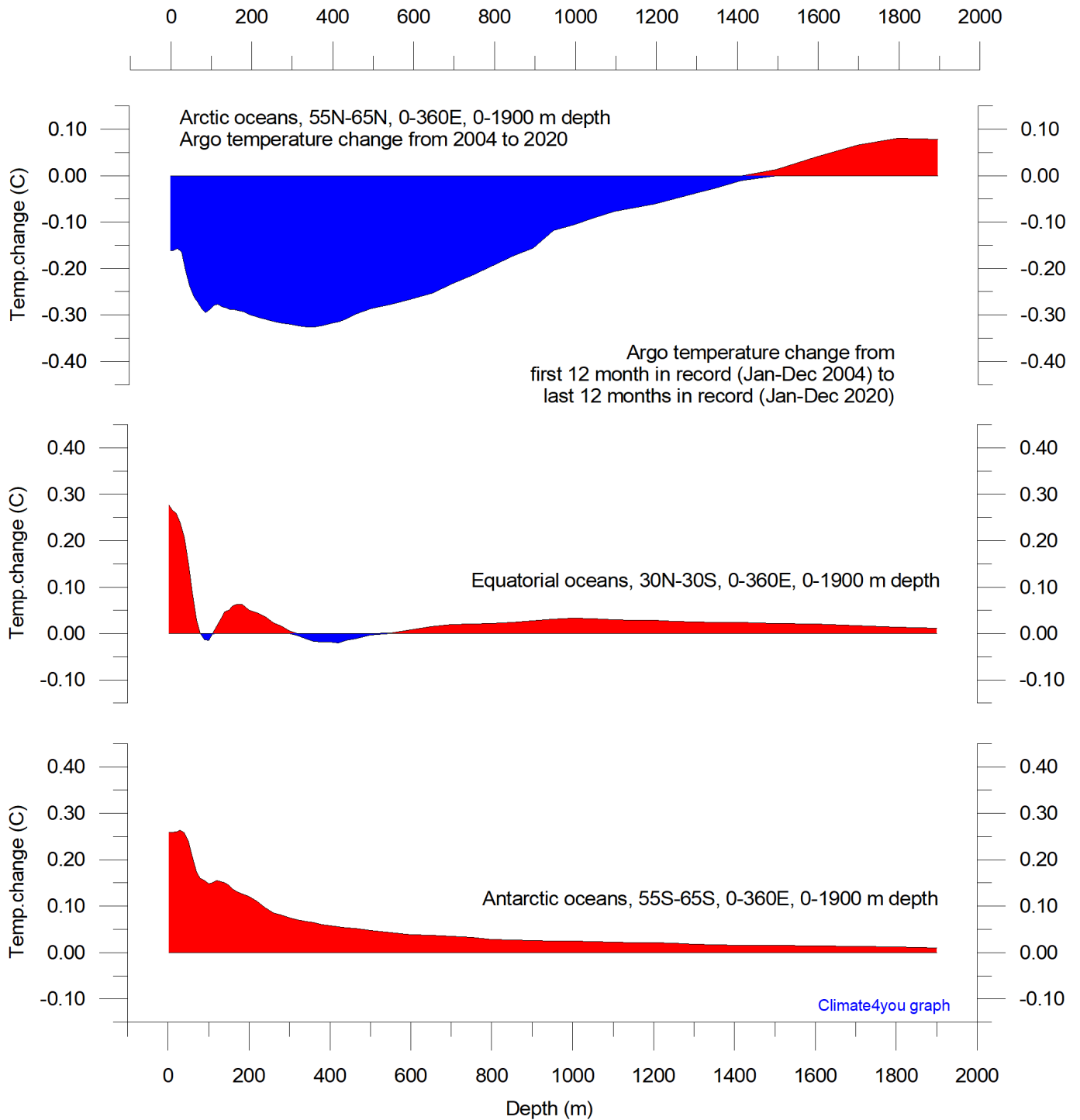
Net temperature change since 2004 from surface to 1900 m depth in different parts of the global oceans, using *Argo*-data. Source: *Global Marine Argo Atlas*. Additional information can be found in: Roemmich, D. and J. Gilson, 2009. The 2004-2008 mean and annual cycle of temperature, salinity, and steric height in the global ocean from the Argo Program. *Progress in Oceanography*, 82, 81-100. Please note that due to the spherical form of Earth, northern and southern latitudes represent only small ocean volumes, compared to latitudes near the Equator.

La Niña and El Niño episodes, Oceanic Niño Index (ONI), updated to November 2024
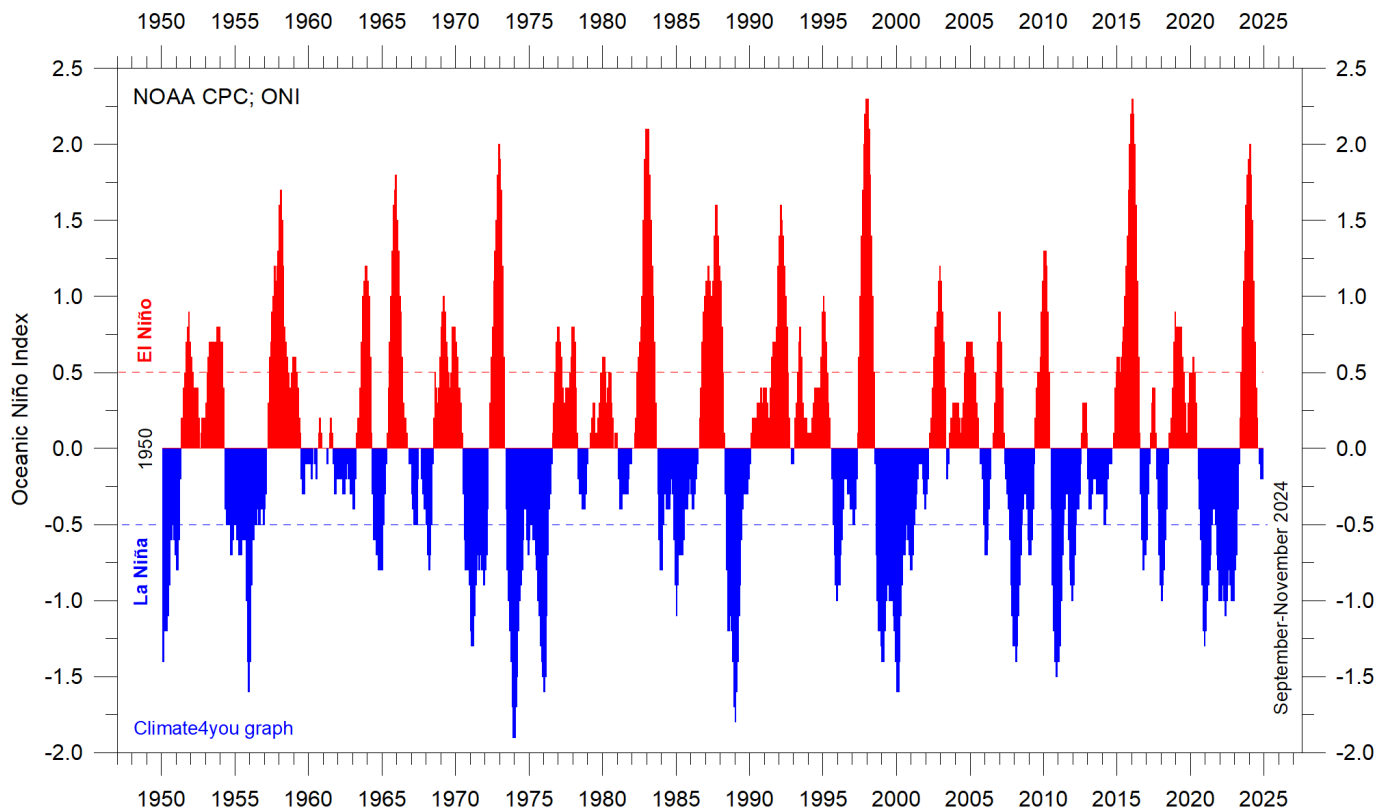
Warm (>+0.5ºC) and cold (<0.5ºC) episodes for the Oceanic Niño Index (ONI), defined as 3 month running mean of ERSSTv4 SST anomalies in the Niño 3.4 region (5ºN-5ºS, 120º-170ºW)]. For historical purposes cold and warm episodes are defined when the threshold is met for a minimum of 5 consecutive over-lapping seasons. Anomalies are centred on 30-yr base periods updated every 5 years.

In the Pacific Ocean, trade winds usually blow west along the equator, pushing warm water from South America towards Asia. To replace that warm water, cold water rises from the depths near South America. During El Niño episodes, trade winds weaken, and warm water is spreading back east, toward South America. In contrast, during La Niña episodes, trade winds are stronger than usual, pushing more warm water than usual toward Asia, and upwelling of cold water near South America therefore increases.

The 2015-16 El Niño episode is among the strongest since the beginning of the record in 1950. Considering the entire record, however, recent variations between El Niño and La Niña episodes do not appear abnormal in any way.

A Fourier frequency analysis (not shown here) shows the ONI record to be influenced by a significant 3.6-year cycle, and feasibly also by a longer 5.6-year cycle.

Zonal lower troposphere temperatures from satellites, updated to November 2024
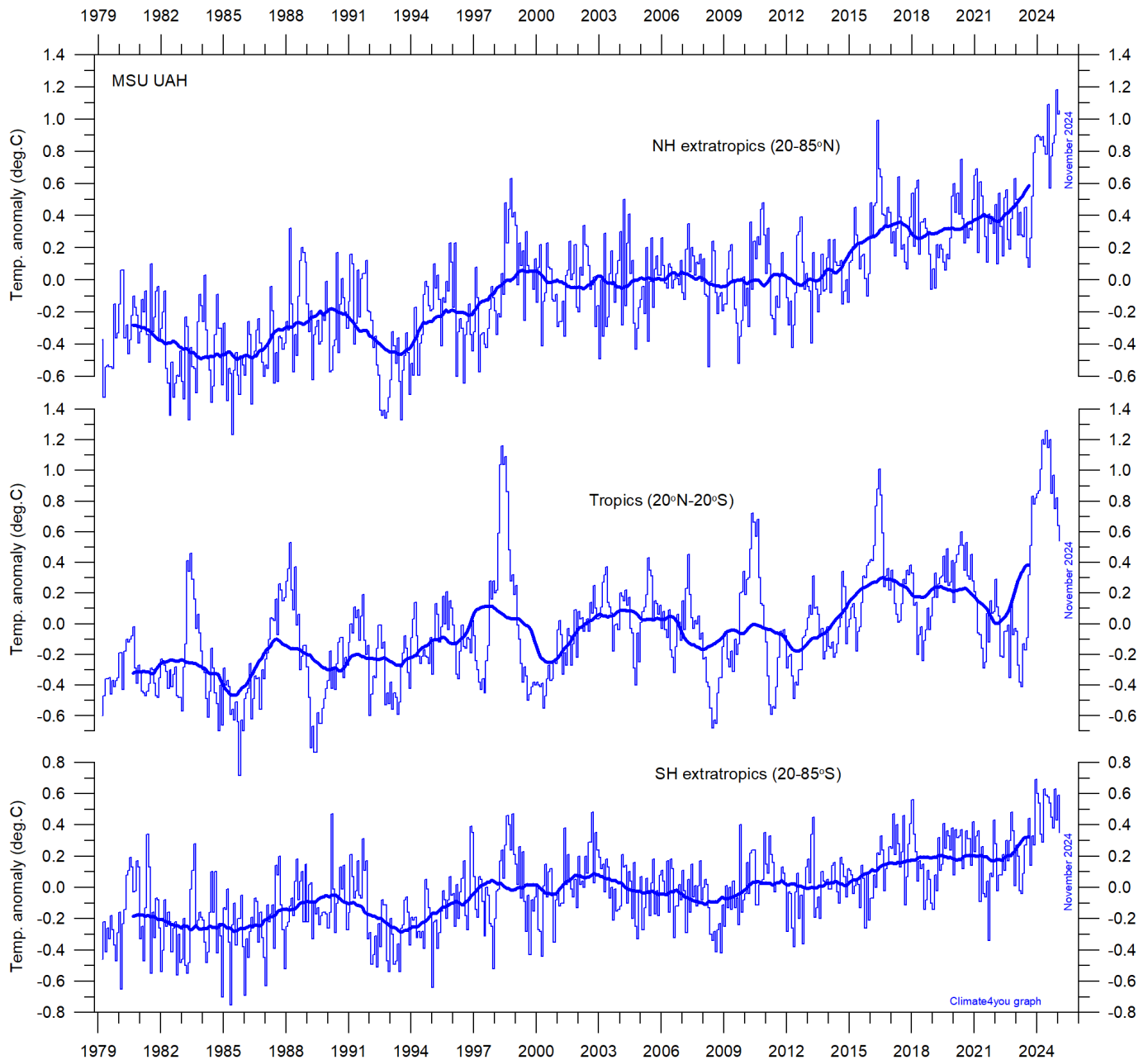
Global monthly average lower troposphere temperature since 1979 for the tropics and the northern and southern extratropics, according to University of Alabama at Huntsville, USA. Thin lines show the monthly temperature. Thick lines represent the simple running 37-month average, nearly corresponding to a running 3-year average. Reference period 1981-2010.

The overall warming since 1980 has dominantly been a northern hemisphere phenomenon, and mainly played out as a marked change between 1994 and 1999. However, this rather rapid temperature change is probably influenced by the Mt. Pinatubo eruption 1992-93 and the subsequent 1997 El Niño episode. The diagram also shows the temperature effects of the strong Equatorial El Niño's in 1997 and 2015-16, as well as the moderate El Niño in 2019. Apparently, these effects were spreading to higher latitudes in both hemispheres with some delay. Recently, a new El Niño was playing out in the Pacific Ocean (p.25), as is clearly shown by tropics surface air temperatures.

Arctic and Antarctic lower troposphere temperature, updated to November 2024
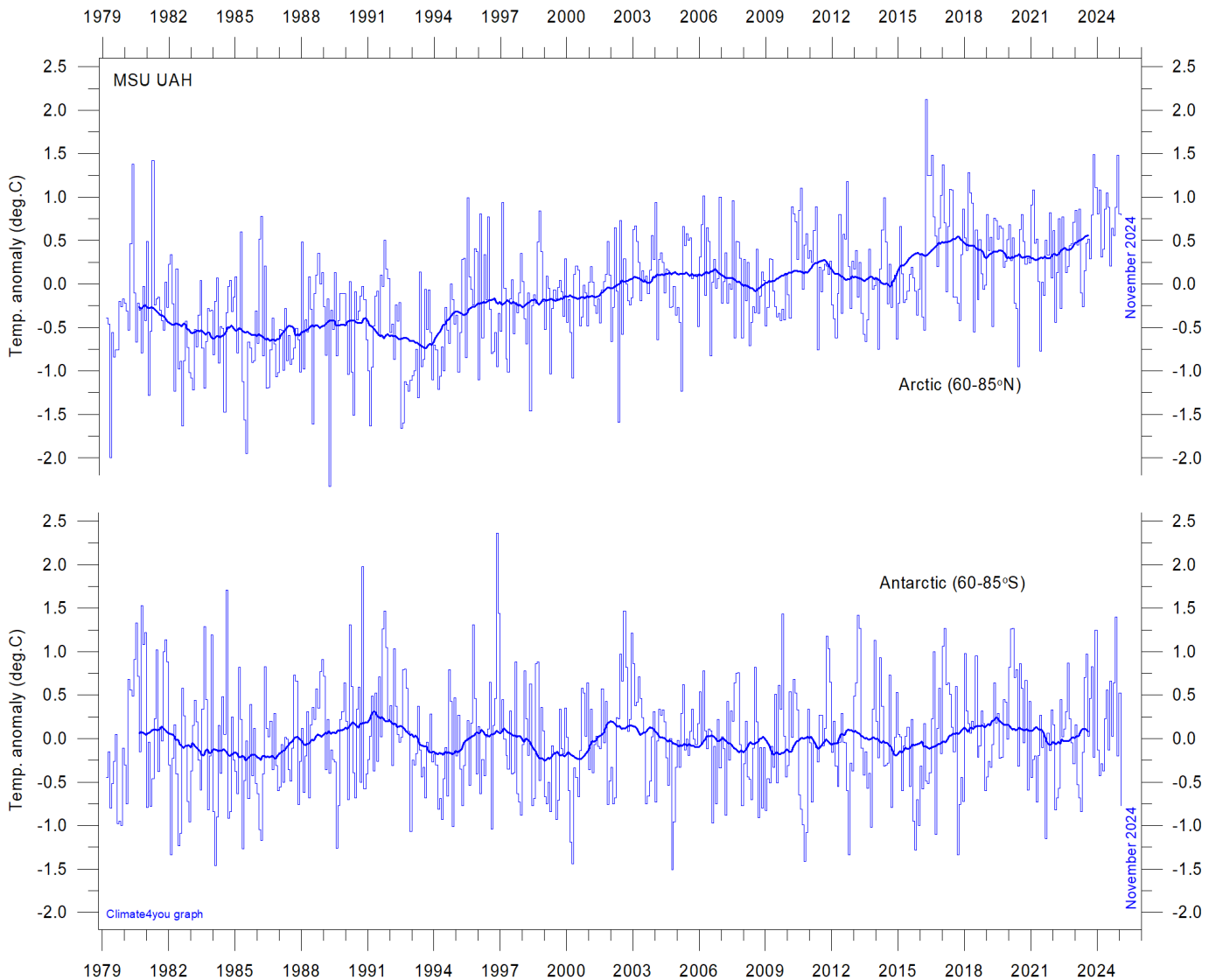
Global monthly average lower troposphere temperature since 1979 for the North Pole and South Pole regions, based on satellite observations (University of Alabama at Huntsville, USA). Thin lines show the monthly temperature. The thick line is the simple running 37-month average, nearly corresponding to a running 3-year average. Reference period 1991-2020.

In the Arctic region, warming mainly took place 1994-96, and less so subsequently. In 2016, however, temperatures peaked for several months, presumably because of oceanic heat given off to the atmosphere during the 2015-15 El Niño (see also diagram on page 25) and subsequently advected to higher latitudes.

This underscores how Arctic air temperatures may be affected not only by variations in local conditions but also by variations playing out in geographically remote regions.

A slight temperature decrease characterised the Arctic since the marked 2016 El Niño peak. However, the recent (2023-24) El Niño episode is recorded by Arctic temperatures in a less pronounced way.

In the Antarctic region, temperatures have basically remained stable since the onset of the satellite record in 1979. In 2016-17 a small temperature peak visible in the monthly record may be interpreted as the subdued effect of the recent El Niño episode.

Arctic and Antarctic surface air temperature, updated to December 2021

Diagram showing area weighted Arctic (70-90ºN) monthly surface air temperature anomalies (HadCRUT4) since January 2000, in relation to the WMO normal period 1961-1990. The thin line shows the monthly temperature anomaly, while the thicker line shows the running 37-month (c. 3 year) average.

Diagram showing area weighted Antarctic (70-90ºS) monthly surface air temperature anomalies (HadCRUT4) since January 2000, in relation to the WMO normal period 1961-1990. The thin line shows the monthly temperature anomaly, while the thicker line shows the running 37-month (c. 3 year) average.

Diagram showing area weighted Arctic (70-90ºN) monthly surface air temperature anomalies ([HadCRUT4](#)) since January 1957, in relation to the WMO [normal period](#) 1961-1990. The thin line shows the monthly temperature anomaly, while the thicker line shows the running 37-month (c. 3 year) average.

Diagram showing area weighted Antarctic (70-90ºS) monthly surface air temperature anomalies ([HadCRUT4](#)) since January 1957, in relation to the WMO [normal period](#) 1961-1990. The thin line shows the monthly temperature anomaly, while the thicker line shows the running 37-month (c. 3 year) average.
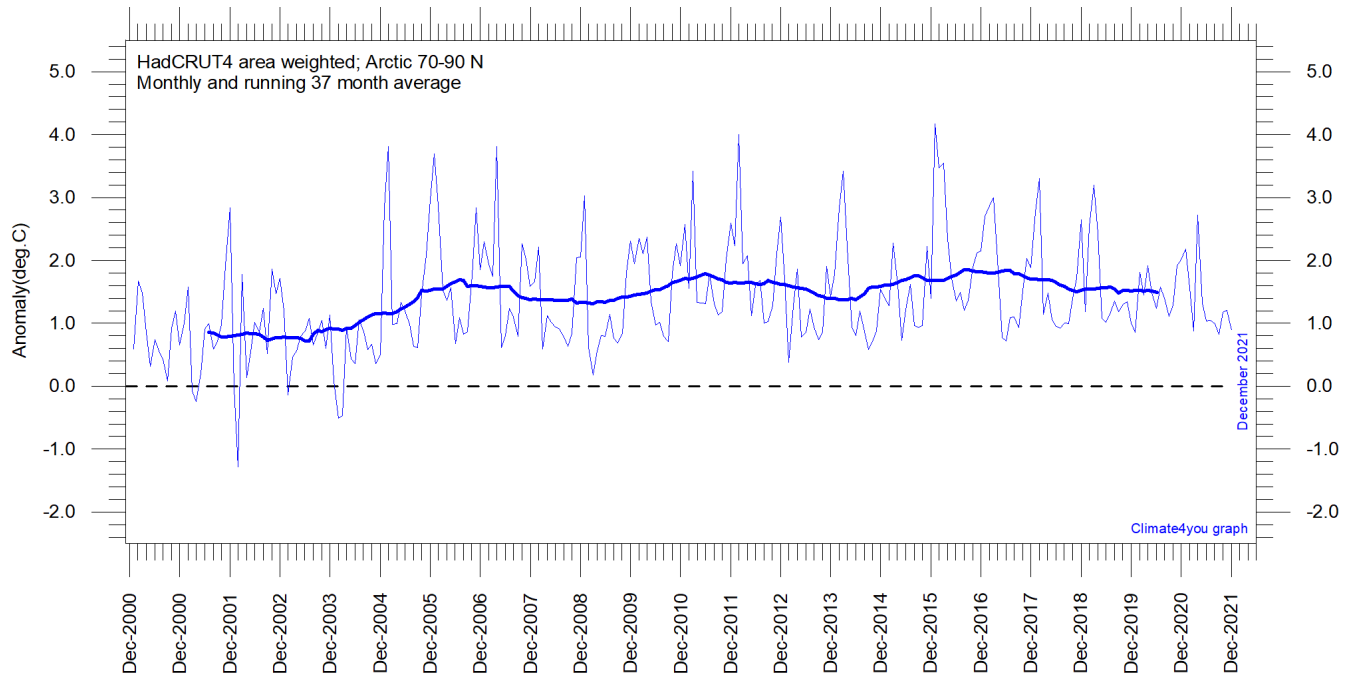
Diagram showing area-weighted Arctic (70-90°N) monthly surface air temperature anomalies ([HadCRUT4](#)) since January 1920, in relation to the WMO [normal period](#) 1961-1990. The thin line shows the monthly temperature anomaly, while the thicker line shows the running 37-month (c. 3 year) average.
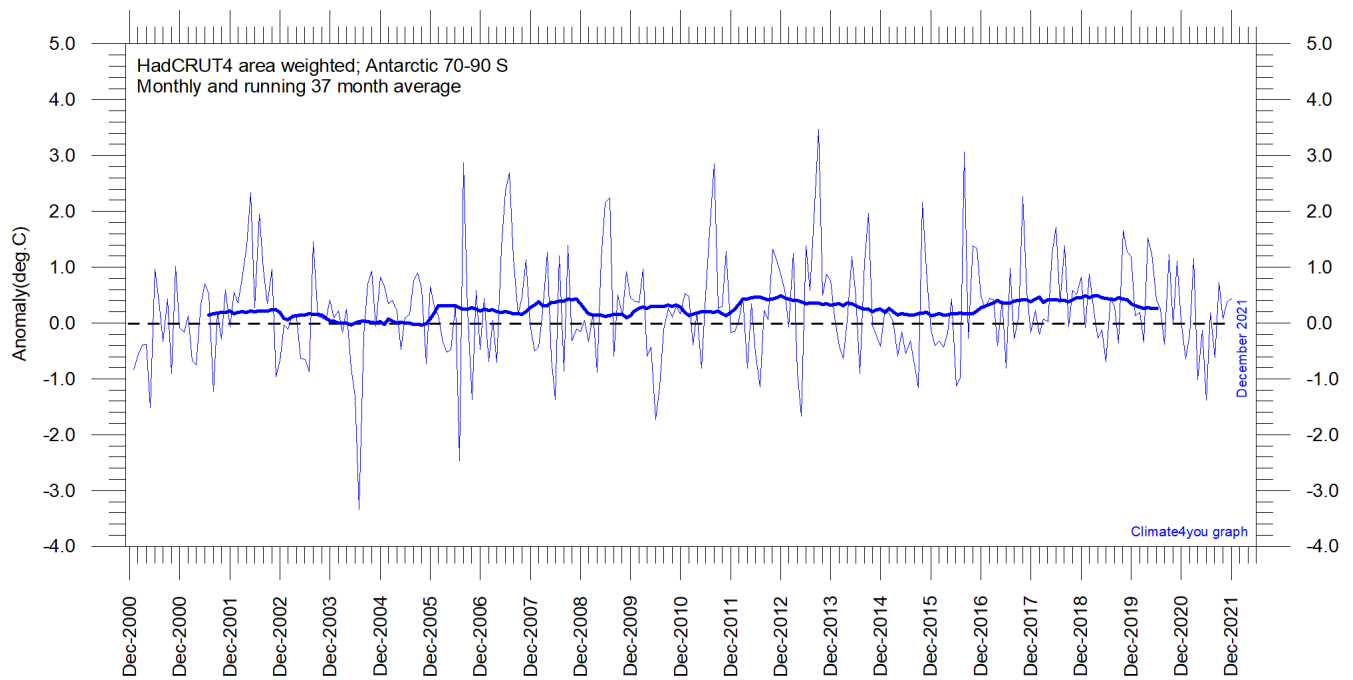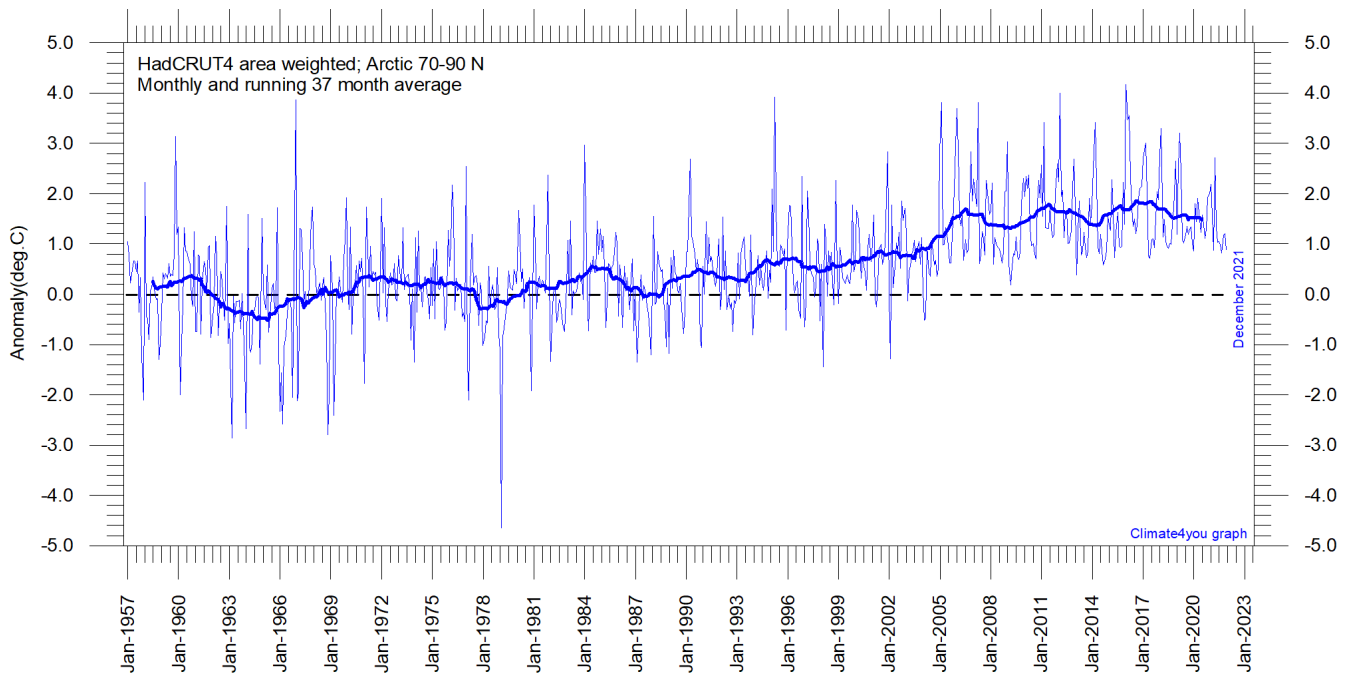
Because of the relatively small number of Arctic stations before 1930, month-to-month variations in the early part of the Arctic temperature record 1920-2018 are higher than later (diagram above).

The period from about 1930 saw the establishment of many new Arctic meteorological stations, first in Russia and Siberia, and following the 2nd World War, also in North America, explaining the above difference.

The period since 2005 is warm, about as warm as the period 1930-1940.

As the HadCRUT4 data series has improved high latitude coverage data coverage (compared to the HadCRUT3 series), the individual 5°x5° grid cells have been weighted according to their surface area. This area correction is especially important for polar regions, where longitudes converge rapidly. This approach differs from the approach used by Gillet et al. 2008, which calculated a simple average, with no correction for the substantial latitudinal surface area effect in polar regions.

The area weighted Arctic HadCRUT4 surface air temperature anomalies (p.28-30) correspond rather well to the lower troposphere temperature anomalies recorded by satellites (p.27).

Literature:

Gillett, N.P., Stone, D.A., Stott, P.A., Nozawa, T., Karpechko, A.Y.U., Hegerl, G.C., Wehner, M.F. and Jones, P.D. 2008. Attribution of polar warming to human influence. *Nature Geoscience* 1, 750-754.

Long Arctic annual surface air temperature series, updated to year 2023
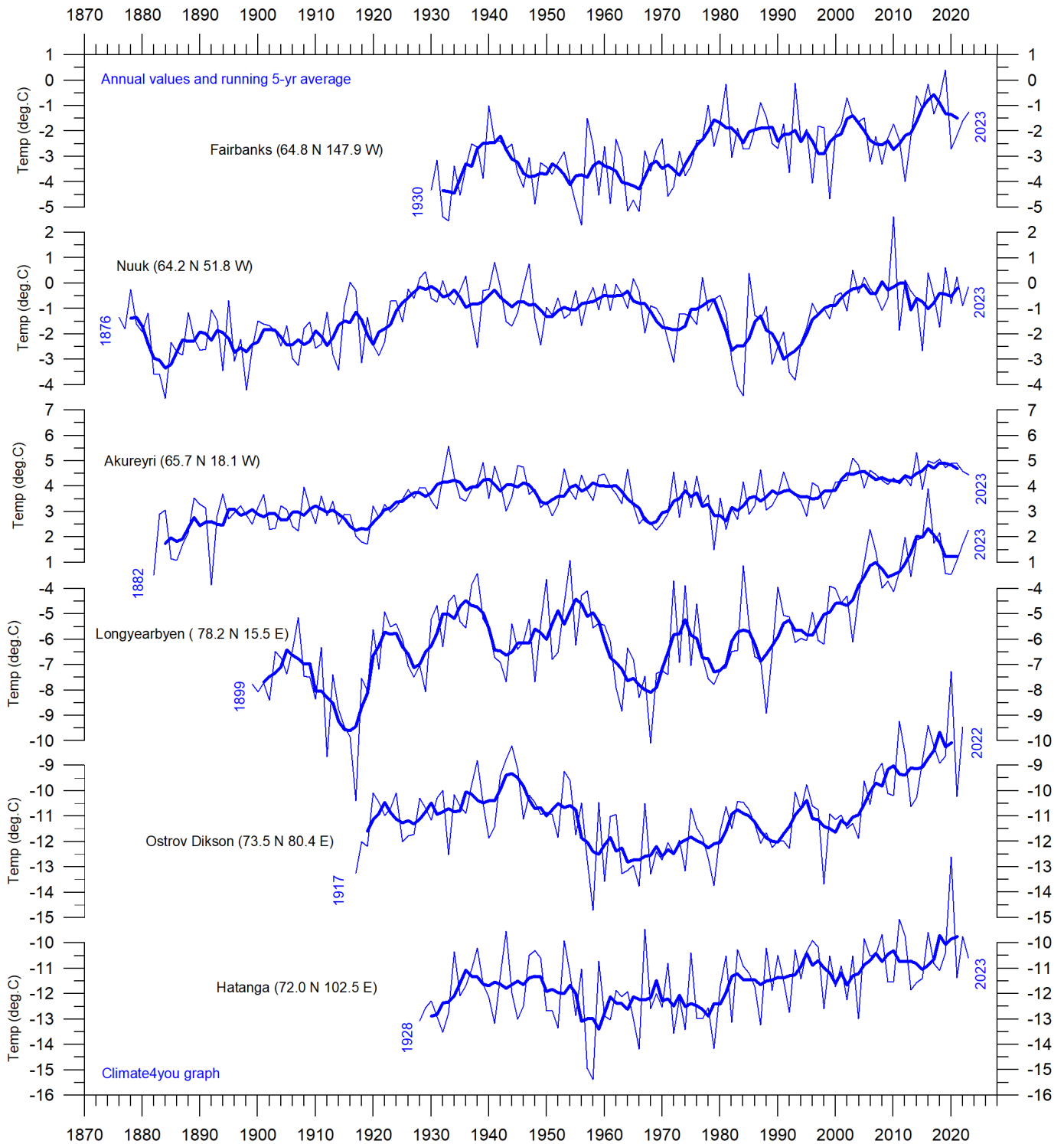
Arctic annual surface air temperature series, selected because of their length of observation time. The thin blue line represents the mean annual air temperature, and the thick blue line is the running 5-year average. Annual values were calculated from monthly average temperatures. More info on Climate4you.

Long Antarctic annual surface air temperature series, updated to year 2023
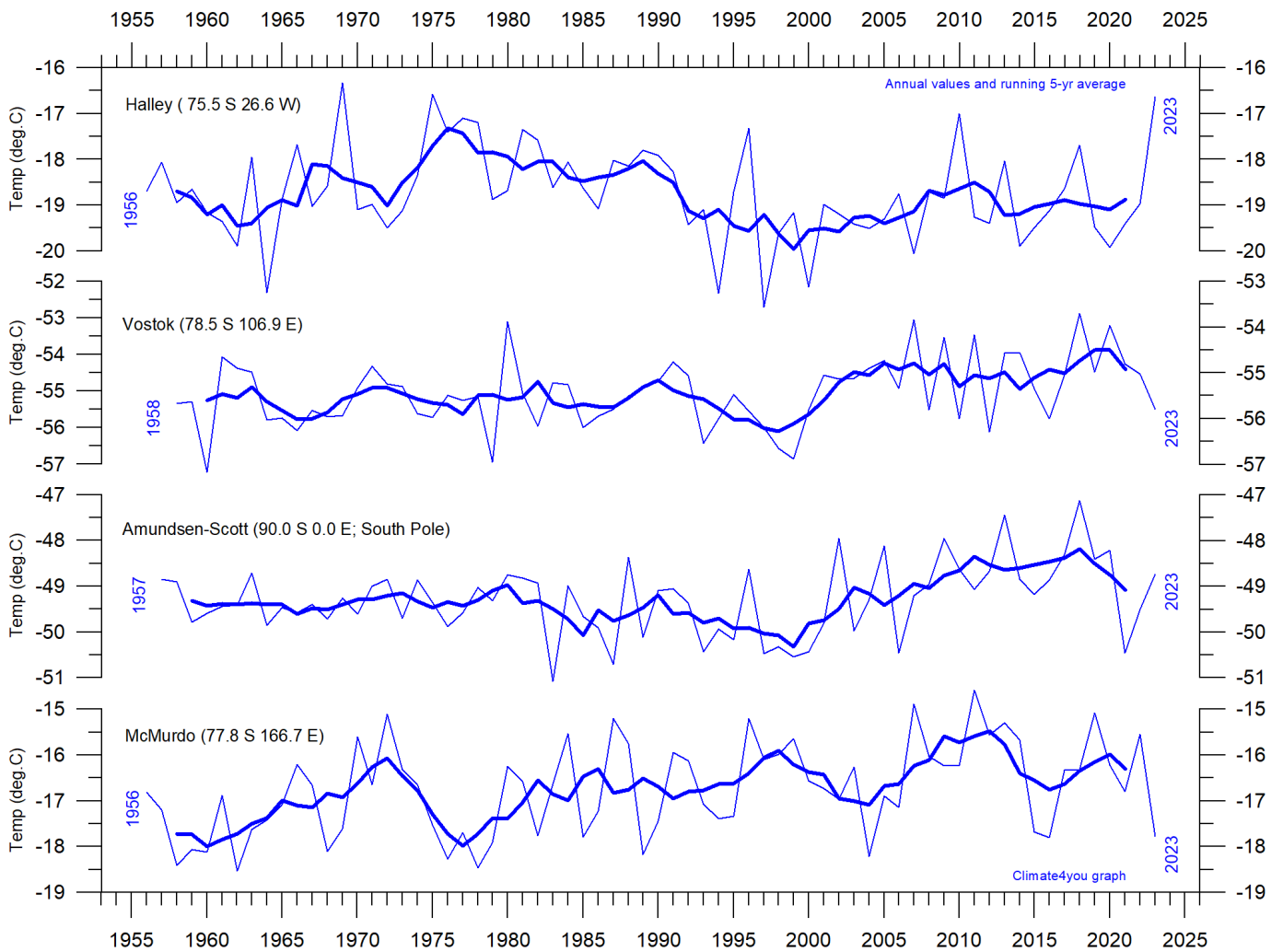
Antarctic annual surface air temperature series, selected because of their length of observation time. The thin blue line represents the mean annual air temperature, and the thick blue line is the running 5-year average. Annual values were calculated from monthly average temperatures. More info on Climate4you.

Temperature over land versus over oceans, updated to November 2024
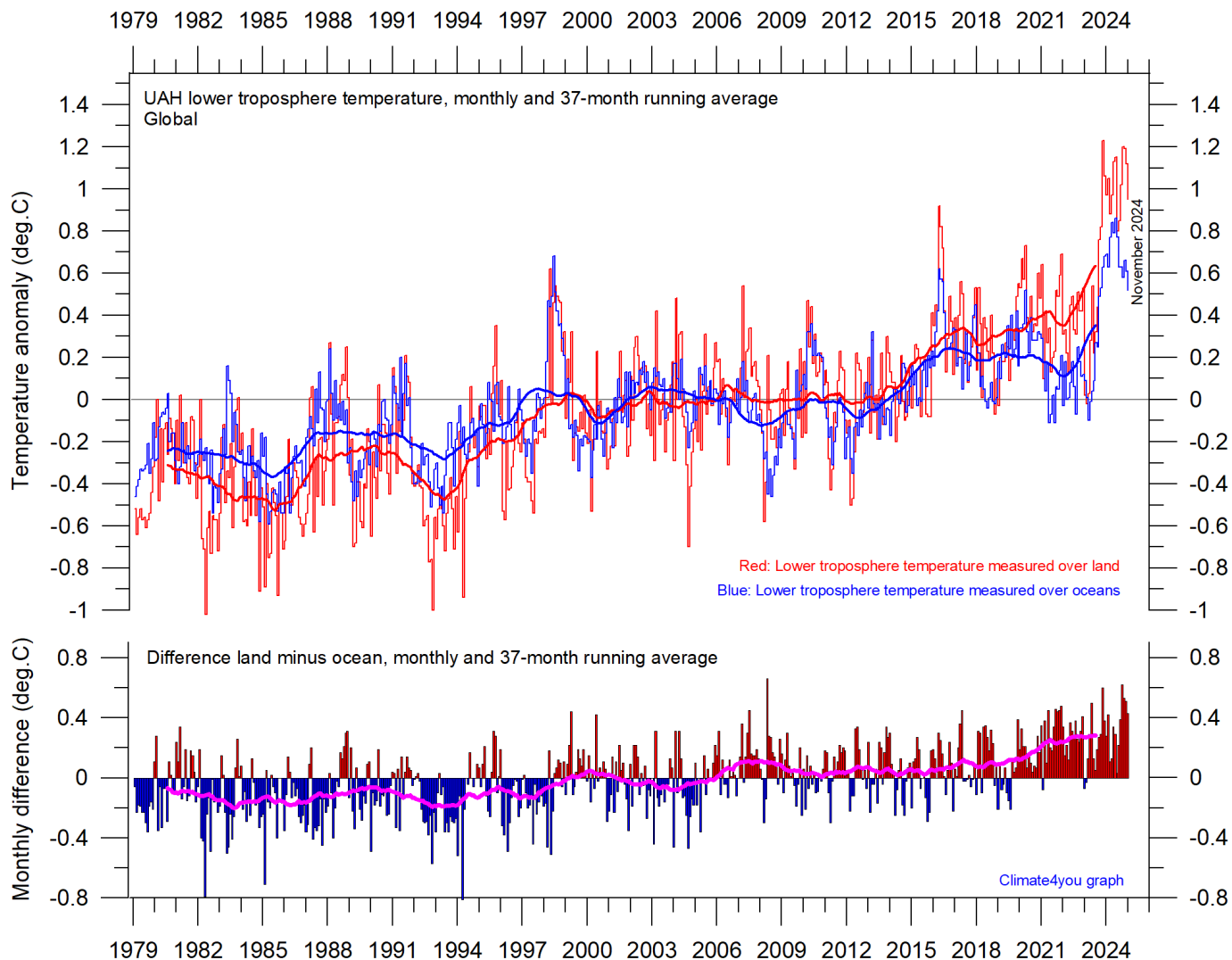
Global monthly average lower troposphere temperature since 1979 measured over land and oceans, respectively, according to [University of Alabama](#) at Huntsville, USA. Thick lines are the simple running 37-month average, nearly corresponding to a running 3-year average. Reference period 1991-2020.

Since 1979, the lower troposphere over land has warmed much more than over oceans, suggesting that the overall warming is derived mainly from incoming solar radiation. In addition, there may be supplementary reasons for this divergence, such as, e.g., variations in cloud cover and changes in land use. Compare also with cloud cover diagram on page 60.

The temperature effect of the recent (2023-24) El Niño episode was recorded more pronounced over land regions, compared to ocean regions.

Troposphere and stratosphere temperatures from satellites, updated to November 2024
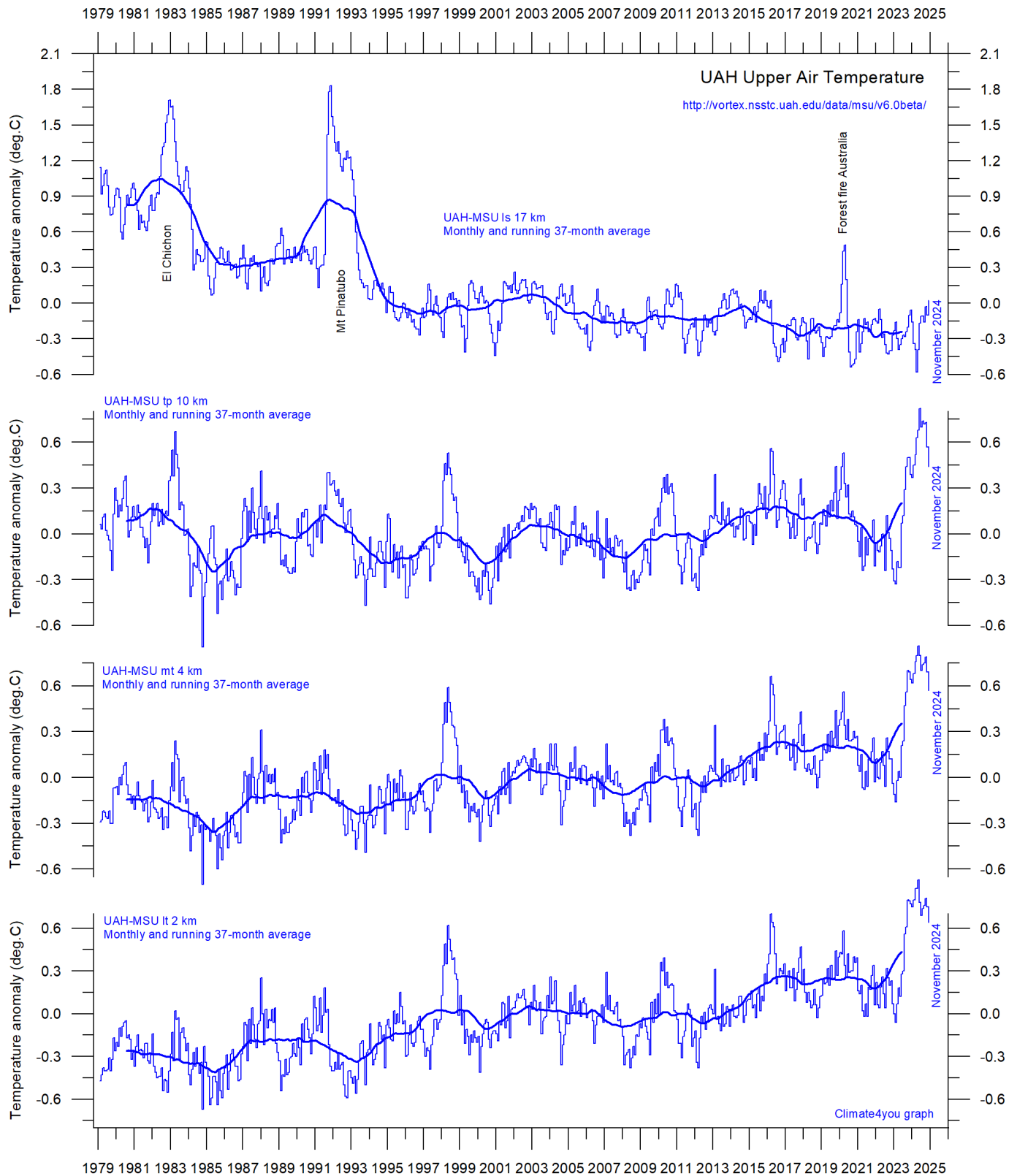
Global monthly average temperature in different according to University of Alabama at Huntsville, USA. The thin lines represent the monthly average, and the thick line the simple running 37-month average, nearly corresponding to a running 3-year average. Reference period 1991-2020.

Arctic and Antarctic sea ice, updated to November 2024
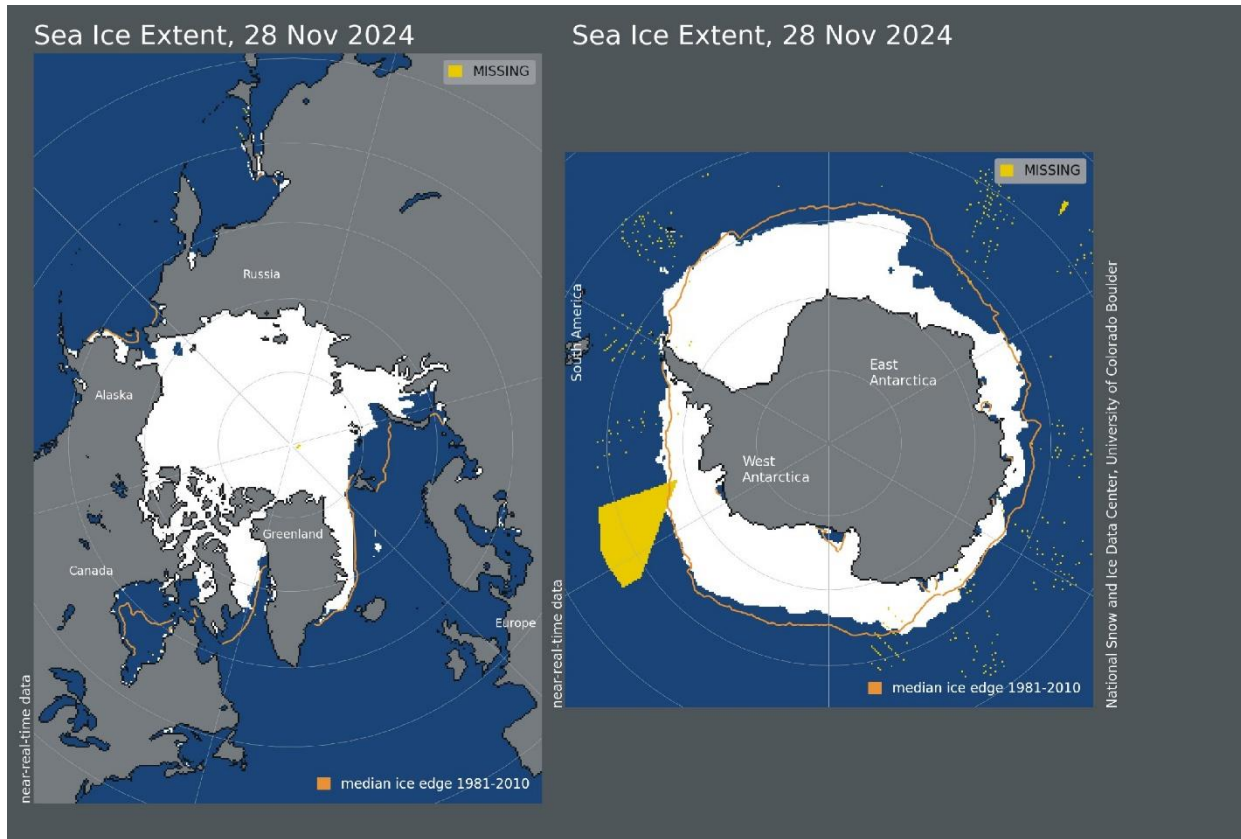
Sea ice extent 28 November 2024. The median limit of sea ice (orange line) is defined as 15% sea ice cover, according to the average of satellite observations 1981-2010 (both years included). Sea ice may therefore well be encountered outside and open water areas inside the limit shown in the diagrams above. Map source: National Snow and Ice Data Center (NSIDC).
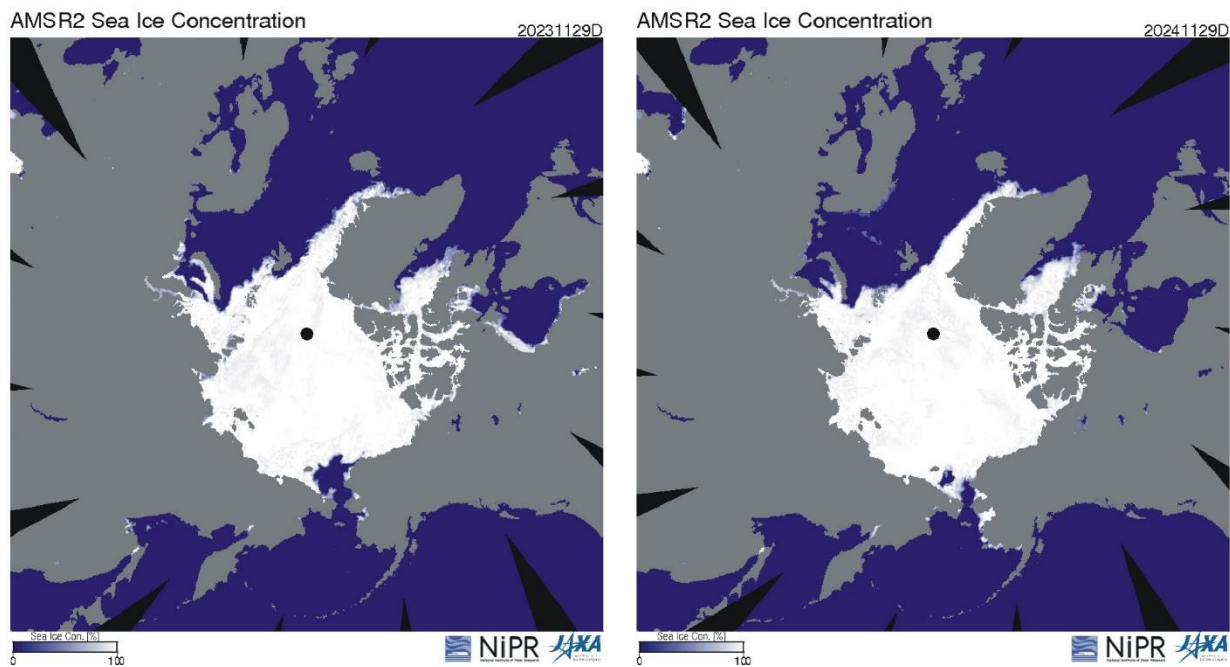
Diagrams showing Arctic sea ice extent and concentration 29 November 2023 (left) and 2024 (right), according to the Japan Aerospace Exploration Agency (JAXA).
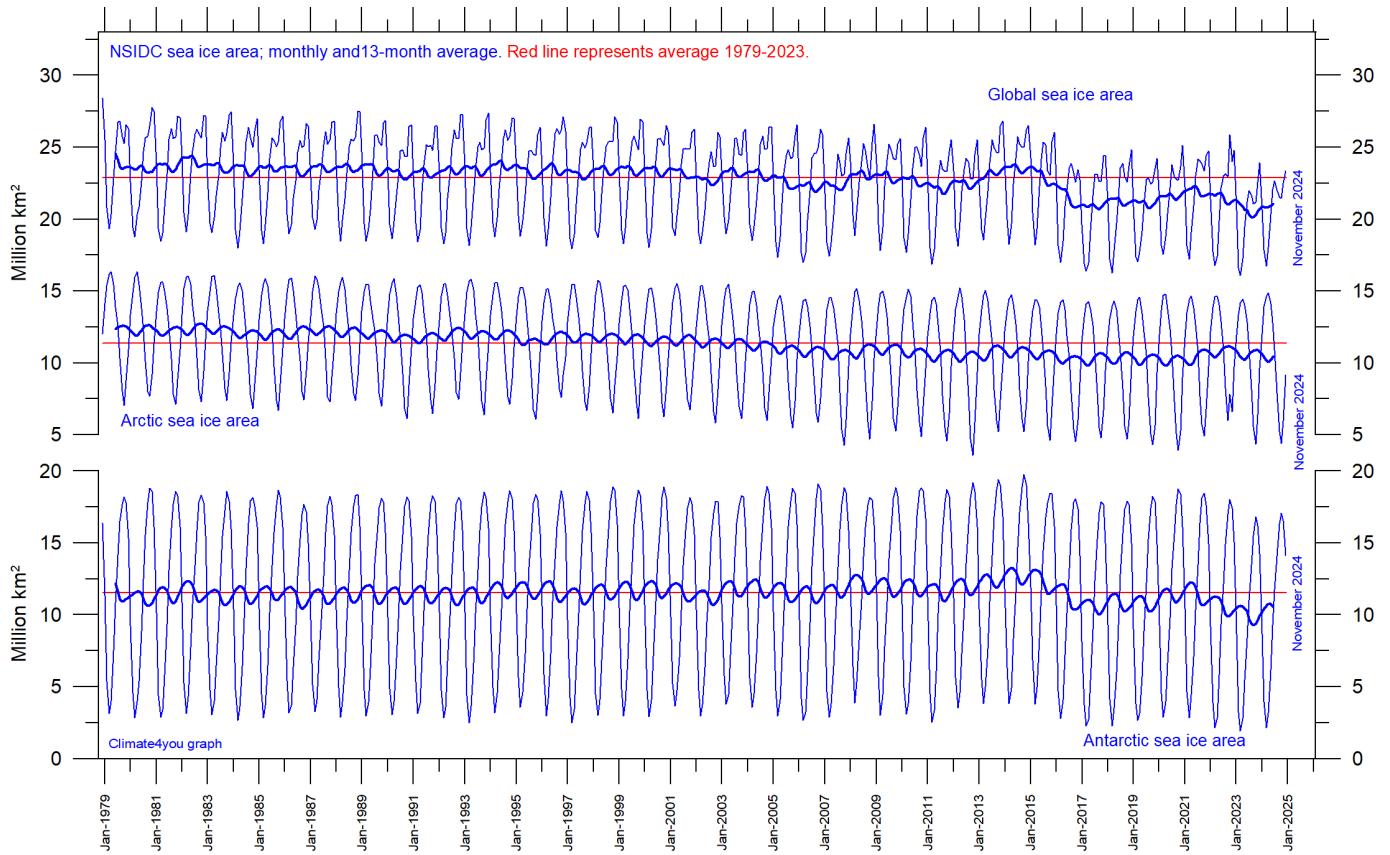
Graphs showing monthly Antarctic, Arctic, and global sea ice extent since November 1978, according to the _National Snow and Ice data Center_ (NSIDC).
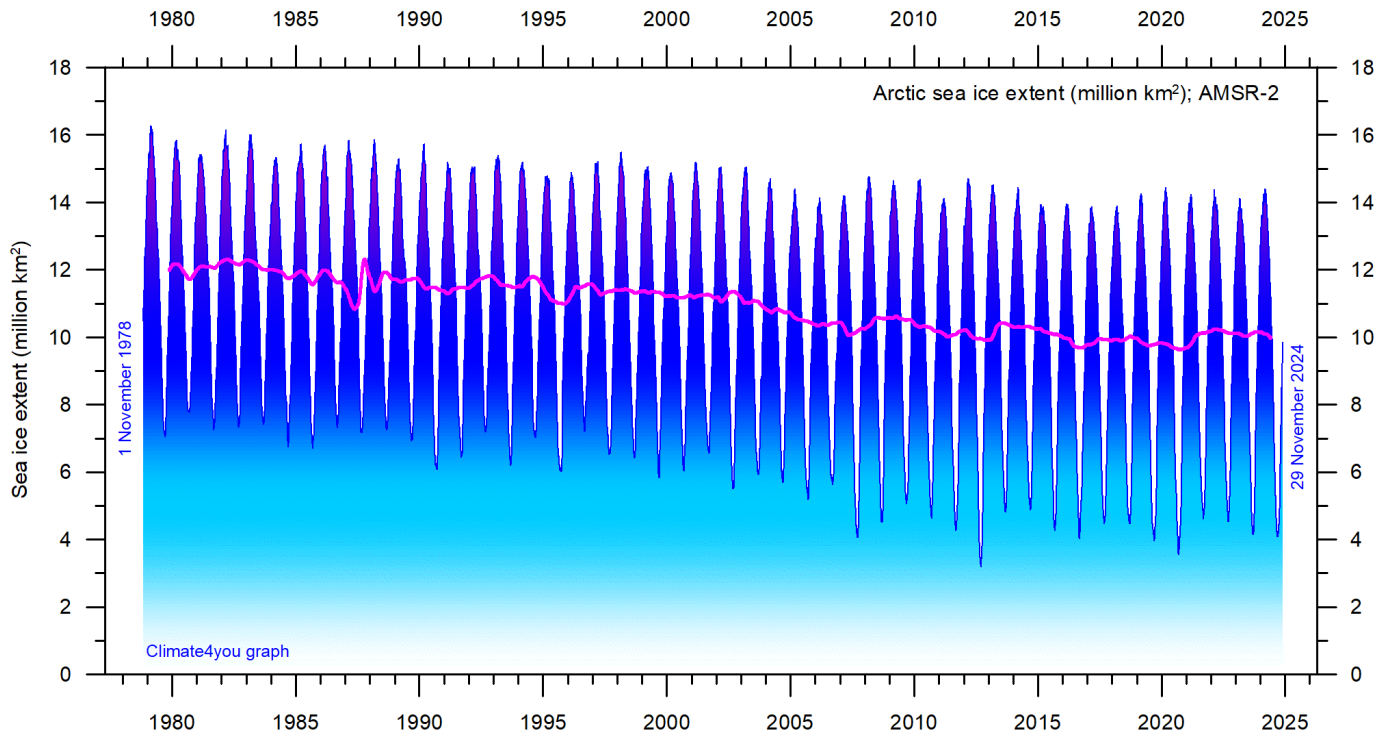
Diagram showing daily Arctic sea ice extent since November 1978, to 29 November 2024, data courtesy of _Japan Aerospace Exploration Agency_ (JAXA).

Sea Ice Thickness, 29-Nov-2024
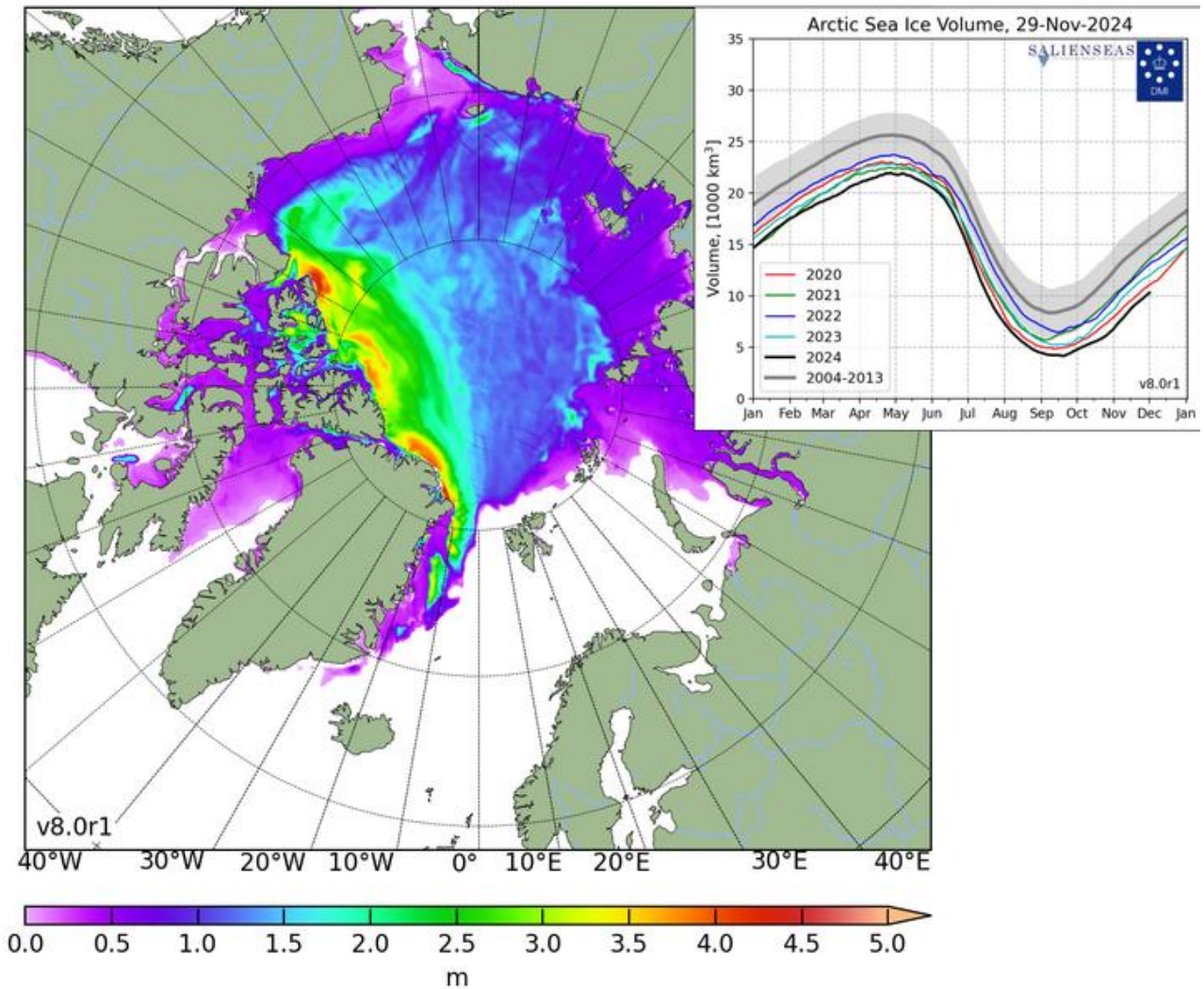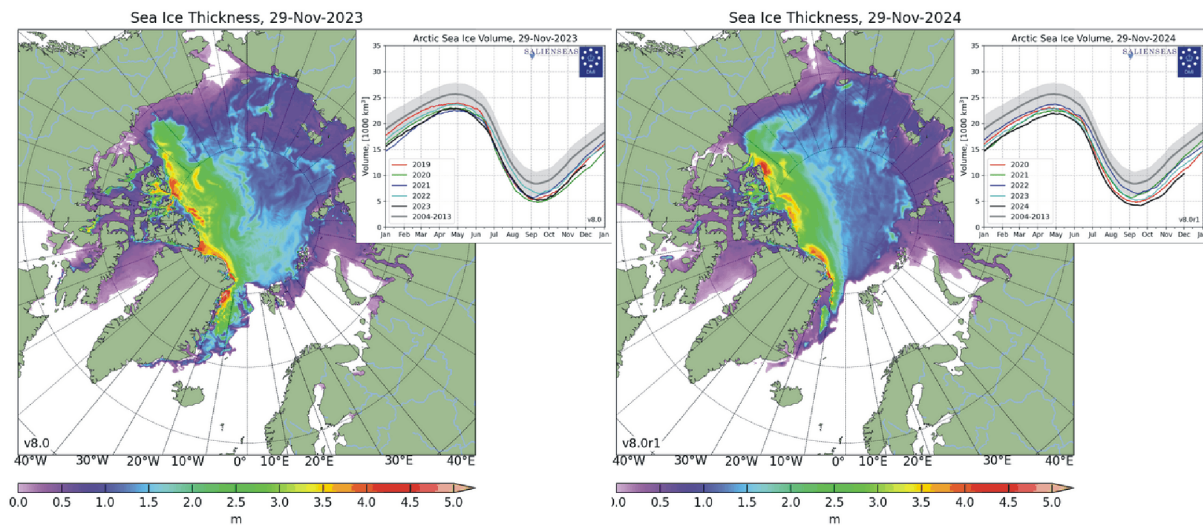
Diagrams showing Arctic sea ice extent and thickness 29 November 2023 (left) and 2024 (right and above) and the seasonal cycles of the calculated total arctic sea ice volume, according to [The Danish Meteorological Institute (DMI)](). The mean sea ice volume and standard deviation for the period 2004-2013 are shown by grey shading. Please note that DMI on 7 December 2021 changed their sea ice calculation model. DMI's description of the model version change can be read here: http://polarportal.dk/en/sea-ice-and-icebergs/sea-ice-thickness-and-volume/
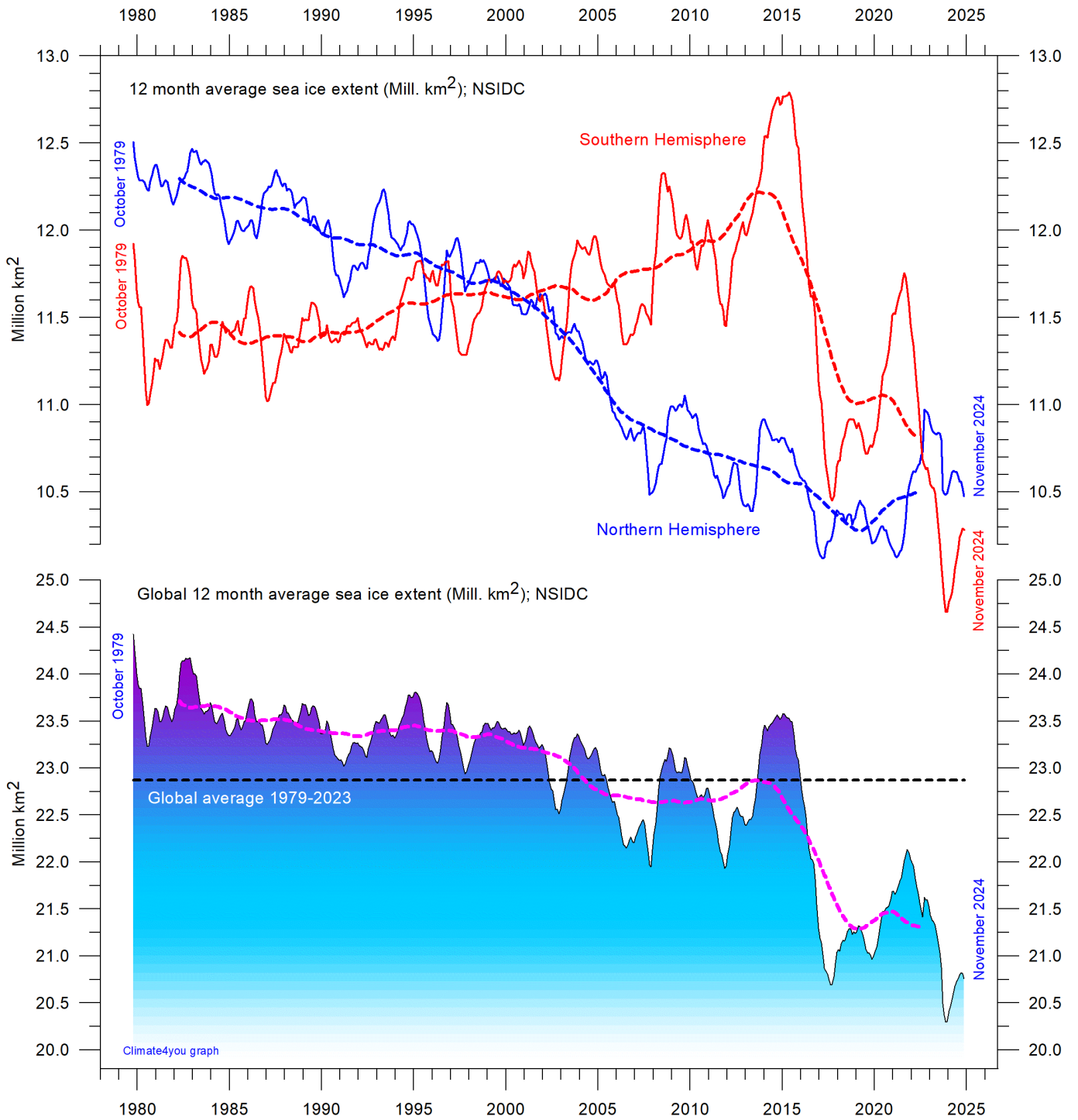
12 month running average sea ice extension, global and in both hemispheres since 1979, the satellite-era. The October 1979 value represents the monthly 12-month average of November 1978 - October 1979, the November 1979 value represents the average of December 1978 - November 1979, etc. The stippled lines represent a 61-month (ca. 5 years) average. Data source: National Snow and Ice Data Center (NSIDC).

Sea level in general

Global (or eustatic) sea-level change is measured relative to an idealised reference level, the geoid, which is a mathematical model of planet Earth's surface (Carter et al. 2014). Global sea-level is a function of the volume of the ocean basins and the volume of water they contain. Changes in global sea-level are caused by – but not limited to - four main mechanisms:

1. Changes in local and regional air pressure and wind, and tidal changes introduced by the Moon.
2. Changes in ocean basin volume by tectonic (geological) forces.
3. Changes in ocean water density caused by variations in currents, water temperature and salinity.
4. Changes in the volume of water caused by changes in the mass balance of terrestrial glaciers.

In addition to these there are other mechanisms influencing sea-level, such as storage of ground water, storage in lakes and rivers, evaporation, etc.

Mechanism 1 is controlling sea-level at many sites on a time scale from months to several years. As an example, many coastal stations show a pronounced annual variation reflecting seasonal changes in air pressures and wind speed. Longer-term climatic changes playing out over decades or centuries will also affect measurements of sea-level changes. Hansen et al. (2011, 2015) provide excellent analyses of sea-level changes caused by recurrent changes of the orbit of the Moon and other phenomena.

Mechanism 2 – with the important exception of earthquakes and tsunamis - typically operates over long (geological) time scales and is not significant on human time scales. It may relate to variations in the seafloor spreading rate, causing volume changes in mid-ocean mountain ridges, and to the slowly changing configuration of land and oceans. Another effect may be the slow rise of basins due to isostatic offloading by deglaciation after an ice age. The floor of the Baltic Sea and the Hudson Bay are presently rising, causing a slow net transfer of water from these basins into the adjoining oceans. Slow changes of excessively big glaciers (ice sheets) and movements in the mantle will affect the gravity field and thereby the vertical position of the ocean surface. Any increase of the total water mass as well as sediment deposition into oceans increase the load on their bottom, generating sinking by viscoelastic flow in the mantle below. The mantle flow is directed towards the surrounding land areas, which will rise, thereby partly compensating for the initial sea level increase induced by the increased water mass in the ocean.

Mechanism 3 (temperature-driven expansion) only affects the uppermost part of the oceans on human time scales. Usually, temperature-driven changes in density are more important than salinity-driven changes. Seawater is characterised by a relatively small coefficient of expansion, but the effect should however not be overlooked, especially when interpreting satellite altimetry data. Temperature-driven expansion of a column of seawater will not affect the total mass of water within the column considered and will therefore not affect the potential at the top of the water column. Temperature-driven ocean water expansion will therefore not in itself lead to any lateral displacement of water, but only locally lift the ocean surface. Near the coast, where people are living, the depth of water approaches zero, so no measurable temperature-driven expansion will take place here (Mörner 2015). Mechanism 3 is for that reason not important for coastal regions.

Mechanism 4 (changes in glacier mass balance) is an important driver for global sea-level changes along coasts, for human time scales. Volume changes of floating glaciers – ice shelves – has no influence on the global sea-level, just like volume changes of floating sea ice has no influence. Only the mass-balance of grounded or land-based glaciers is important for the global sea-level along coasts.

Summing up: Presumably, mechanism 1 and 4 are the most important for understanding sea-level changes along coasts.

References:

Carter R.M., de Lange W., Hansen, J.M., Humlum O., Idso C., Kear, D., Legates, D., Mörner, N.A., Ollier C., Singer F. & Soon W. 2014. Commentary and Analysis on the Whitehead& Associates 2014 NSW Sea-Level Report. Policy Brief, NIPCC, 24. September 2014, 44 pp. http://climatechangereconsidered.org/wp-content/uploads/2014/09/NIPCC-Report-on-NSW-Coastal-SL-9z-corrected.pdf
Hansen, J.-M., Aagaard, T. and Binderup, M. 2011. Absolute sea levels and isostatic changes of the eastern North Sea to central Baltic region during the last 900 years. Boreas, 10.1111/j.1502-3885.2011.00229.x. ISSN 0300–9483.
Hansen, J.-M., Aagaard, T. and Huijpers, A. 2015. Sea-Level Forcing by Synchronization of 56- and 74-YearOscillations with the Moon's Nodal Tide on the Northwest European Shelf (Eastern North Sea to Central Baltic Sea). Journ. Coastal Research, 16 pp.
Mörner, Nils-Axel 2015. Sea Level Changes as recorded in nature itself. Journal of Engineering Research and Applications, Vol.5, 1, 124-129.

Global sea level from satellite altimetry, updated to September 2023
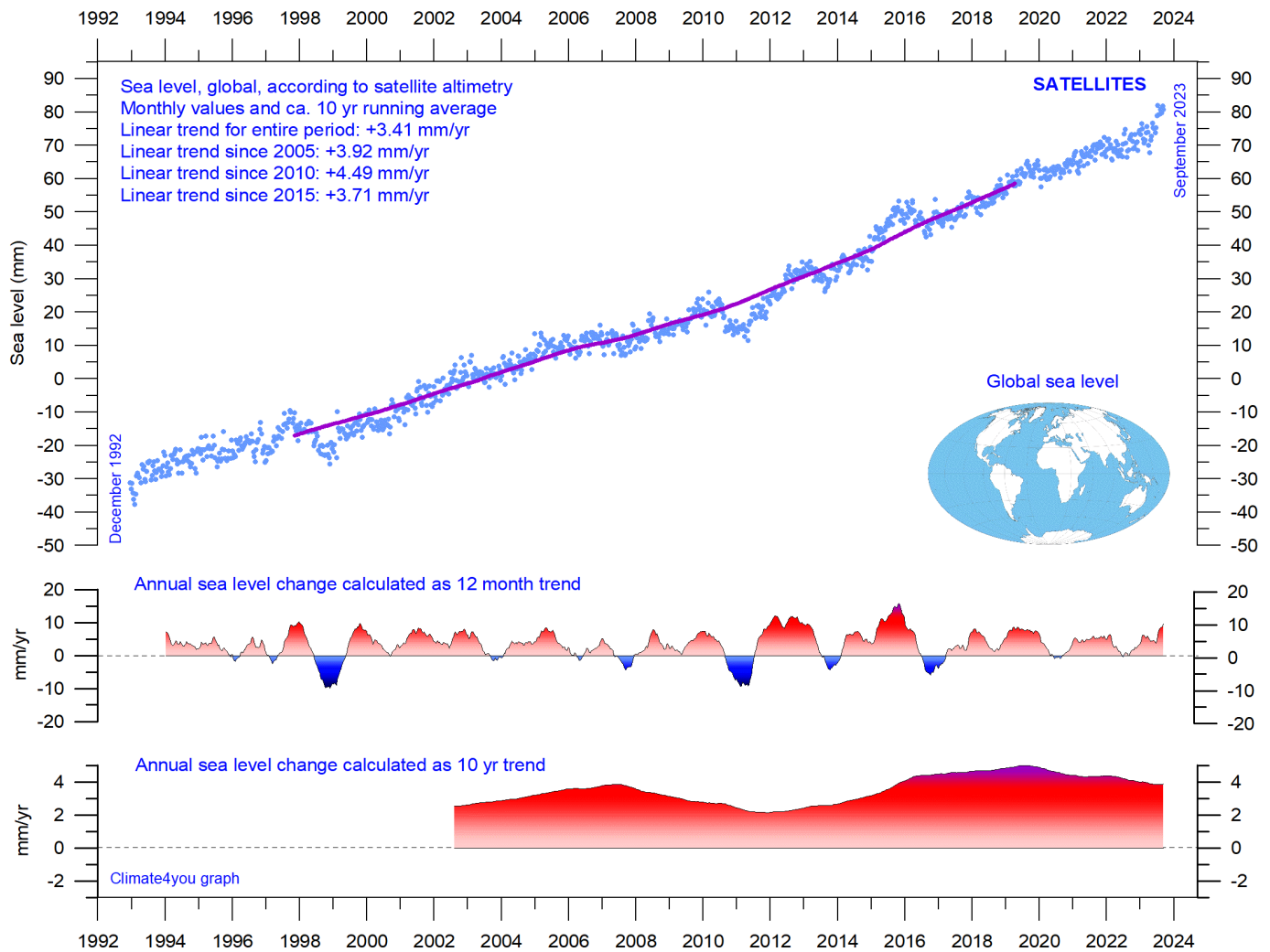
Global sea level since December 1992 according to the Colorado Center for Astrodynamics Research at University of Colorado at Boulder. The blue dots are the individual observations, and the purple line represents the running 121-month (ca. 10 year) average. The two lower panels show the annual sea level change, calculated for 1 and 10-year time windows, respectively. These values are plotted at the end of the interval considered. Compare with tide-gauge diagram on page 41.

Ground truth is a term used in various fields to refer to information provided by direct observation as opposed to information provided by inference, such as, e.g., by satellite observations.

In remote sensing using satellite observations, ground truth data refers to information collected on location. Ground truth allows the satellite data to be related to real features observed on the planet surface. The collection of ground truth data enables calibration of remote-sensing data, and

aids in the interpretation and analysis of what is being sensed or recorded by satellites. Ground truth sites allow the remote sensor operator to correct and improve the interpretation of satellite data.

For satellite observations on sea level ground true data are provided by the classical tide gauges (example diagram on next page), that directly measures the local sea level many places distributed along the coastlines on the surface of the planet.

Global sea level from tide-gauges, extended Holgate-9, updated to December 2022

Sea level, extended **Holgate-9** since 1900, Honolulu, Newlyn, Balboa, San Diego, Key West, New York, Stockholm, Ketchikan, Perth, Sydney, Montevideo, Port Elisabeth, Wajima, Visakhapatnam, Argentine Islands.
Monthly values and 121-month running average
Linear trend for entire period: +1.19 mm/yr
Linear trend since December 1992: +2.46 mm/yr

Annual sea level change calculated as 12 month trend

Annual sea level change calculated as 10 yr trend

Climate4you graph

Extended Holgate-9 monthly tide-gauge data from PSMSL Data Explorer. Holgate (2007) suggested 9 stations to capture the global variability found in a larger number of stations over the last half century studied previously. However, some of the stations suggested by Holgate has not reported values for several years, leading to the southern hemisphere now being seriously underrepresented in his original data set. Therefore, in the above diagram several other long tide-gauge series have been included, to provide a more balanced representation of both hemispheres (15 stations in total). The blue dots are the individual average monthly observations, and the purple line represents the running 121-month (ca. 10 year) average. The two lower panels show the average annual sea level change, calculated for moving 1 and 10-year windows, respectively. These values are plotted at the end of the time window considered, month by month.

Data from tide-gauges all over the world suggest an average global sea-level rise of 1-2 mm/year, while the modern satellite-derived record (since 1992, page 40) suggest a rise of about 3.4 mm/year, or more. The difference between the two data sets is remarkable. It is however known that satellite observations are facing several complications in areas near the coast. Vignudelli et al. (2019) provide an updated overview of the current limitations of classical satellite altimetry in coastal regions. Since 2015 a sea level increase rate may be suggested by the above composite record.

References:

Holgate, S.J. 2007. On the decadal rates of sea level change during the twentieth century. Geophys. Res. Letters, 34, L01602, doi:10.1029/2006GL028492

Vignudelli et al. 2019. Satellite Altimetry Measurements of Sea Level in the Coastal Zone. *Surveys in Geophysics, Vol.* 40, p. 1319–1349.
https://link.springer.com/article/10.1007/s10712-019-09569-1

This month's selected sea level station (tide-gauge): Bundaberg, NE Australia
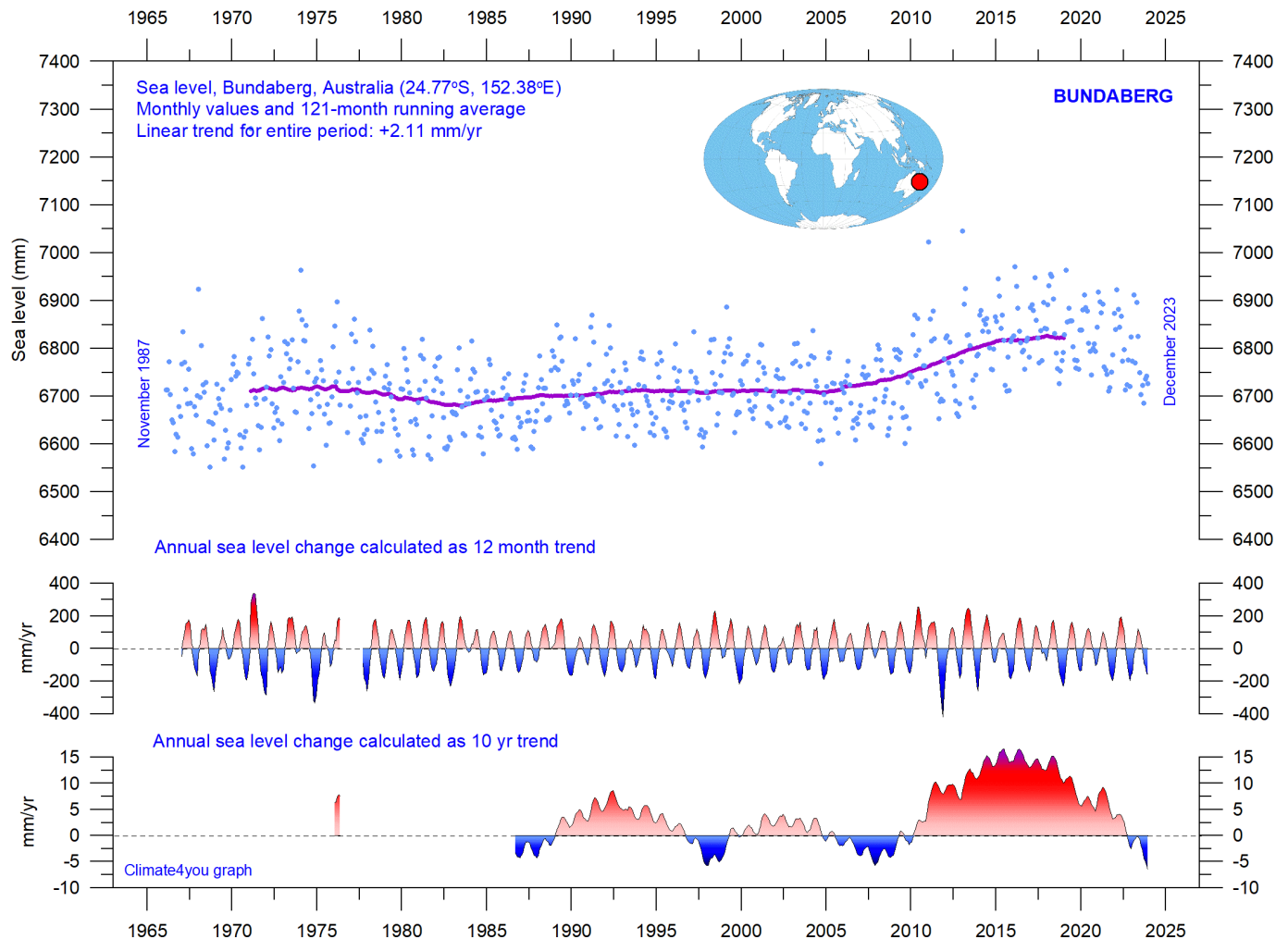
Bundaberg, NE Australia, monthly tide gauge data from [PSMSL Data Explorer](). The blue dots are the individual monthly observations, and the purple line represents the running 121-month (ca. 10 yr) average. The two lower panels show the annual sea level change, calculated for 1 and 10 yr time windows, respectively. These values are plotted at the end of the interval considered.

Bundaberg

Bundaberg is in northeastern Australia, about 250 km north of Brisbane. If the observed development since 1987 continues, relative sea level at Bundaberg will have increased about 16 cm by year 2100. If the higher short-term rate 2005-2020 is applied instead, relative sea level at Bundaberg will have increased about 90 cm by year 2100. This last development is,

however, entirely unlikely, as the high change rate mainly is the result of an about 11-year cyclic variation, as clearly displayed by the lower panel in the diagram. Much is still to be learnt about sea level changes.

Australia

Australia (the Commonwealth of Australia) is a continent-wide nation comprising the mainland of the Australian continent, the island of Tasmania, and numerous smaller islands. The total area is about 7,692,000,000 km^2. Australia is away from active tectonic plate boundaries. Therefore, in contrast to the neighbouring geologically highly active New Zealand, the Australian continent has been relatively stable since the uplift of the Great Dividing Range in eastern Australia about 80 million years ago. However, while Australia largely may be considered a relatively stable continent, it is also subject to widespread small-magnitude tectonic movements.

Northern Hemisphere weekly and seasonal snow cover, updated to November 2024
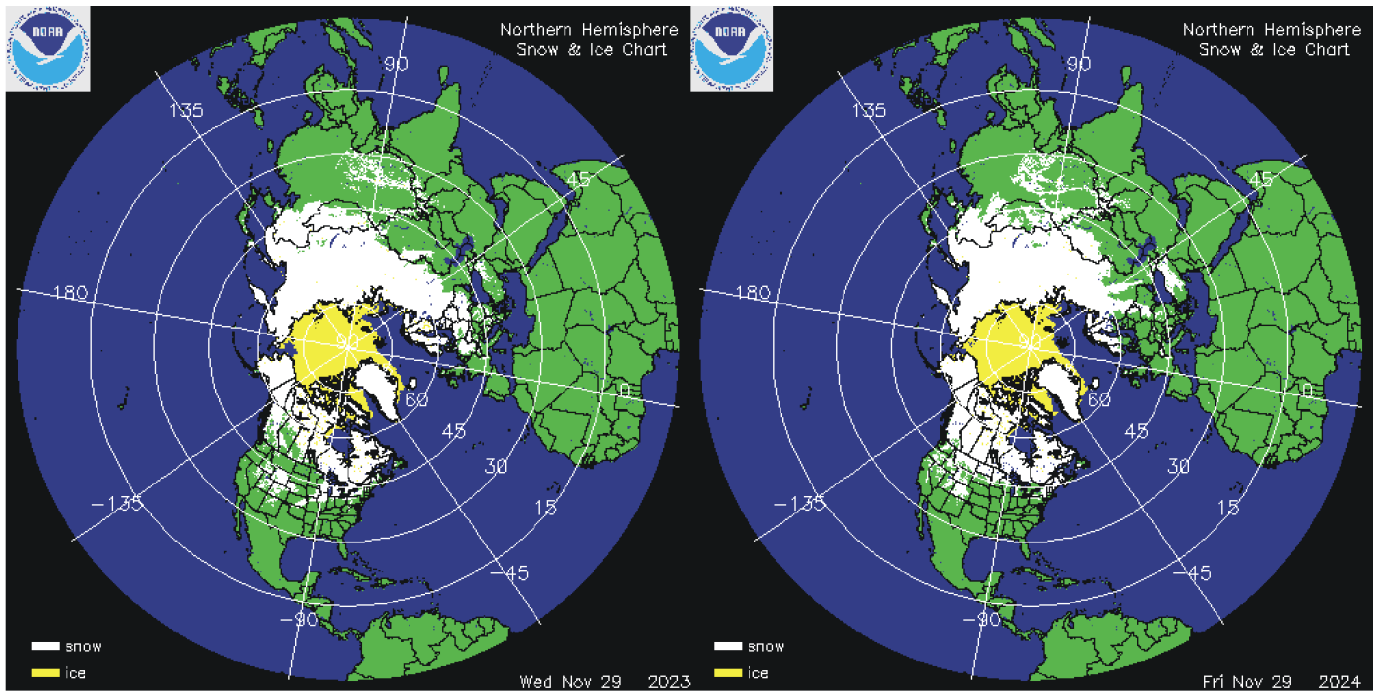
Northern hemisphere snow cover (white) and sea ice (yellow) 29 November 2023 (left) and 2024 (right). Map source: National Ice Center (NIC).
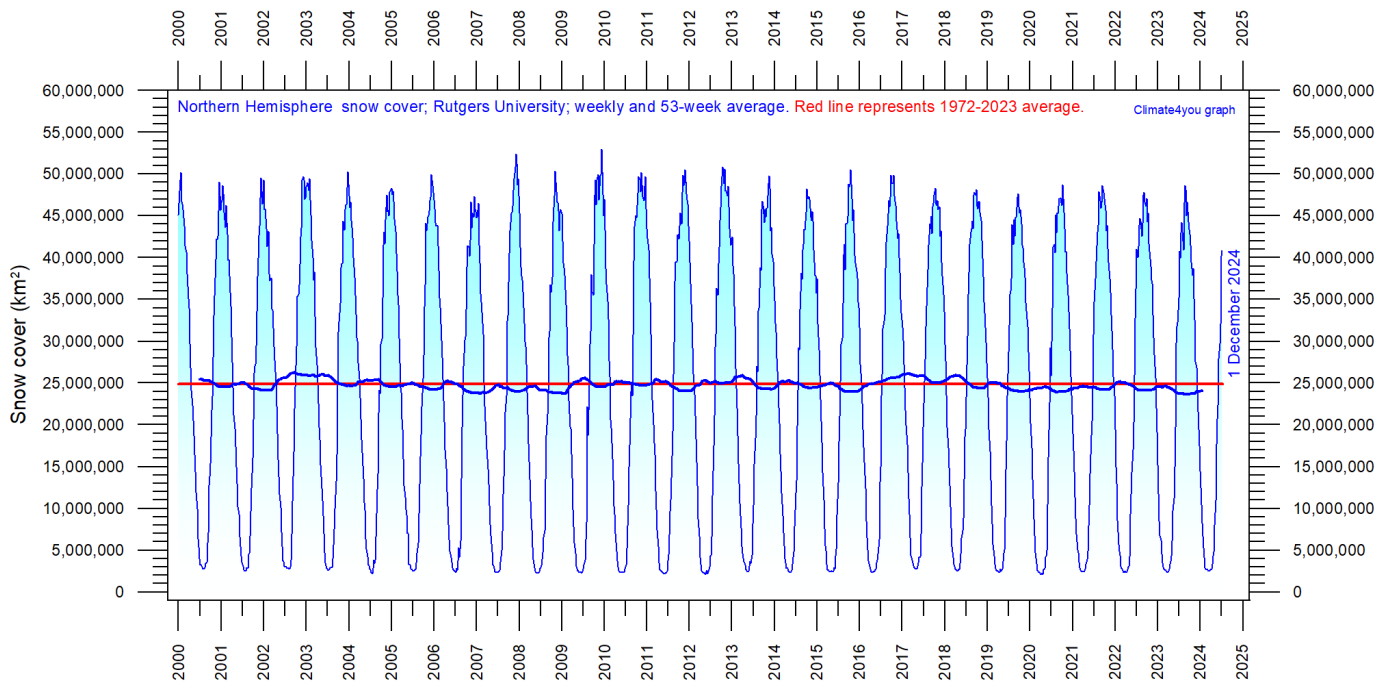
Northern hemisphere weekly snow cover since January 2000 according to Rutgers University Global Snow Laboratory. The thin blue line is the weekly data, and the thick blue line is the running 53-week average (approximately 1 year). The horizontal red line is the 1972-2023 average.
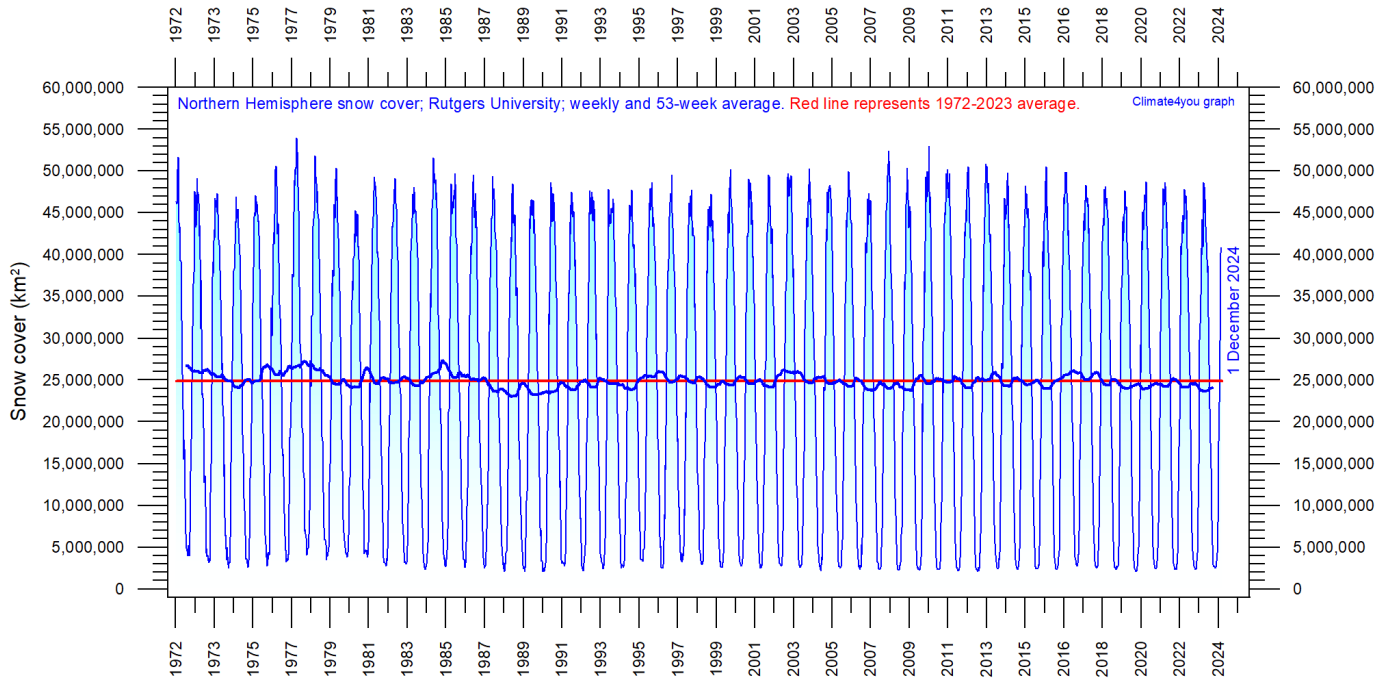
Northern hemisphere weekly snow cover since January 1972 according to Rutgers University Global Snow Laboratory. The thin blue line is the weekly data, and the thick blue line is the running 53-week average (approximately 1 year). The horizontal red line is the 1972-2023 average.
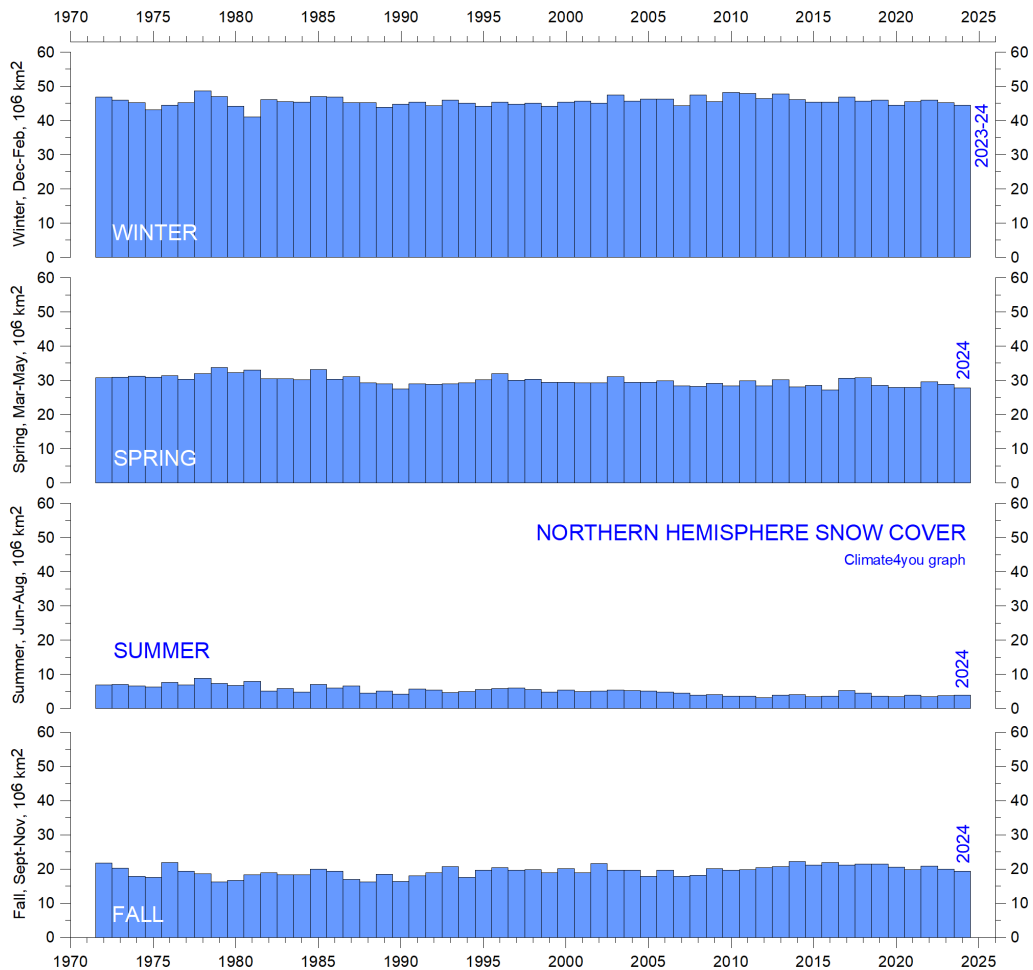
Northern hemisphere seasonal snow cover since January 1972 according to Rutgers University Global Snow Laboratory.

Greenland Ice Sheet net surface mass balance, updated to November 2024
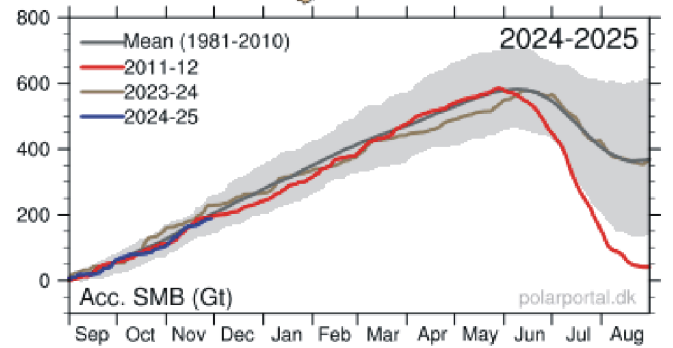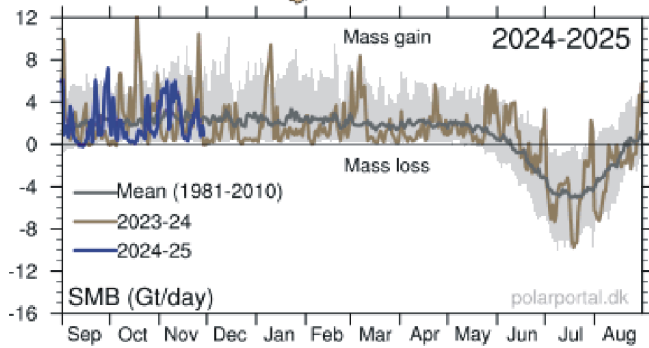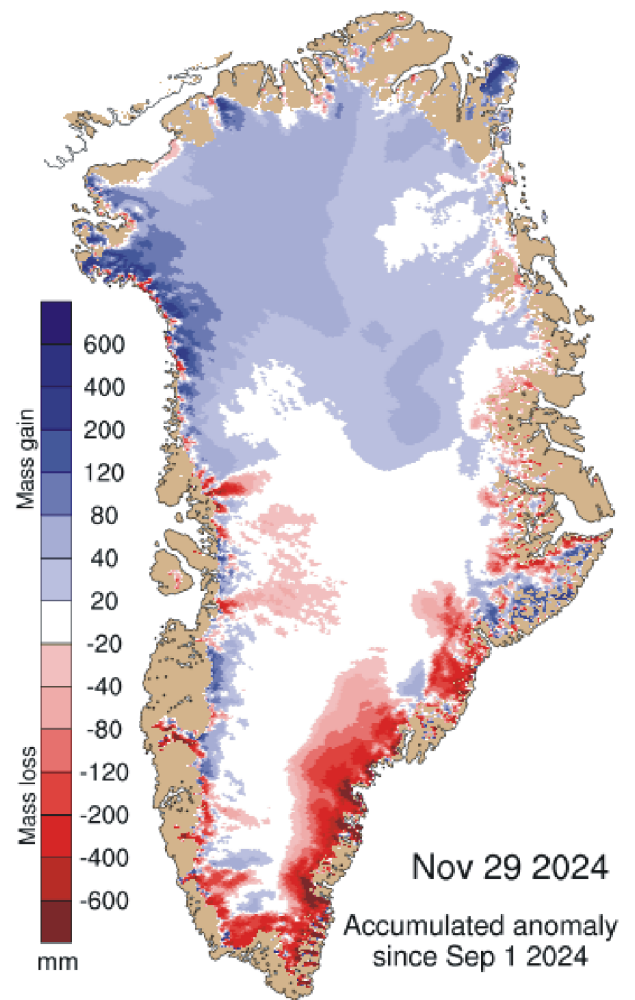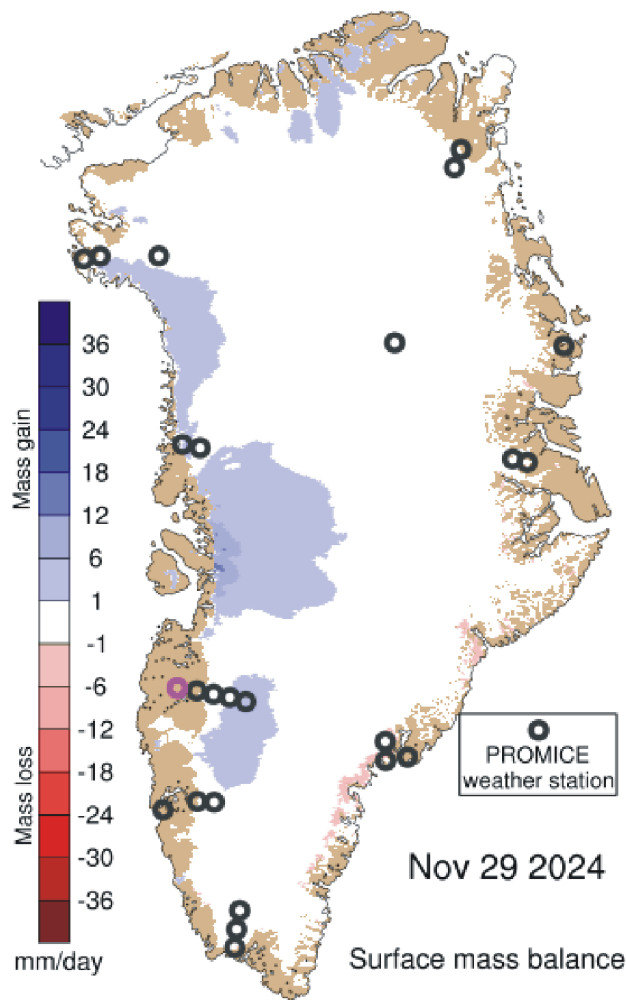
Left: Surface mass balance 29 November 2024. Right: Net surface mass balance anomaly since September 1, 2024. Courtesy of Danish Meteorological Institute (DMI).

Atmospheric relative and specific humidity, updated to November 2024
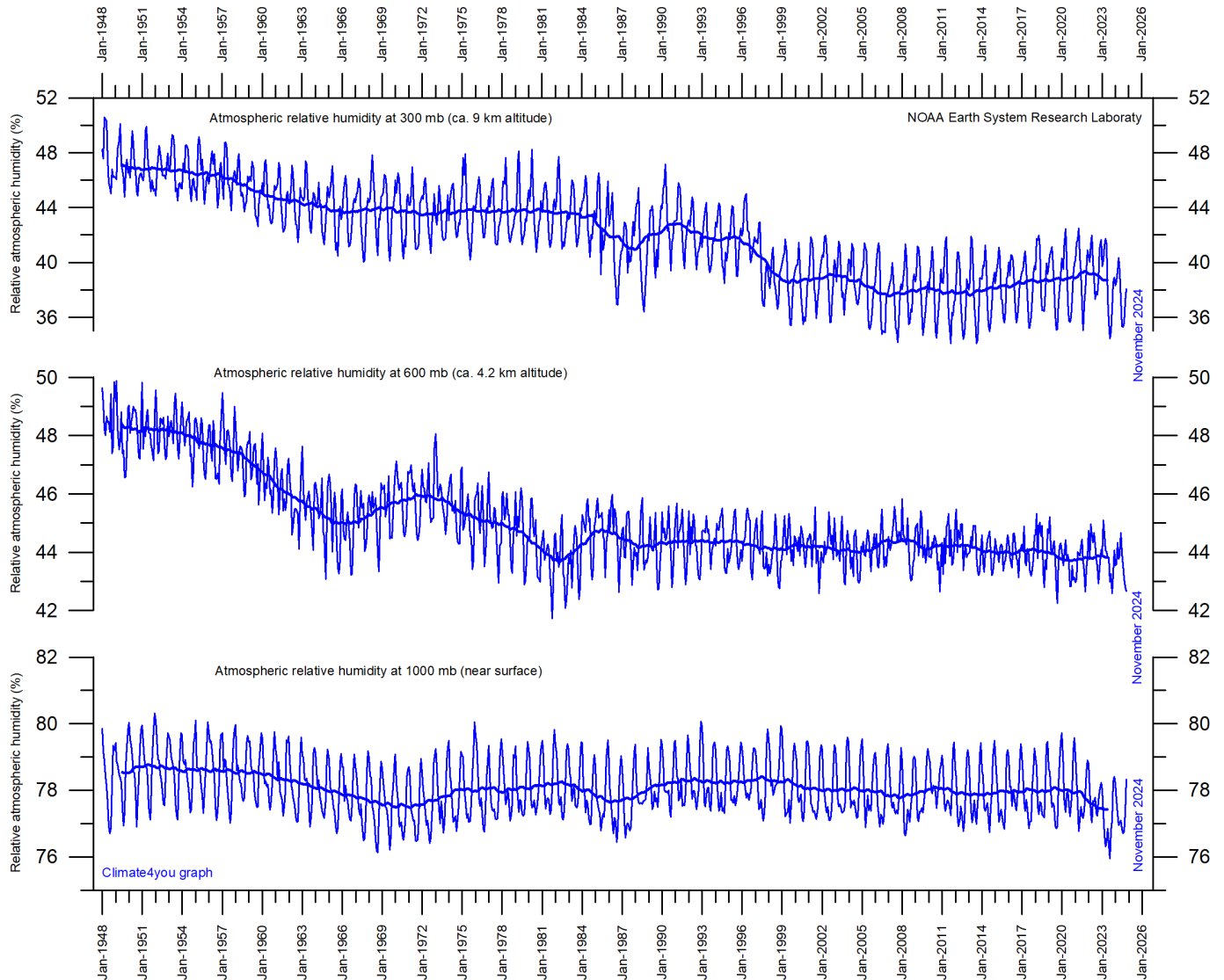
Relative atmospheric humidity (g/kg) at three different altitudes in the lower part of the atmosphere (*the Troposphere*) since January 1948 (*Kalnay et al. 1996*). The thin blue lines show monthly values, while the thick blue lines show the running 37-month average (about 3 years). Data source: *Earth System Research Laboratory (NOAA)*.
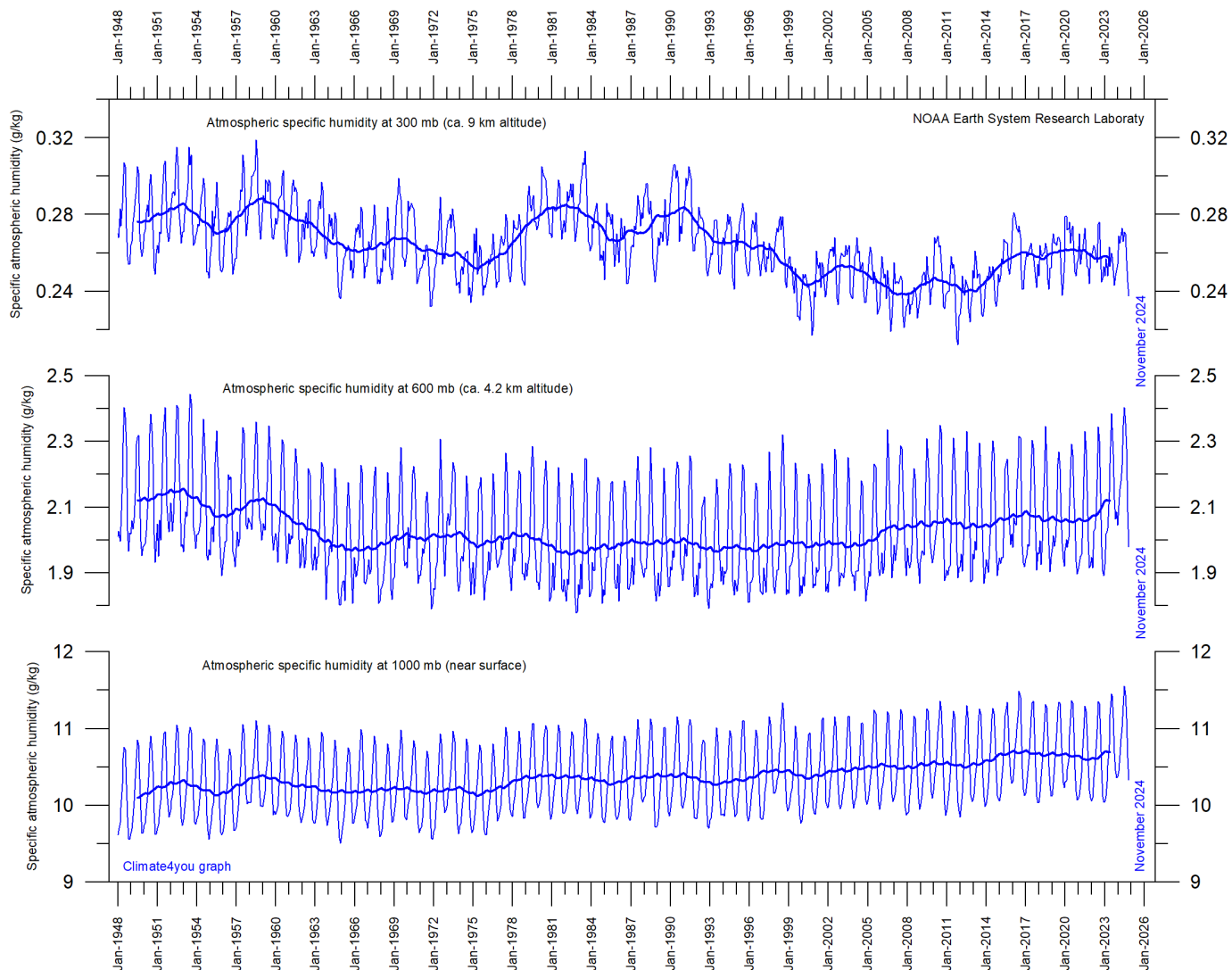
Specific atmospheric humidity (g/kg) at three different altitudes in the lower part of the atmosphere (the Troposphere) since January 1948 (Kalnay et al. 1996). The thin blue lines show monthly values, while the thick blue lines show the running 37-month average (about 3 years). Data source: Earth System Research Laboratory (NOAA).

Water vapor is the most important greenhouse gas in the Troposphere. The highest concentration is found within a latitudinal range from 50°N to 60°S. The two polar regions of the Troposphere are comparatively dry.

Climate models assume that the atmosphere during a CO_2 induced warming should display rising specific humidity but maintain a constant relative humidity.

The diagram above shows the specific atmospheric humidity to be stable or slightly increasing up to about 4-5 km altitude. At higher levels in the Troposphere (about 9 km), the specific humidity has been decreasing for the duration of the record (since 1948), although with shorter variations superimposed on the falling trend.

The persistent decrease in specific humidity at about 9 km altitude is particularly noteworthy, as this altitude roughly corresponds to the level where the theoretical temperature effect of increased atmospheric CO_2 is expected initially to play out. In contrast, climate models assume specific humidity to increase at this height.

A Fourier frequency analysis (not shown here) suggests these changes are influenced, not only by the significant annual variation, but feasibly also by a longer variation of about 35-years' duration. Much is still to be learnt on controls on atmospheric water vapor, and its climatic significance.

Atmospheric CO₂, updated to November 2024
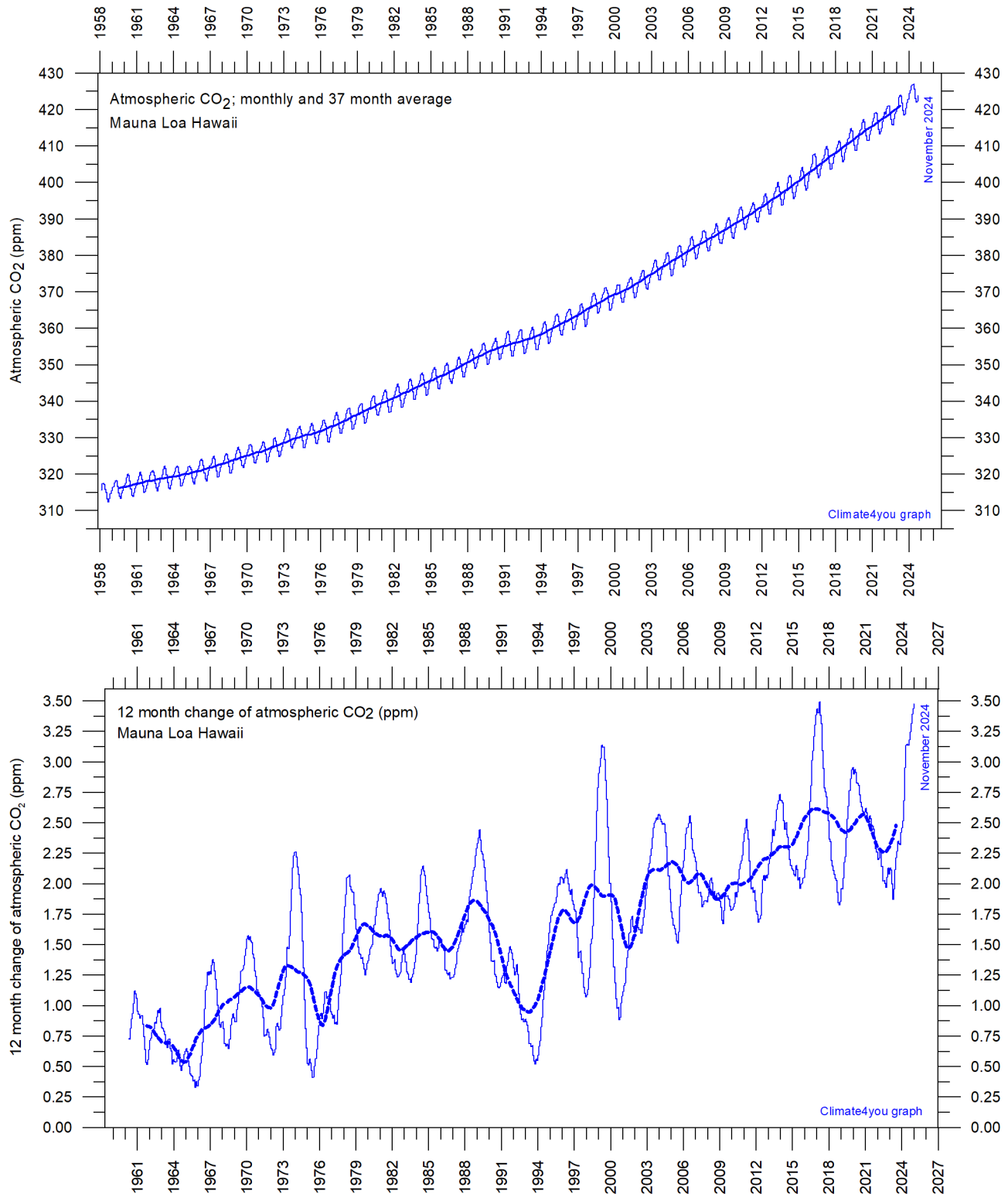
Monthly amount of atmospheric CO₂ (upper diagram) and annual growth rate (lower diagram); average last 12 months minus average preceding 12 months, thin line) of atmospheric CO₂ since 1959, according to data provided by the Mauna Loa Observatory, Hawaii, USA. The thick, stippled line is the simple running 37-observation average, nearly corresponding to a running 3-year average. A Fourier frequency analysis (not shown here) shows the 12-month change of Tropospheric CO2 to be influenced especially by periodic variations of 2.5- and 3.8-years' duration.

The relation between annual change of atmospheric CO_2 and La Niña and El Niño episodes, updated to November 2024
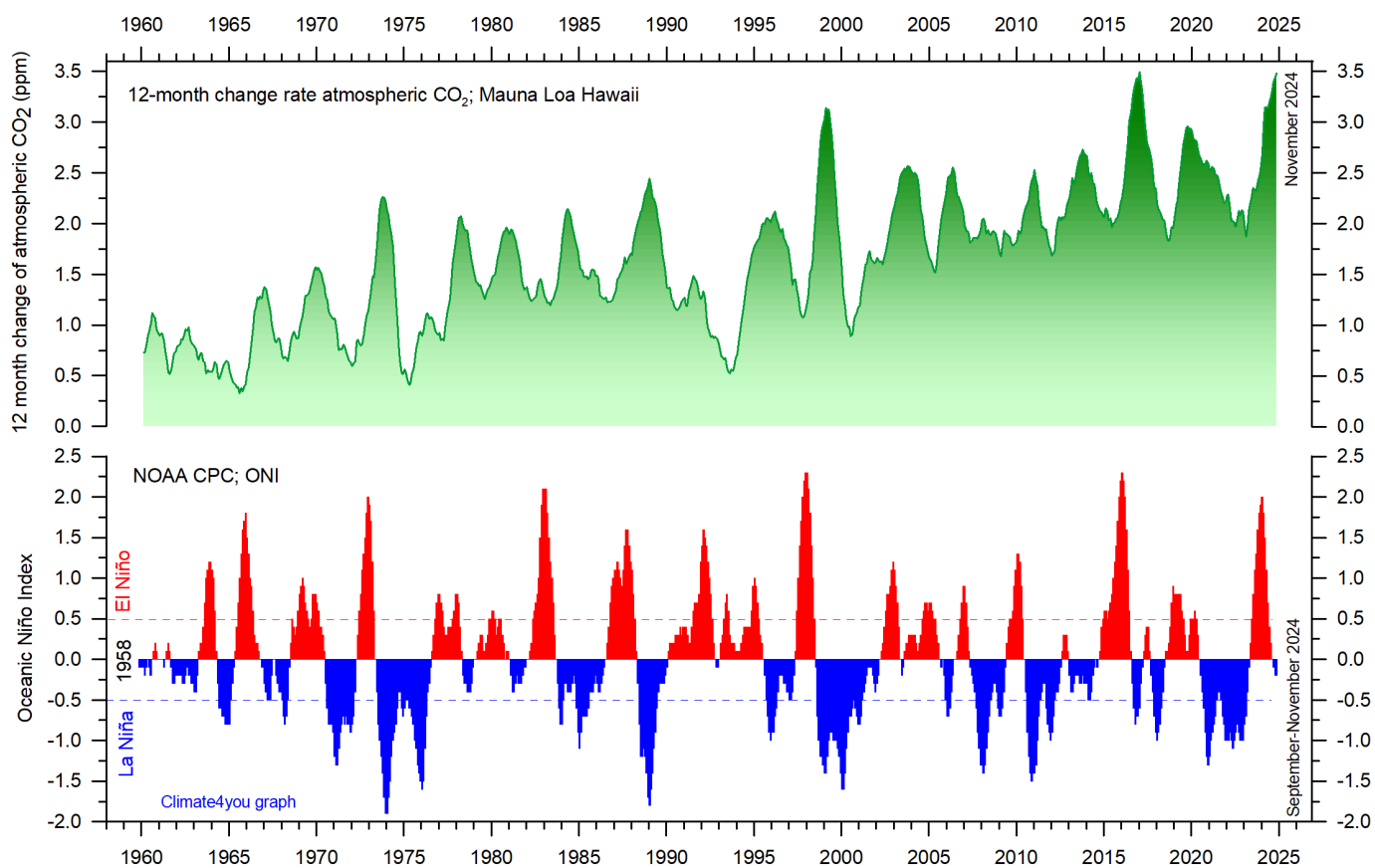
Visual association between annual growth rate of atmospheric CO_2 (upper panel) and Oceanic Niño Index (lower panel). See also diagrams on page 47 and 25, respectively.

Changes in the global atmospheric CO_2 is seen to vary roughly in concert with changes in the Oceanic Niño Index. The typical sequence of events is that changes in the global atmospheric CO_2 to a certain degree follows changes in the Oceanic Niño Index, but clearly not in all details. Many processes, natural as well as anthropogenic, controls the amount of atmospheric CO_2, but oceanographic processes are clearly particularly important (see also diagram on next page).

Atmospheric CO_2 and the recent coronavirus pandemic

Modern political initiatives usually assume the human influence (mainly the burning of fossil fuels) to represent the main reason for the observed increase in atmospheric CO_2 since 1958.

The coronavirus pandemic since January 2020 resulted in a marked reduction in the global consumption of fossil fuels, lasting at least to 2022. However, there was no effect to be seen of this reduction in the atmospheric amount of CO_2 (see, e.g., diagrams on page 49) The explanation for this is the fact that human contributions are too small compared to the numerous natural sources and sinks for atmospheric CO_2 to make the above reduction appear in diagrams showing the amount of atmospheric CO_2.

Much is still to be learnt on controls on the atmospheric amount of CO_2, and its climatic significance.

The phase relation between atmospheric CO₂ and global temperature, updated to October 2024
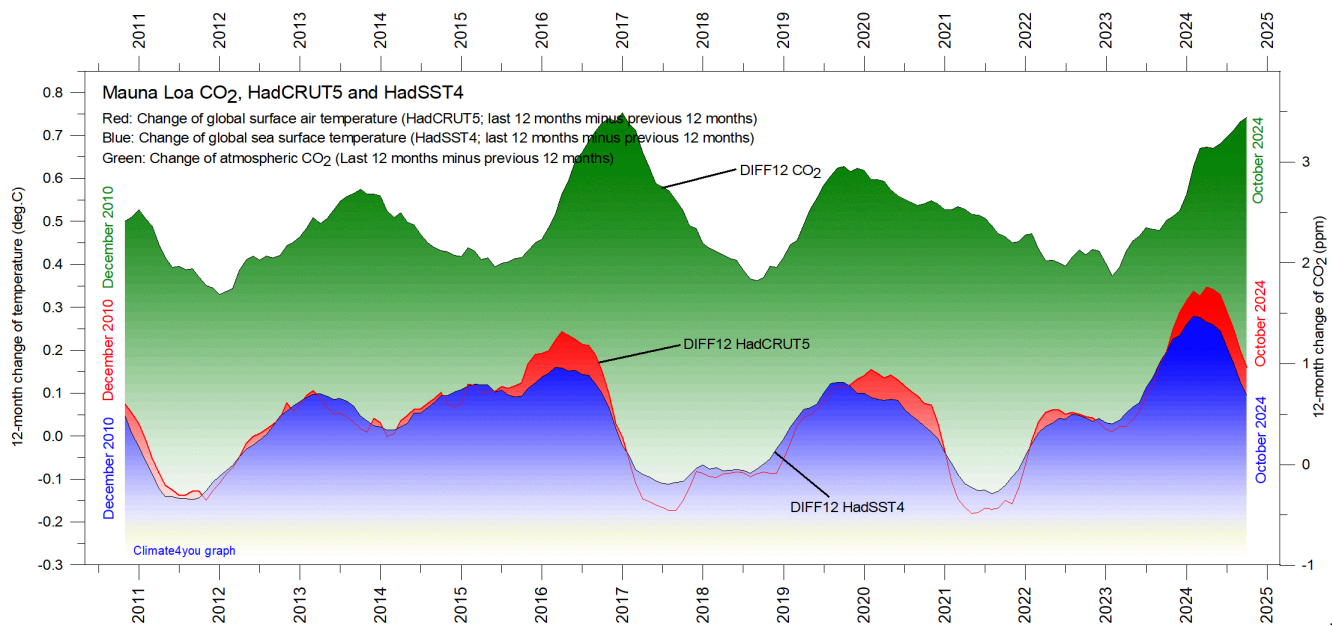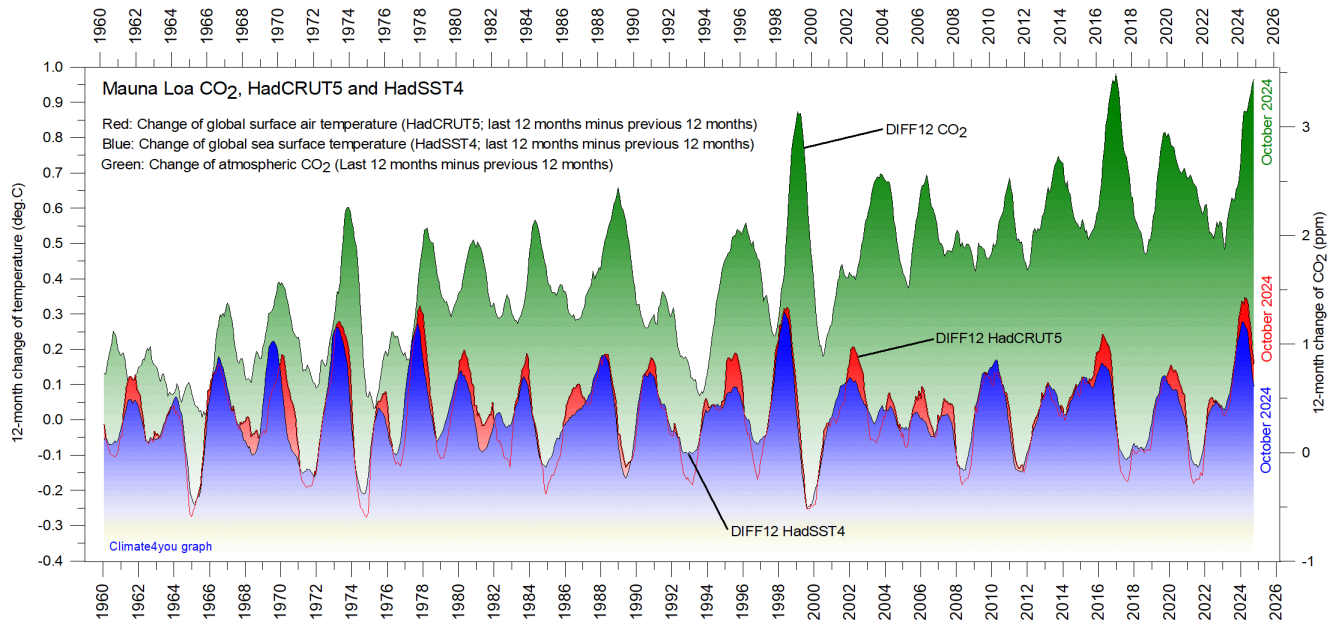
12-month change of global atmospheric CO₂ concentration (Mauna Loa; green), global sea surface temperature (HadSST4; blue) and global surface air temperature (HadCRUT5; red dotted). Entire data series since 1958 in upper figure, and last 15 years in lower figure, to enhance modern dynamics. All graphs are showing monthly values of DIFF12, the difference between the average of the last 12 month and the average for the previous 12 months for each data series.

The typical sequence of events is seen to be that changes in the global atmospheric CO₂ follow changes in global surface air temperature, which again follow changes in global ocean surface temperatures. Thus, changes in global atmospheric CO₂ usually are lagging 9.5–10 months behind changes in global air surface temperature, and 11–12 months behind changes in global sea surface temperature.

Reference: Humlum, O., Stordahl, K. and Solheim, J-E. 2012. The phase relation between atmospheric carbon dioxide and global temperature. Global and Planetary Change, August 30, 2012.
http://www.sciencedirect.com/science/article/pii/S0921818112001658?v=s5

51

Global air temperature and atmospheric CO₂, updated to November 2024

Measured global temperature anomaly (UAH MSU), and running 37-month average
Theoretical temperature change derived from atmospheric CO₂
Atmospheric CO₂ (Mauna Loa)

UAH temperature average 1981-2010

October 2024

Climate4you graph

Measured global temperature anomaly (RSS MSU), and running 37-month average
Theoretical temperature change derived from atmospheric CO₂
Atmospheric CO₂ (Mauna Loa)

RSS temperature average 1979-1998

November 2024

Climate4you graph

52

Diagrams showing UAH, RSS, HadCRUT5, NCDC and GISS monthly global air temperature estimates (blue) and the monthly atmospheric CO_2 content (red) according to the [Mauna Loa Observatory](), Hawaii. Purple line (running along red CO_2 curve) shows theoretical temperature change due to changing atmospheric CO2. The Mauna Loa data series begins in March 1958, and 1958 was therefore chosen as starting year for all diagrams above. Reconstructions of past atmospheric CO_2 concentrations (before 1958) are not incorporated in this diagram, as such past CO_2 values are derived by other means (ice cores, stomata, or older measurements using different methodology), and therefore are not directly comparable with direct atmospheric measurements.

From a theoretical point of view, it is generally agreed that the atmospheric temperature effect ΔT of increasing atmospheric CO_2 may be expressed as (see, e.g. Myhre et al. 1998 and IPCC Third Assessment Report, section 6.1):

$$\Delta T = \Delta F * \lambda$$

where $\Delta F = 5,35\ln(C1/Co)$ W/m^2, and where Co and C1 indicates the concentration of atmospheric CO_2 at the beginning and end of the time interval considered. The factor λ is a so-called climate sensitivity parameter (expressing the global mean surface temperature response to the imposed radiative CO_2 forcing). This factor has been determined to about 0,26^{o}CW^{-1}m^2. The relation shows that as the concentration of atmospheric CO_2 increases, its

theoretical greenhouse effect increases in a logarithmic fashion, not linear. Therefore, for each increase in CO_2 concentration, the effect on temperature is smaller and smaller.

If all other effects in the real world are ignored, the above relation shows that any doubling of atmospheric CO_2 concentration produces a temperature increase of nearly 1°C (0.96^{o}C), no matter how high the initial concentration of CO_2.

The purple line in the above diagrams (p.50-52) is calculated using the observed concentration of atmospheric CO_2 since March 1958. The axis for CO_2 is adjusted to show overlap between CO_2 (red) and the

calculated accumulated temperature effect (purple). In all graphs, the temperature anomaly axis has been adjusted to position the initial calculated effect of CO_2 roughly at the average for the beginning of the observed temperature graph (blue). This is done to make it possible to compare the theoretical CO_2 temperature development (purple) with the observed development (blue).

All these diagrams show the observed temperature development to be much more complicated than the theoretical development from atmospheric CO_2 alone. With exception of the UAH diagram, the overall observed temperature increases since 1958 is much larger than calculated from CO_2 alone. In addition, the observed temperature development is characterised by recurrent intervals characterised by increasing and decreasing temperatures, respectively, a development extremely different from the calculated temperature (purple graph). Clearly many other factors than only CO_2 is in control of the real-world atmospheric temperature.

At today's CO_2 atmospheric concentration (about 426 parts per million; see diagram on p.49), CO_2 has little ability to absorb additional heat and is therefore only a weak greenhouse gas. Previously, at lower atmospheric concentrations CO_2 was a stronger greenhouse gas, relative to other greenhouse gasses. At today's concentration, however, its ability to warm the planet at higher concentration levels is small. Thus, the often-cited assumption that carbon dioxide is the main driver of climate change is not correct in year 2024.

Nevertheless, in contrast to the above real-world observations, climate models are programmed to give the greenhouse gas carbon dioxide CO_2 a leading role on control on the global air temperature. The fact that the observed real-world temperature has been changing much more than expected just from CO_2, is usually ascribed to an added greenhouse effect of atmospheric water vapour in the upper Troposphere, the concentration of which by the models is expected to increase along with CO_2 (see, e.g. Schneider et. al. 1999).

However, measurements of water vapour in the upper Troposphere apparently show this assumption to be mistaken (see, e.g., diagrams on p.47-48). Therefore, the quite substantial difference between modelled and observed atmospheric temperature must be caused by other factors (see, e.g., Koutsoyiannis and Vournas 2023). In addition, the very dynamic change pattern displayed by the observed temperature also needs to be explained before a sound understanding of global climate dynamics can be claimed.

All temperature-CO_2 diagrams (p.52-54) shows both atmospheric temperature and atmospheric CO_2 to be increasing since 1959. However, this fact does not demonstrate that temperature is controlled by CO_2. In fact, it might just as well demonstrate the opposite relation (temperature controlling CO_2), or, that both temperature and CO_2 is controlled by a third factor. See also diagrams on page 51.

Litterature:

Demetris Koutsoyiannis & Christos Vournas 2023. *Revisiting the greenhouse effect – a hydrological perspective*. Hydrological Sciences Journal, doi: 10.1080/02626667.2023.2287047

Myhre, G., E. Highwood, K. Shine, and F. Stordal 1998. *New estimates of radiative forcing due to well mixed greenhouse gases*, Geophys. Res. Lett., 25(14), 2715–2718, doi:10.1029/98GL0190

Schneider, E.K., Kirtman, B.P., and Lindzen, R.S. 1999. *Tropospheric Water Vapor and Climate Sensitivity.* Journal of the Atmospheric Sciences, 56, 1649-1658.

Latest 20-year QC1 global monthly air temperature changes, updated to November 2024
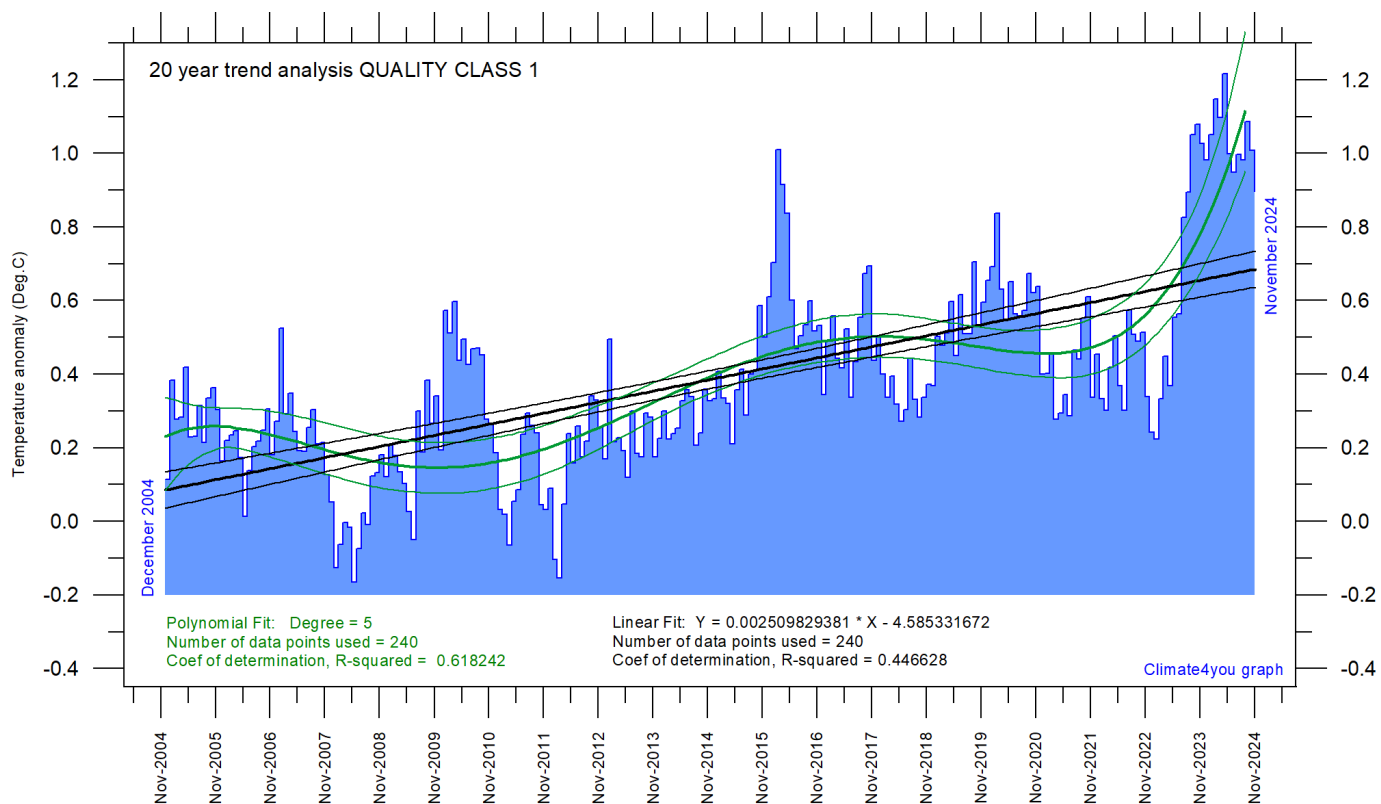
Last 20 years' global monthly average air temperature according to Quality Class 1 (UAH and RSS; see p.6 and 9) global monthly temperature estimates. The thin blue line represents the monthly values. The thick black line is the linear fit, with 95% confidence intervals indicated by the two thin black lines. The thick green line represents a 5-degree polynomial fit, with 95% confidence intervals indicated by the two thin green lines. A few key statistics are given in the lower part of the diagram (please note that the linear trend is the monthly trend).

In the enduring scientific climate debate, the following question is often put forward: Is the surface air temperature still increasing or has it basically remained without significant changes during the last 15-16 years?

The diagram above may be useful in this context and demonstrates the differences between two often used statistical approaches to determine recent temperature trends. Please also note that such fits only attempt to describe the past, and usually have small, if any, predictive power.

In addition, before using any linear trend (or other) analysis of time series a proper statistical model should be chosen, based on statistical justification.

For global temperature time series, there is no *a priori* physical reason why the long-term trend should be linear in time. In fact, climatic time series often have trends for which a straight line is not a good approximation, as is clearly demonstrated by several of the diagrams shown in the present report.
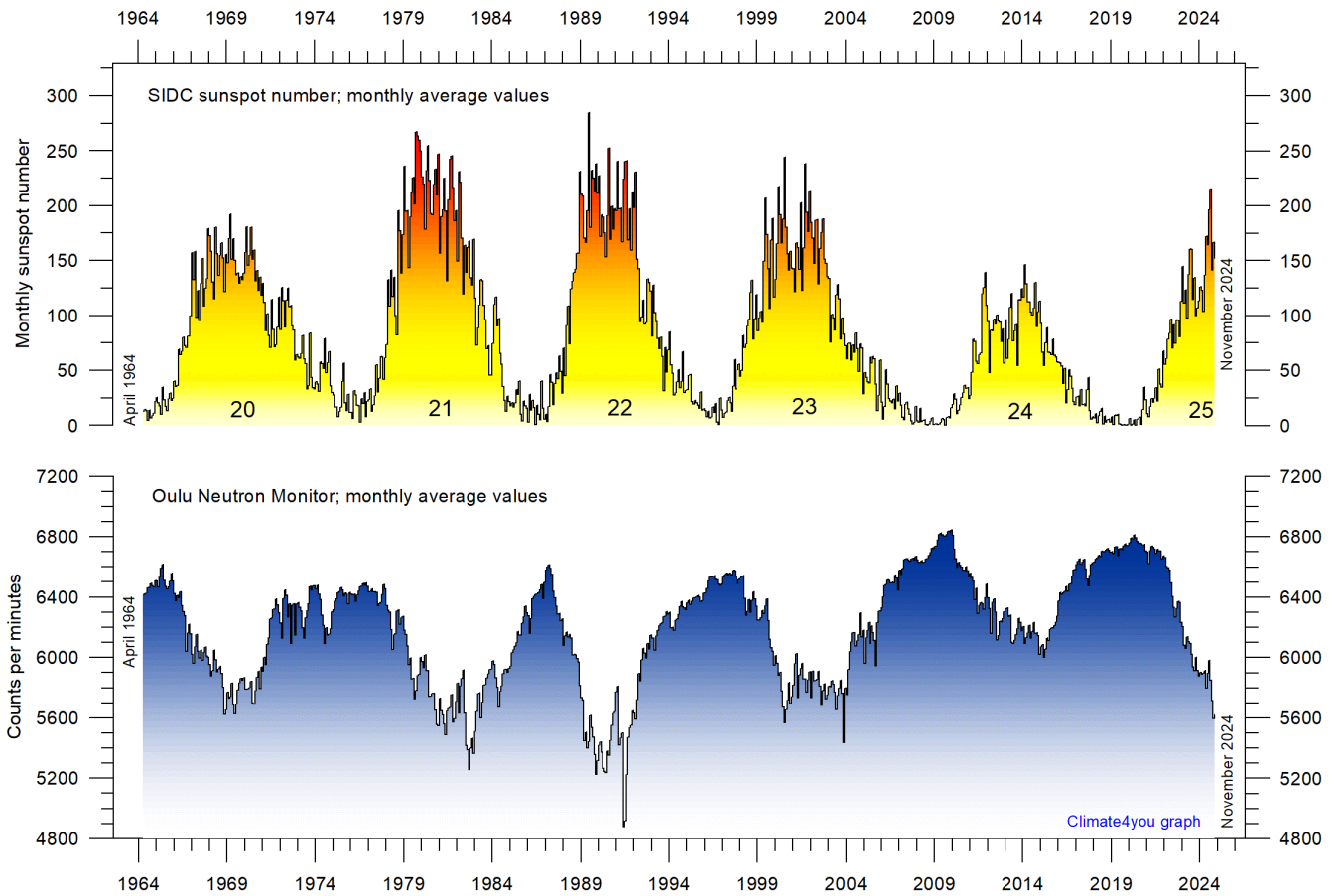
For an commendable description of problems often encountered by analyses of temperature time series analyses, please see Keenan, D.J. 2014: Statistical Analyses of Surface Temperatures in the IPCC Fifth Assessment Report.
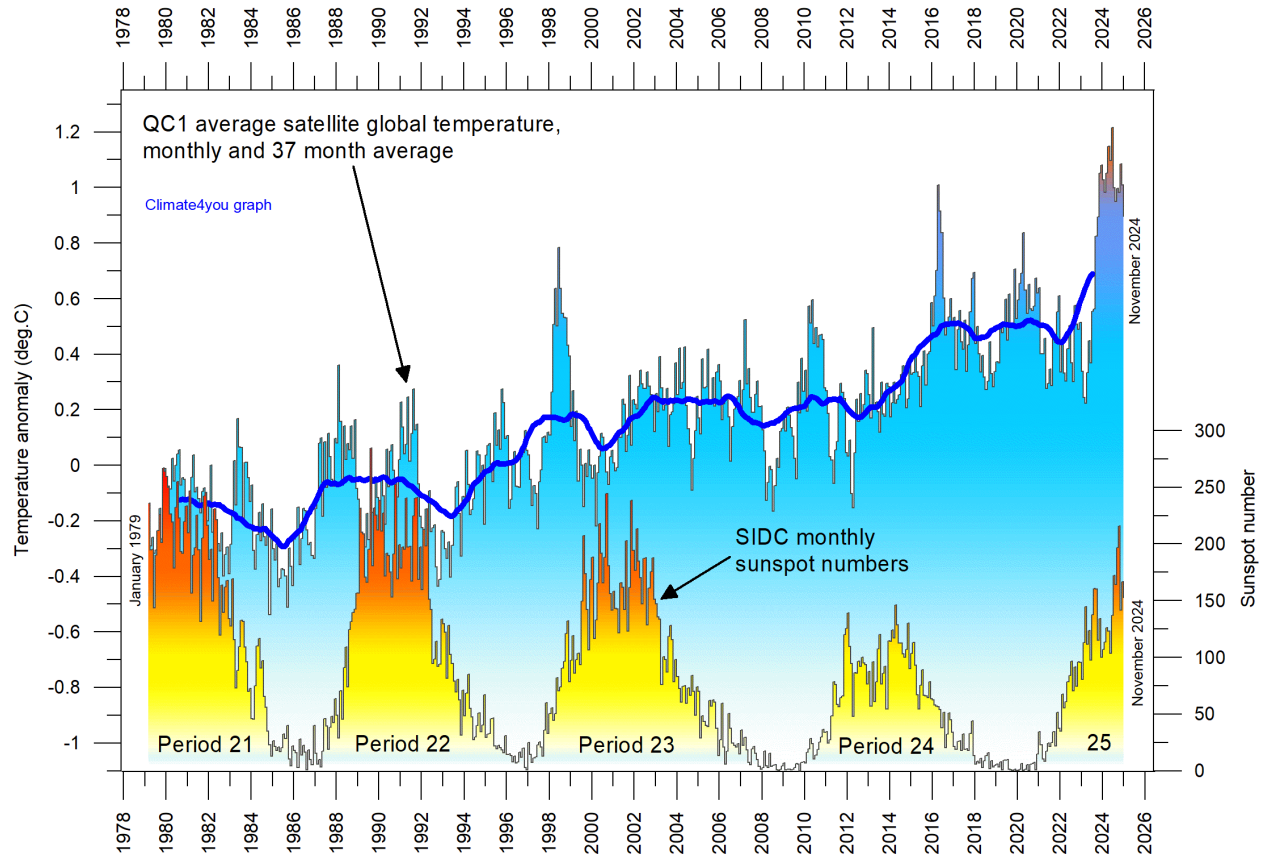
Variation of global monthly air temperature according to Quality Class 1 (UAH and RSS; see p.4) and observed sunspot number as provided by the Solar Influences Data Analysis Center (SIDC), since 1979. The thin lines represent the monthly values, while the thick line is the simple running 37-month average, nearly corresponding to a running 3-year average. The asymmetrical temperature 'bump' around 1998 is influenced by the oceanographic El Niño phenomenon in 1998, as is the case also for 2015-16. Temperatures in year 2019-20 was influenced by a moderate El Niño. In summer 2023 a new El Niño episode has begun (see diagram on p.25).

Observed monthly sunspot number (Solar Influences Data Analysis Center (SIDC) since April 1964, and (lower panel) monthly average counts of the Oulu (Finland) neutron monitor, adjusted for barometric pressure and efficiency.

Monthly sunspot activity (SIDC), Oceanic Niño Index (ONI), and change rates of atmospheric CO_2 and specific humidity, updated to November 2024
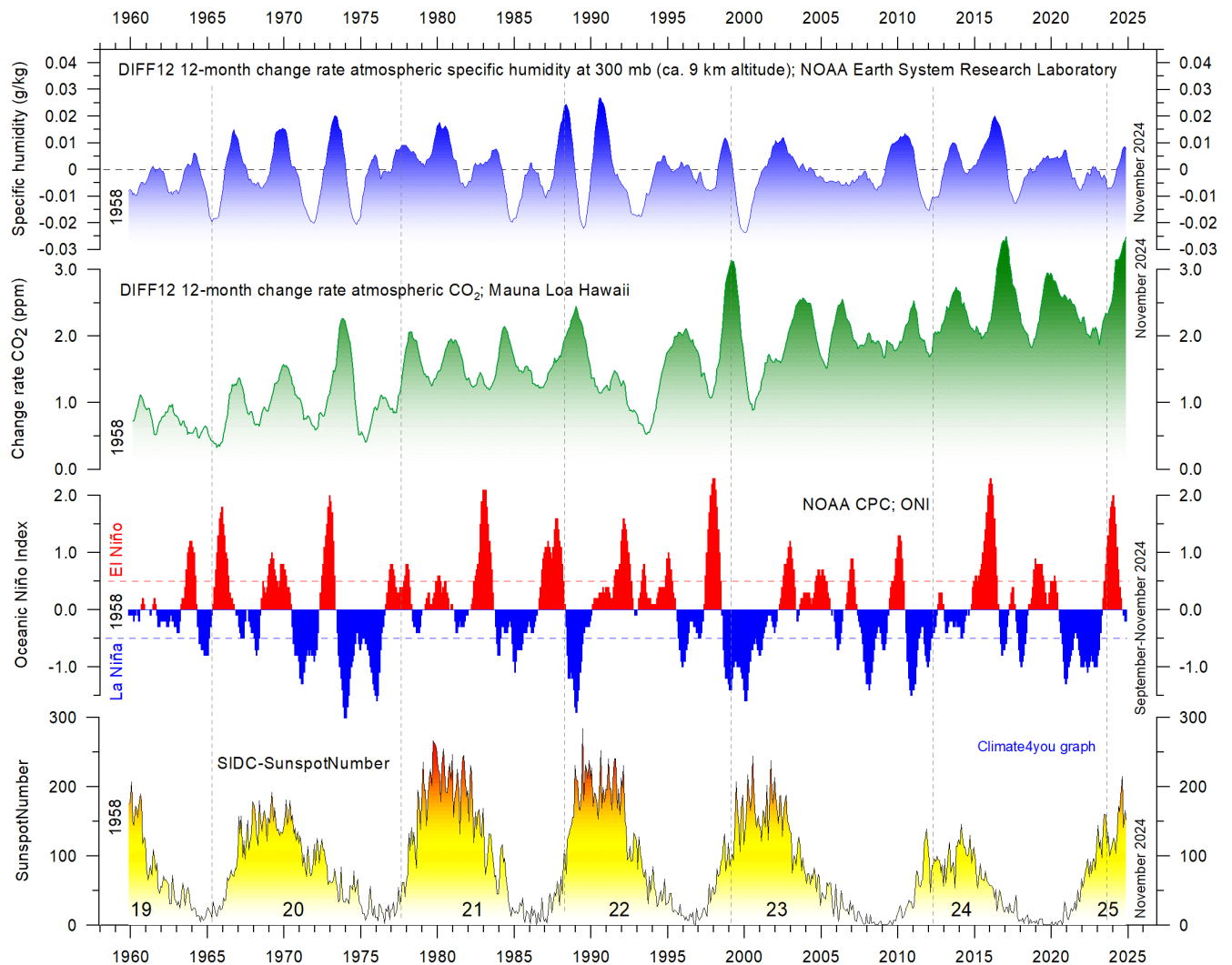

Visual association since 1958 between (from bottom to top) Sunspot Number, Oceanic Niño Index (ONI) and annual change rate of atmospheric CO2. and specific humidity at 300 mb (ca. 9 km altitude). Upper two panels: Annual (12 month) change rate of atmospheric CO2 and specific humidity at 300 mb since 1959, calculated as the average amount of atmospheric CO2/humidity during the last 12 months, minus the average for the preceding 12 months (see also diagrams on page 43+44). Niño index panel: Warm (>+0.5ºC) and cold (<0.5ºC) episodes for the Oceanic Niño Index (ONI), defined as 3 month running mean of ERSSTv4 SST anomalies in the Niño 3.4 region (5ºN-5ºS, 120º-170ºW)]. For historical purposes cold and warm episodes are defined when the threshold is met for a minimum of 5 consecutive over-lapping seasons. Anomalies are centred on 30-yr base periods updated every 5 years. Thin vertical stippled lines indicate the visually estimated timing of sunspot minima. The typically sequence following a sunspot minimum appears to be a warm El Niño episode followed by a cold La Niña episode. Effects on change rates of atmospheric CO_2 and atmospheric specific humidity are visually apparent, with ONI variations being followed by changes in first humidity, and then (last) by CO_2.

The above diagram is inspired by the Leamon et al. 2021 publication: *Robert J. Leamon, Scott W. McIntosh, Daniel R. Marsh. Termination of Solar Cycles and Correlated Tropospheric Variability. Earth and Space Science, 2021; 8 (4) DOI: [10.1029/2020EA001223](10.1029/2020EA001223)*

Monthly lower troposphere temperature (UAH) and global cloud cover, updated to April 2021
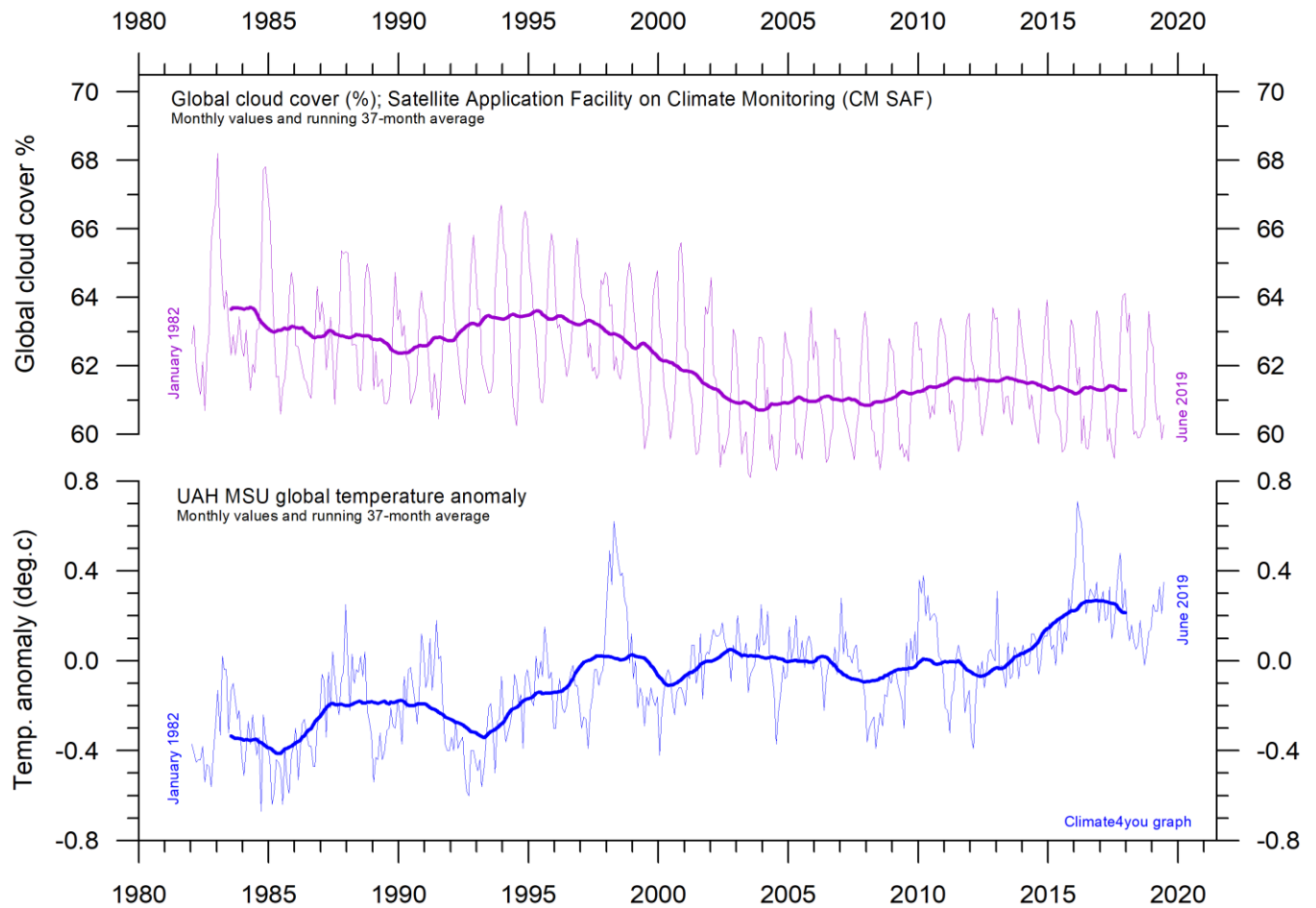
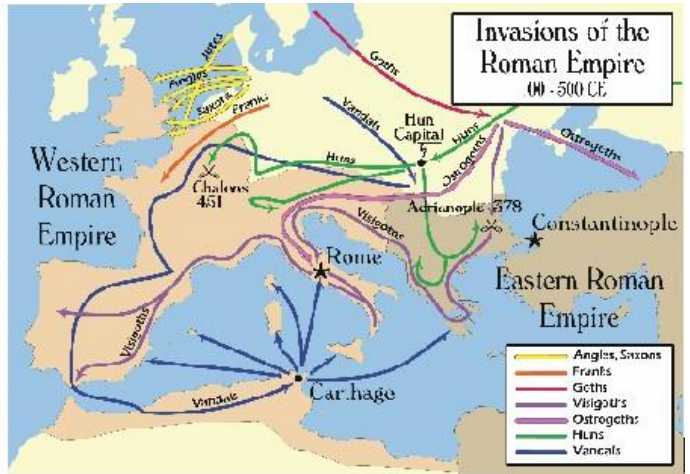*Lower tropospheric air temperature and global cloud cover. Upper panel: Global cloud cover according to Satellite Application Facility on Climate Monitoring. Lower panel: Global monthly average lower troposphere temperature (thin line) since 1979 according to University of Alabama at Huntsville, USA. The thick lines represent the simple running 37-month average. Reference period for UAH is 1991-2020.*

Climate and history; one example among many

AD 476: Collapse of the Roman Empire

Karl Bruillov's 'Sack of Rome' (left). Map of the "barbarian" invasions of the Roman Empire showing the major incursions from 100 to 500 AD (right).

The decline of the Roman Empire refers to the gradual societal collapse of the Western Roman Empire. This slow decline occurred over a period of four centuries, culminating on September 4, 476 AD, when Romulus Augustus, the last Emperor of the Western Roman Empire, was deposed by Odoacer, a Germanic chieftain. The following text is based mainly on Büntgen et al. (2011), Lubick 2011 and Wikipedia.

The decline of the Roman Empire is one of the events traditionally marking the end of Classical Antiquity and the beginning of the European Middle Ages. Throughout the 5th century, the Empire's territories in western Europe and northwestern Africa, including Italy, fell to various invading or indigenous peoples in what is often known as the Migration period, a 250 year period of turmoil in Europe. Although the eastern half of the original Roman Empire still survived with borders essentially intact for several centuries, the Empire as a whole had initiated major cultural and political transformations since the Crisis of the Third Century, with the shift towards a more openly autocratic and ritualized form of government, the adoption of Christianity as the state religion, and a general rejection of the traditions and values of Classical Antiquity.

The European Middle Ages following the decline of the Roman Empire is important, as it witnessed the first sustained urbanisation of northern and western Europe. Many modern European states owe their origins to events unfolding in the Middle Ages; present European political boundaries are, in many regards, the result of the military and dynastic achievements during this tumultuous period.

By the late 3rd century, the city of Rome no longer served as an effective capital for the Emperor and various cities were used as new administrative capitals. Successive emperors, starting with

Constantine, privileged the eastern city of Byzantium, which he had entirely rebuilt after a siege. Later renamed Constantinople, and protected by formidable walls in the late 4th and early 5th centuries, it was to become the largest and most powerful city of Christian Europe in the Early Middle Ages. Since the Crisis of the Third Century, the Roman Empire was intermittently ruled by more than one emperor at once (usually two), presiding over different regions. At first a haphazard form of power sharing, this eventually settled on an East-West administrative division between the Western Roman Empire (centred on Rome, but now usually presided from other seats of power such as Trier, Milan, and especially Ravenna), and the Eastern Roman Empire, also known as the Byzantine Empire.

Throughout the 5th century, Western emperors were usually figureheads, while the Eastern emperors maintained more independence. For most of the time, the actual rulers in the West were military strongmen who took the titles of magister militum (master of the soldiers), patrician, or both. Although Rome was no longer the capital in the West, it remained the West's largest city and its economic centre. But the city was sacked by rebellious Visigoths in 410 AD and by the Vandals in 455 AD, events that shocked contemporaries and signalled the disintegration of Roman authority.

In June 474 AD, Julius Nepos became Western Emperor but in the next year the magister militum Orestes revolted and made his son Romulus Augustus emperor. Romulus, however, was not recognized by the Eastern Emperor Zeno, who used to have good connections to Nepos. Romulus, therefore, was technically a usurper, and Nepos still being the legal Western Emperor. Nevertheless, Romulus Augustus is often known as the last Western Roman Emperor. In 476 AD, after being refused lands in Italy, Orestes' Germanic mercenaries under the leadership of the chieftain Odoacer captured and executed Orestes and took

Ravenna, the Western Roman capital at the time, deposing Romulus Augustus. The whole of Italy was quickly conquered, and Odoacer was granted the title of patrician by Zeno, effectively recognizing his rule in the name of the Eastern Empire. Odoacer returned the Imperial insignia to Constantinople and ruled as King in Italy. Although Roman political authority in the West was lost, Roman culture would last in most parts of the former Western provinces into the 6th century and beyond.

The English historian Edward Gibbon, author of The History of the Decline and Fall of the Roman Empire (1776) made the concept of the decline of the Roman Empire part of the framework of the English language. In six volumes, Gibbon painstakingly charted the Empire's final demise, using original reference material where possible. Gibbon blamed the fall on several factors: a loss of civic virtue, the use of barbarians as mercenaries rather than Roman soldiers, and the rise of Christianity, which led to increased pacifism and widespread beliefs that a better life awaited Roman citizens after death.

Gibbon, however, was not the first to speculate on why and when the Empire collapsed. In 1984, the German professor Alexander Demandt published a collection of 210 theories on why Rome fell, and new theories have emerged since then. One of the last was recently proposed by Büntgen et al. (2011).

The Büntgen research team compared modern tree-ring data with instrumental climate records to quantify the relationship between tree-ring growth and climate (precipitation and summer temperature). They used this relationship to reconstruct climate information from the ancient tree rings before instrumental records became available. To avoid getting strong local signals from one or a handful of trees in a particular forest or mountain site, Büntgen et al. (2011) used data for thousands of pieces of oak wood across Central Europe. Precipitation was reconstructed by using

over 7000 oak trees across France and Germany. And about 1500 stone pine trees from the Austrian Alps region provided information about temperature.

From these data interesting climate information emerge. From the beginning of the Roman Empire to its peak (c. 50 BC to AD 250), the climate was relatively stable, with warm and dry summers. During the two-and-half centuries or so that followed Europe apparently experienced very unfavourable conditions for agriculture, with summers being wet and cool. This time period corresponds to what today is known as the Migration period - a 250-year-period of turmoil and waves of migration in Europe.
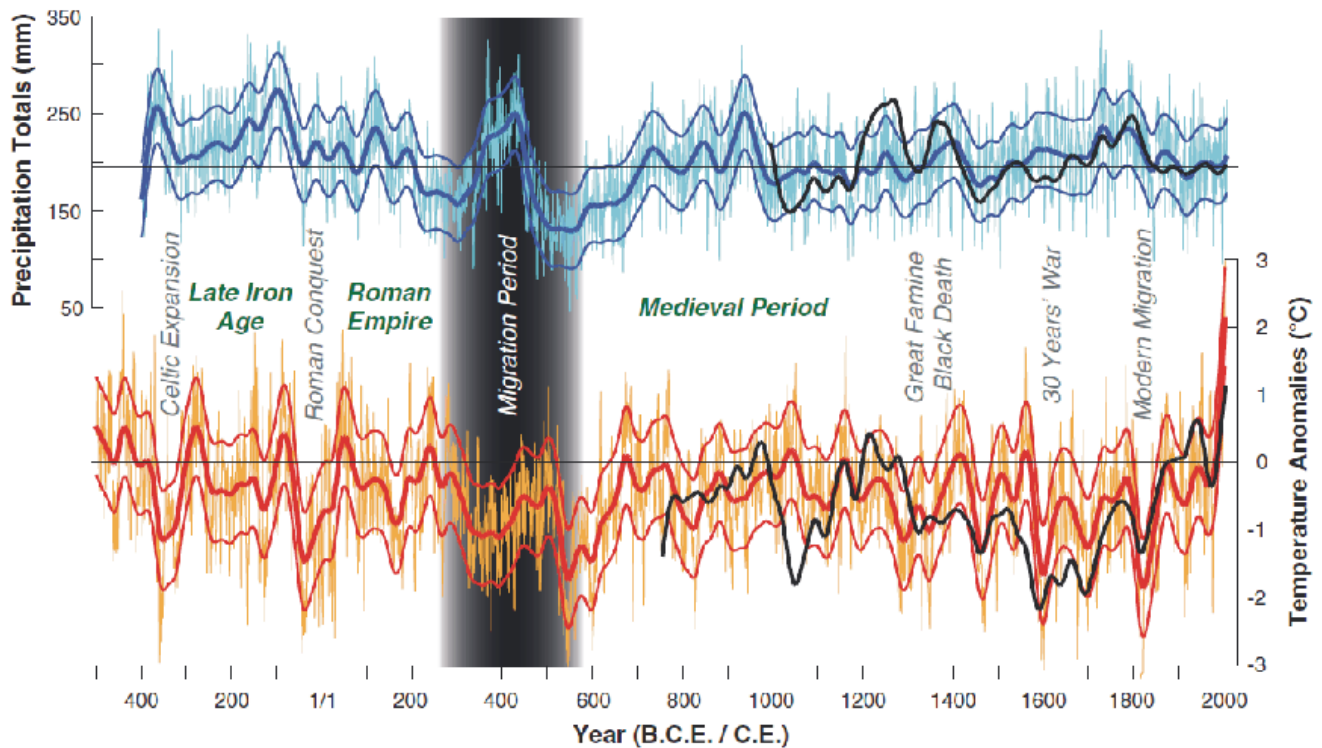
Reconstructed precipitation (upper panel) and summer (JJA) temperature anomaly, with respect to the average of the 1901-2000 period ([Büntgen et al. (2011)](#)).

Wet weather apparently may have made harvest conditions very difficult around the end of the Roman Empire in the fifth century. In this way cool and moist summer climate may have contributed to the Decline of the Roman Empire. Later climate then transitioned to a very dry and cold period around AD 550. Better conditions returned around AD 700, and the subsequent reduced climate variability from AD 1000 to 1200 was coincident with prosperity and a growing population.

Sources and References:

Büntgen, U., Tegel, W., Nicolussi,K., McCormick, M., Frank, D., Trouet, V., Kaplan, J.O., Herzig, F., Heussner, K.-U., Wanner, H., Luterbacher, J. and Esper. J. 2011. 2500 Years of European Climate Variability and Human Susceptibility. *Science* 331 (6017): 578-582, doi: 10.1126/science.1197175.

Lubick, N. 2011. Did rain bring down the Roman Empire?. *Global Change* 77, 8-11.

Wikipedia. http://www.wikipedia.org/

*****

All diagrams in this report, along with any supplementary information, including links to data sources and previous issues of this newsletter, are freely available for download on www.climate4you.com

64

Season's Greetings,

yours sincerely,

Ole Humlum (Ole.Humlum@gmail.com)

Arctic Historical Evaluation and Research Organisation, Longyearbyen, Svalbard

20 December 2024.

Planned publication of next newsletter: around 25 January 2025.